UNIVERSITA' DEGLI STUDI DI NAPOLI "FEDERICO II"

FACOLTA' DI SCIENZE MATEMATICHE, FISICHE E NATURALI

DOTTORATO DI RICERCA IN SCIENZE CHIMICHE

(XXI ciclo 2005-2008)

INDIRIZZO DI SINTESI, STRUTTURA E REATTIVITÀ DI MOLECOLE ORGANICHE

CHEMISTRY AND BIOACTIVITY OF NATURAL POLYPHENOLS.

Candidato

Dott. MARIA DE LUCIA

Tutore

Ch.ma Prof. ssa ALESSANDRA NAPOLITANO

Relatore

Prof. CRISTINA DE CASTRO

UNIVERSITA' DEGLI STUDI DI NAPOLI "FEDERICO II"

FACOLTA' DI SCIENZE MATEMATICHE, FISICHE E NATURALI

DOTTORATO DI RICERCA IN SCIENZE CHIMICHE

(XXI ciclo 2005-2008)

INDIRIZZO DI SINTESI, STRUTTURA E REATTIVITÀ DI MOLECOLE ORGANICHE

CHIMICA E BIOATTIVITÀ DI COMPOSTI POLIFENOLICI DI ORIGINE NATURALE

Candidato

Dott. MARIA DE LUCIA

Tutore

Ch.ma Prof. ssa ALESSANDRA NAPOLITANO

Relatore

Prof. CRISTINA DE CASTRO

INDEX

ABSTRACT

Natural polyphenols exhibit several beneficial effects most notably protection against oxidative stress and degenerative diseases, which can be ascribed largely to their intrinsic capabilities to act as antioxidant or antinitrosating agents. This work has led to definition of the reaction pathways of a number of polyphenols, with special reference to their transformations when acting as antioxidant or antinitrosating agents under conditions of physiological relevance.

The H_2O_2-dependent oxidative pathway of hydroxytyrosol, the well known antioxidant from extra virgin olive oil, was defined evidencing the marked nucleophilic character of hydroxylated compounds generated by addition of hydrogen peroxide to the *ortho*-quinone of hydroxytyrosol.

The reactions of stilbene resveratrol and piceatannol, occurring in red wines and grapes, toward acidic nitrite showed the tendency of these compounds to undergo nitration at the stilbene double bond and their susceptibility to oxidative cleavage under mild conditions.

The nitrite scavenging effects of the dietary catechols caffeic acid, chlorogenic acid, piceatannol, hydroxytyrosol and their *s*-glutathionyl conjugates were assessed by the 2,3-diaminonaphthalene (DAN) nitrosation and tyrosine nitration assays. In the DAN assay the 5-*S*-glutathionylpiceatannol was found to be the most active, while in the tyrosine assay chlorogenic acid was the best inhibitor, suggesting that the antinitrosating properties do not correlate straightforwardly with the antioxidant activity for these compounds. The antioxidant properties of a new derivative of hydroxytyrosol with dihydrolipoic acid, 5-*S*-lipoylhydroxytyrosol, were also evaluated showing a higher radical scavenging activity with respect to the parent compound.

In a related study the reactivity of menthofuran, a naturally occurring furan derivative found in mint oils, with nitric acid and nitrous acid was comparatively investigated. In the presence of sulfuric acid, nitric acid induced mainly fragmentation/dimerization reactions to give bis-furanyl adducts. By contrast, exposure to nitrous acid led to a complex pattern of products, including an unusual dimer with three different nitrogen functionalities.

Among polyphenol metabolites of mammals cysteinyldopas, viz. the 5*S* and 2*S* isomers, the biosynthetic precursors of epidermal pheomelanins, characteristic of red-haired individuals have attracted particular interest. In this study the first direct synthesis of 2-S-cysteinyldopa by a three-step procedure with an overall 30% yield was developed which allows preparation of the compound on gram-scale for reactivity studies in the field.

A detailed analysis of the chemical and spectrophotometric features of the main intermediates derived from cysteinyldopas in the build up of the pheomelanin chromophore allowed also to dissect the contribution of different structural units disproving the axiom that pheomelanin chromophore is determined only by benzothiazine systems.

1. INTRODUCTION

1.1 Classification of dietary polyphenols.

Over the past 20 years, there has been an increasing interest in plant-derived polyphenols with respect to human health.[1-5] Many of these compounds are found in plant foods that have been in common use in different societies around the world for many centuries. Since by definition a food is not toxic at the levels normally consumed, it has been assumed that the polyphenols in the food are also non toxic. This has encouraged the use of such foods and the polyphenols therein for their chemoprevention properties and/or as adjuvants in chemotherapy of cancer.[6-12] It is worth noting that all the compounds in plants have been selected by evolution to have biological importance and that plants also generate novel compounds with extreme stereospecificity. It is not therefore surprising that 50% of the anticancer therapeutic agents used in modern medicine are derived from plants.[13] Plant-based chemoprevention agents include the vast array of polyphenols (bioflavonoids, stilbenoids, etc.) and non polyphenols (isothiocyanates, terpenoids, etc., as well as the more familiar vitamins A, C, D, and E).[14-19]

Dietary polyphenols represent a group of secondary metabolites which widely occur in fruit and beverages (fruit juice, wine, tea, coffee, chocolate and beer) and, to a lesser extent, vegetables, dry legumes and cereals. They are mostly derivatives, and/or isomers of flavones, isoflavones, flavonols, catechins, and phenolic acids. Dietary polyphenols are the most abundant antioxidants in human diets. With over 8,000 structural variants, they denote many substances with aromatic ring(s) bearing one or more hydroxyl moieties. They are subdivided into groups (Figure 1) by the number of phenolic rings and of the structural elements that link these rings:[20] (1) The phenolic acids with the subclasses derived from hydroxybenzoic acids such as gallic

acid and from hydroxycinnamic acid, containing caffeic, ferulic, and coumaric acid; (2) Flavonoids, which are the most abundant polyphenols in human diets, and are mainly divided into: (a) anthocyanins, glycosylated derivative of anthocyanidin, present in colorful flowers and fruits; (b) anthoxanthins, a group of colorless compounds further divided in several categories, including flavones, flavans, flavonols, flavanols, isoflavones, and their glycosides. Flavonols are mainly represented by myricetin, fisetin, quercetin and kaempferol; (3) Stilbenes, which are structurally characterized by the presence of a 1,2-diphenylethylene nucleus with hydroxyls substitued on the aromatic rings, and exist in the form of monomers or oligomers. The best known compound is *trans*-resveratrol, possessing a trihydroxystilbene skeleton; (4) Tannins, a group of water-soluble polyphenols having molecular weights from 500 to 3,000 which are commonly found complexed with alkaloids, polysaccharides and proteins, particularly the latter. Finally there are also some other polyphenols such as hydroxytyrosol, a simple polyphenol occurring in olive fruits and olive oil. Phenolic acids account for about one third of the total intake and flavonoids account for the remaining two thirds.

Flavonoids are biosynthesized by first reacting phenylalanine and malonyl CoA to form 4-coumaroyl CoA, followed by condensation with further malonyl CoA by chalcone synthase to yield naringenin. This flavonoid is the precursor to a variety of flavonoids, flavanoids, isoflavonoids, anthocyanins, proanthocyanins, and coumestanes.[21] Stilbenoids are formed in a similar way from 4-coumaroyl CoA and malonyl CoA and stilbene synthase.[22, 23]

Many of these compounds in the plant are in a pro-form, i.e., they are structurally modified to limit their biological activity or to allow them to be sequestered within the plant at high concentrations. This allows them to be made

available quickly to the plant under stress conditions or when it is under attack.

Figure 1. Classification of dietary polyphenols.

For the biosynthesis of many natural products, including polyphenols and terpenes, glycosylation is the final step necessary for storage (and therefore accumulation) of the metabolite in the plant. Therefore, most polyphenols exist in plants in glycosidic forms. Most of the polyphenol *O*-glycosides undergo intestinal

hydrolysis to release the respective aglycons by intestinal glucosidases/hydrolases, both from the host and intestinal bacteria. Because the aglycons and their metabolites are more hydrophobic, they are more efficiently transported across the wall of the gastrointestinal tract than their respective glycosides. They are converted both in the gut wall and the liver, as well as at peripheral tissue sites, into phase I and phase II metabolites. A second level of defense occurs in the form of phase I and phase II metabolism. The principal reaction is the formation of glucuronides, but methylation and sulfonation also occur.

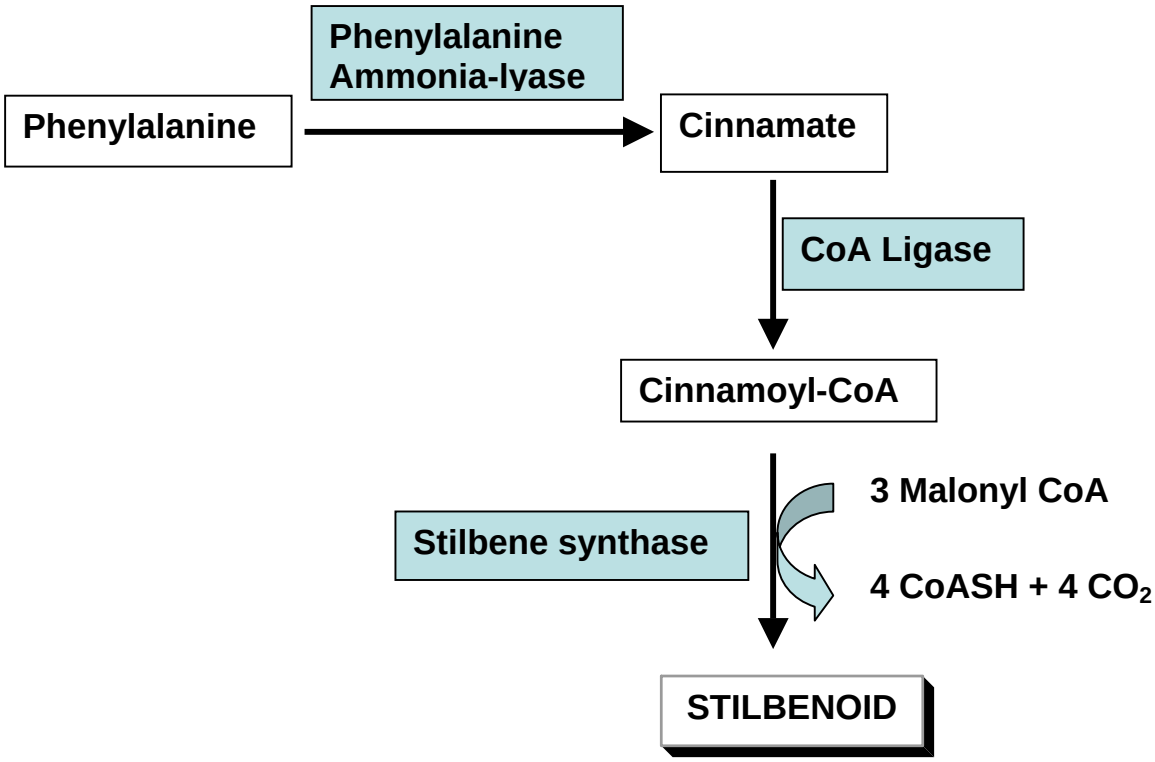
Phenylalanine Ammonia-lyase
Phenylalanine
Cinnamate
CoA Ligase
Cinnamoyl-CoA
3 Malonyl CoA
Stilbene synthase
4 CoASH + 4 CO2
STILBENOID

1.2 Bioactivities of dietary polyphenols.

Dietary polyphenols exhibit many biologically significant functions, such as protection against oxidative stress and degenerative diseases such as atherosclerosis, cardiovascular disease, type II diabetes and cancer. [24-26]

Experimental data indicate that most of these biological actions can be ascribed to their intrinsic antioxidant capabilities. A dietary antioxidant is a substance in food that significantly decreases the adverse effects of reactive oxygen and nitrogen species on physiological functions in humans.

Oxygen free radicals or, more generally, reactive oxygen species (ROS), as well as reactive nitrogen species (RNS), are products of normal cellular metabolism. ROS and RNS are well recognised for playing a dual role as both deleterious and beneficial species, since they can be either harmful or beneficial to living systems.[27] Beneficial effects of ROS/RNS occur at low/moderate concentrations and involve physiological roles in cellular responses to noxious stimuli as, for example, in defence against infectious agents and in the functioning of a number of cellular signalling systems. One further beneficial example of ROS at low/moderate concentrations is the induction of a mitogenic response.The harmful effect of free radicals causing potential biological damage is termed oxidative stress and nitrosative stress.[28-30] This occurs in biological systems when there is an overproduction of ROS/RNS on one side and a deficiency of enzymatic and non-enzymatic antioxidants on the other. In other words, oxidative stress results from the metabolic reactions that use oxygen and represents a disturbance in the equilibrium status of prooxidant/antioxidant reactions in living organisms.

The excess ROS can damage cellular lipids, proteins or DNA inhibiting their normal function. Because of this, oxidative stress has been implicated in a number of human diseases as well as in the ageing process. The delicate balance between beneficial and harmful effects of free radicals is highly important for living organisms and is achieved by mechanisms called "redox regulation". The process of "redox regulation" protects living organisms from oxidative stress in different forms and maintains "redox homeostasis" by controlling the redox status *in vivo*.[31] Free radicals can be defined as molecules or molecular fragments containing one or more unpaired electrons in atomic or molecular orbitals.[32] This unpaired electron(s) usually gives a considerable degree of reactivity to the species. The addition of one electron to dioxygen forms the superoxide anion radical ($O_2^{\bullet-}$);[33] the production of superoxide occurs mostly within mitochondria. Superoxide anion, arising either through metabolic processes or following oxygen "activation" by physical irradiation, is considered the "primary" ROS, and can further interact with other molecules to generate "secondary" ROS, either directly or prevalently through enzyme- or metal-catalysed processes.[30] Superoxide can disproportionate by action of superoxide dismutase to yield hydrogen peroxide. In the presence of partially reduced metal ions, in particular iron, hydrogen peroxide is subsequently converted through Fenton and Haber-Weiss reactions to a hydroxyl radical according to equations 1-4:

$$2 \xrightarrow{e^-} O_2^{-\cdot}$$

$$2O_2^{-\cdot} + 2H^+ \longrightarrow H_2O_2 + O_2$$

$$H_2O_2 + Fe^{2+} \longrightarrow {}^{\cdot}OH + {}^{-}OH + Fe^{3+} \text{ (Fenton Reaction)}$$

$$O_2^{-\cdot} + H_2O_2 \xrightarrow{Fe^{3+}} O_2 + {}^{\cdot}OH + {}^{-}OH \text{ (Haber-Weiss Reaction)}$$

The hydroxyl radical, •OH, has a high reactivity, making it a very dangerous radical with an exceedingly short *in vivo* half-life of approx. 10^{-9} s[34] , that is near

diffusion rate. Thus when produced *in vivo* •OH reacts close to its site of formation and can interact with nucleic acids, lipids, and proteins.

Oxygen consumption in peroxisomes leads to H_2O_2 production, which is then used to oxidize a variety of molecules. These organelles also contains catalase, which decomposes hydrogen peroxide and presumably prevents accumulation of this toxic compound. When peroxisomes are damaged and their H_2O_2 consuming enzymes downregulated, H_2O_2 is released into the cytosol which significantly contributes to oxidative stress.

Additional reactive radicals derived from oxygen that can be formed in living systems are peroxyl radicals ($ROO^{\bullet}$). The simplest peroxyl radical is $HOO^{\bullet}$, which is the protonated form of superoxide ($O_2^{\bullet-}$) and is usually termed hydroperoxyl radical. It has been demonstrated that hydroperoxyl radical initiates the process of lipid peroxidation *in vivo*, a process that generates a variety of products including reactive electrophiles such as epoxides and aldehydes. The overall process of lipid peroxidation consists of three stages: initiation, propagation and termination and is presented in Fig. 2. The methylene groups of polyunsaturated fatty acids are highly susceptible to oxidation and their hydrogen atoms, after the interaction with radical R•, are removed to form carbon-centred radicals 1• (reaction (1)). Carbon-centred radicals react with molecular dioxygen to form peroxyl radicals (reactions (2) and (3)). If the peroxyl radical is located at one of the ends of the double bond (3•) it is reduced to a hydroperoxide which is relatively stable in the absence of metals (reaction (4)). A peroxyl radical located in the internal position of the fatty acid (2•) can react by cyclisation to produce a cyclic peroxide adjacent to a carbon-centred radical (reaction (5)). This can then either be reduced to form a hydroperoxide (reaction (6)) or through reaction (7) it can undergo a second cyclisation to form a

bicyclic peroxide which after coupling to dioxygen and reduction yields a molecule structurally analogous to the endoperoxide. This product is an intermediate for the production of malondialdehyde (reaction (8)). Malondialdehyde can react with DNA bases G, A, and C to form adducts M_1G, M_1A and M_1C (reactions (9)–(11)).[37] Peroxyl radicals located in the internal position of the fatty acid (2•) can, besides cyclisation reactions, also abstract hydrogen from the neighbouring fatty acid molecule, creating thus lipid hydroperoxides (reaction (12)). They can further react with redox metals (e.g. iron) to produce reactive alkoxyl radicals (RO•) (reaction (13)) which, after cleavage (reaction (14)) may form, gaseous pentane, a good marker of lipid peroxidation. Malondiadlehyde (MDA), the main by-product of lipid degradation, is a tautomer that is both highly electrophilic and nucleophilic. This characteristic allows not only reaction with cellular nucleophiles, but also the formation of MDA oligomers.[38] MDA and MDA-MDA dimers are mutagenic in bacterial assays as well as in the mouse lymphoma assay.[39] MDA was also shown to induce thyroid tumors in chronically treated rats. The identification of MDA-DNA adducts in humans may be significant as MDA-DNA adducts have been detected in the genome of healthy humans in quantities comparable to those levels generated by exogenous chemicals in rodent carcinogenesis studies. The observed MDA-DNA adducts appear to be promutagenic as they induce mutations in oncogenes and tumor suppressor genes seen in human tumors. MDA-DNA adduct levels also appear to correlate with altered cell cycle control and gene expression in cultured cells.[40]

The major aldehyde product of lipid peroxidation other than malondialdehyde is 4-hydroxy-2-nonenal (HNE). Hydroxynonenal is weakly mutagenic but appears to be the major toxic product of lipid peroxidation.

At high concentrations, ROS can be important mediators of damage to cell structures, nucleic acids, lipids and proteins.[27] The hydroxyl radical is known to react with all components of the DNA molecule, damaging both the purine and pyrimidine bases and also the deoxyribose backbone.[30] The most extensively studied DNA lesion is the formation of 8-OH-G. Permanent modification of genetic material resulting from these "oxidative damage" incidents represents the first step involved in mutagenesis, carcinogenesis, and ageing. Mechanisms involved in the oxidation of proteins by ROS were elucidated by studies in which amino acids, simple peptides and proteins were exposed to ionising radiations under conditions where hydroxyl radicals or a mixture of hydroxyl/superoxide radicals are formed.[41] The side chains of all amino acid residues of proteins, in particular cysteine and methionine residues of proteins, are susceptible to oxidation by the action of ROS/RNS.[41] Oxidation of cysteine residues may lead to the reversible formation of mixed disulphides between protein thiol groups (–SH) and low molecular weight thiols, in particular GSH (*S*-glutathiolation). The concentration of carbonyl groups, generated by many different mechanisms is a good measure of ROS-mediated protein oxidation. A number of highly sensitive methods have been developed for the assay of protein carbonyl groups.[42, 43] Advanced glycation end products (AGEs) is a class of complex products. They are the results of a reaction between carbohydrates and free amino group of proteins. The intermediate products are known, variously, as Amadori, Schiff Base and Maillard products, named after the researchers who first described them.[43] Most of the AGEs are very unstable, reactive compounds and the end products are difficult to be completely analysed.

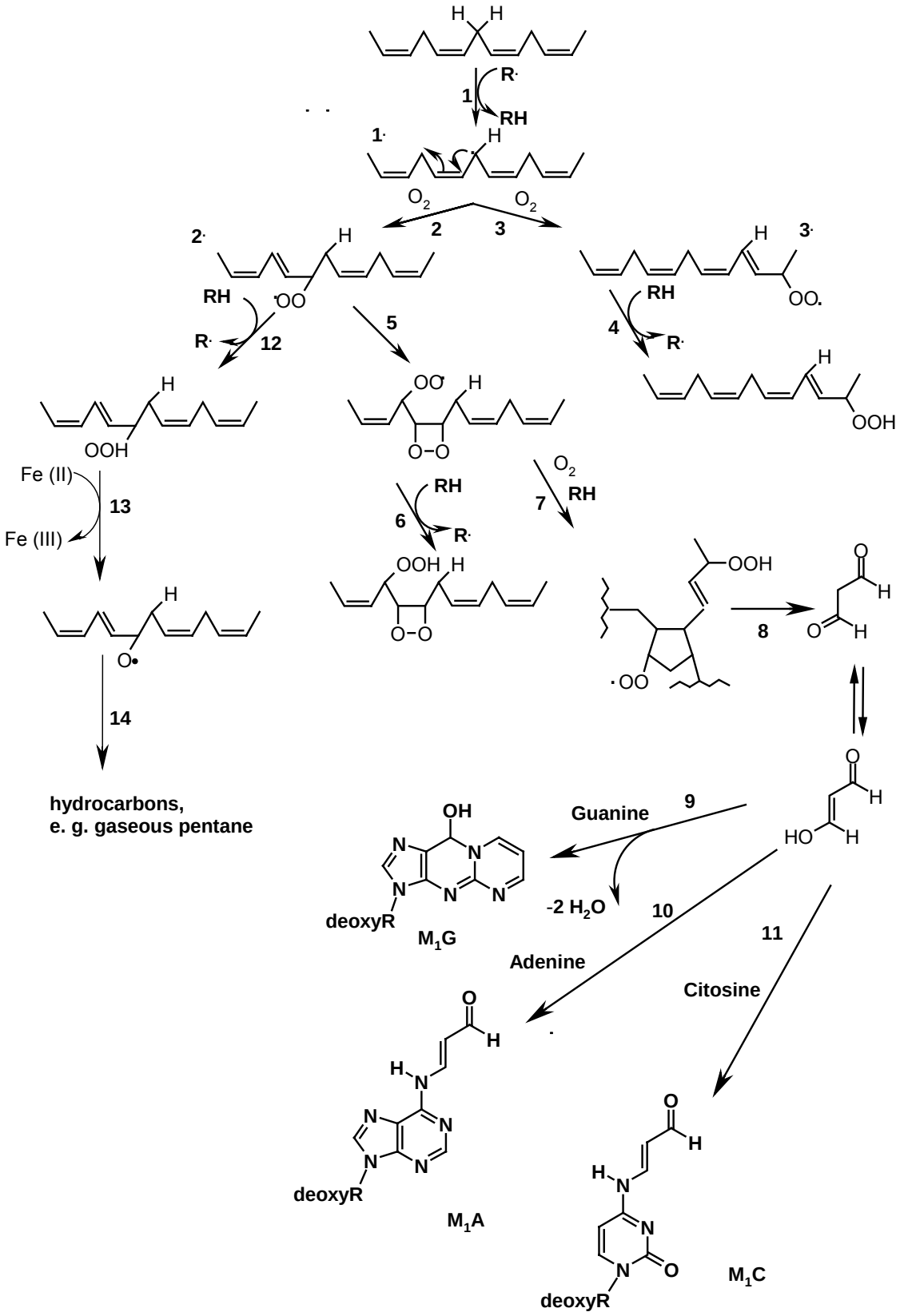

Figure 2. Lipid peroxidation.

The best chemically characterisedAGEs compounds found in human are pentosidine and carboxyl methyl lysine (CML).

Dietary polyphenols have been reported to possess potent antioxidant activity by endogenous and exogenous mechanisms.[44] It was reported that they were able to scavenge free radicals (superoxide anion, hydroxyl and peroxyl radicals), to increase several antioxidant enzyme activities such as glutathione peroxidase (GPx), superoxide dismutase (SOD), catalase (CAT) or glutathione reductase (GR) *in vivo* and *in vitro*, and activate endogenous defense systems *in vitro*. Dietary polyphenols may offer an indirect protection by activating endogenous defense systems and by modulating cellular signaling processes such as NF-κB activation, AP-1 DNA binding, glutathione biosynthesis, PI3-kinase/Akt pathway, MAPK proteins (ERK, JNK and P38) activation, and the translocation into the nucleus of Nrf2, a transcription factor that regulates the basal and inducible expression of numerous detoxifying and antioxidant genes. The Nrf2–Kelch-like ECH-associated protein 1 (Keap1)-ARE system is now recognized as one of the major cellular defence mechanisms against oxidative and xenobiotic stresses.[45]

Studies have shown that some of dietary polyphenols exerted anti-atherosclerosis activity and cardioprotection (Figure 3). For example, hydroxytyrosol could not only lower serum total cholesterol (TC) and low density lipoprotein cholesterol (LDL-C), but also slow the lipid peroxidation process in rats fed a cholesterol rich diet.[46]

Recently, there has been considerable interest in the neuroprotective effects of dietary polyphenols, especially in the context of their modes of action as antioxidants.[47,48] They had been considered as therapeutic agents for altering brain

aging processes, and as possible neuroprotective agents in progressive neurodegenerative disorders such as Parkinson's and Alzheimer's diseases.

Oxidative stress induced inflammation is mediated by the activation of NF-kB and AP-1. It affects a wide variety of cellular signaling processes leading to generation of inflammatory mediators and to expression of pro-inflammatory genes such as interleukin-1beta (IL-1β), IL-8, tumor necrotic factor alpha (TNF-a), and inducible nitric oxide synthase (iNOS). The undesired effects of oxidative stress have been found to be controlled by the antioxidant and/or anti-inflammatory effects of dietary polyphenols, such as curcumin and resveratrol, *in vivo* and *in vitro.*[49-51]

On the other hand, to counteract the effects of oxidative stress, the cells also concomitantly express protective antioxidants such as glutamate cysteine ligase (GCL), manganese superoxide dismutase (MnSOD), and heme oxygenase-1(HO-1).

Dietary polyphenols could modulate diverse biochemical processes involved in carcinogenesis by inhibition of cellular proliferation and angiogenesis, blockade of tumor cell cycle progression, and induction of programmed cell death *in vivo* and *in vitro*.[52, 53] Cellular signaling cascades mediated by NF-κB or AP-1 acted as a centerplay in regulating many of aforementioned biochemical processes.[53, 54]

Consumption of berries and red fruits rich in polyphenols contributed to the reduction of cancer through many mechanisms such as in vitro inhibiting human cytochrome P450-dependent monooxygenases 1A1 (CYP1A1) activities,[55] blocking the epidermal growth factor receptor (EGFR) tyrosine kinase activity,[56] and decreasing protein kinase CKII activity.[57]

Dietary polyphenols may also modulate cellular signaling processes by affecting signal transduction pathways. Several studies have indicated that some polyphenolic compounds were able to induce nitric oxide (NO)-mediated

endothelium-dependent relaxations in isolated arteries. The activation of endothelial NO synthase (eNOS) was due to two distinct mechanisms: (a) an increase in [Ca^{2+}] and (b) a phosphorylation of eNOS by the PI3-kinase/Akt pathway.[58] Polyphenolic compounds could prevent matrix metalloproteinases-2 (MMP-2) activation and vascular endothelial growth factor (VEGF) expression in vascular smooth muscle cells (VSMCs).[59, 60] All these mechanisms might contribute to explain the vasodilatory, vasoprotective and anti-hypertensive effects of polyphenols *in vivo*.

Another main facet of the chemistry of dietary polyphenols is their ability to act as scavengers of nitrosating species, commonly linked to mutagenic and carcinogenic events.

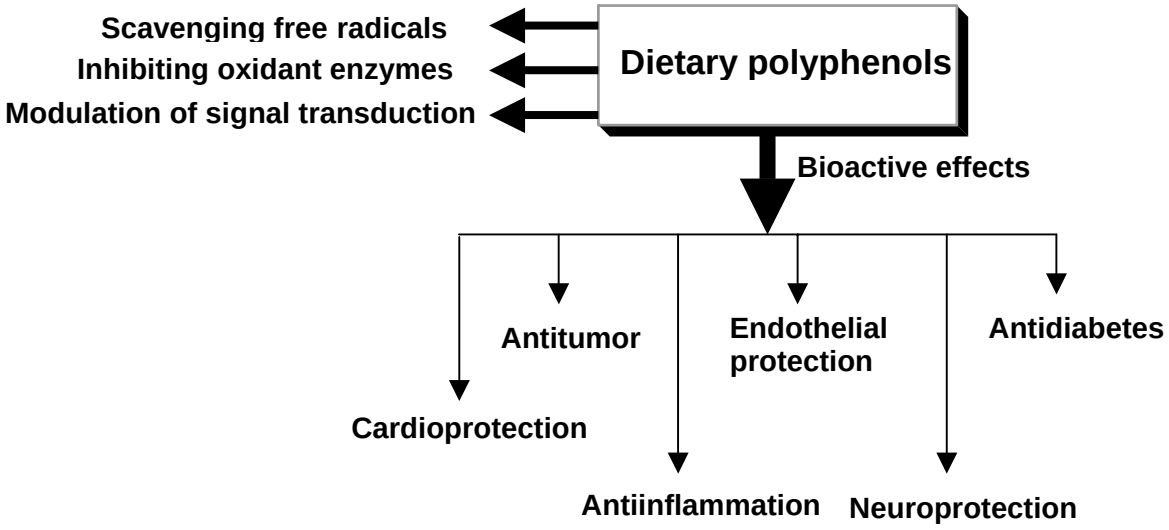

Figure 3. Bioactivities of dietary polyphenols.

Chemically, the term "nitrosation" refers to a reaction in which a nitroso (NO) group is installed onto a functional group, as in *C*-nitroso, *S*-nitroso and *N*-nitroso compounds. In the biomedical circles, however, the term "nitrosylation" (e.g. *S*-nitrosylation) is more frequently used, to indicate those biological modifications

involving coupling with nitric oxide (NO) as a radical.[61] "Nitration", on the other hand, denotes incorporation of a nitro (NO_2) group. Whereas a nitrosation reaction is well defined, the term "nitrosating species" is somewhat ambiguous in a biological context. In fact, under several circumstances, authentic nitrosating species may be accompanied by other species, as in the case of acidic nitrite, and/or may give rise to different processes, including nitration and/or oxidation, depending on the structure and reactivity of the substrate(s)/target(s). Since the focus of the present research is on toxic, cancer-related nitrosation processes, involving primary and secondary amines as main targets, the term "nitrosating species" will be used solely to denote those species, typically N_2O_3 or acidic nitrite, that can nitrosate amine derivatives.

One of the major exogenous sources of nitrosating species is represented by nitrite ions, which are found at mM levels in cured or pickled meats, vegetables, fertilizers and polluted drinking waters.62 In addition, high levels of nitrite are present in human saliva, in the range of 50-200 □M,63, 64 and levels as high as 400 μM may be present in the gastric juice derived from humans consuming 100 g of spinach.65-66 In the acidic environment of the stomach (pH 2.5-3.0 during digestion), nitrite ions are converted to nitrous acid (pKa = 3.25)67 which decomposes to give a range of nitrogen species according to the following equations**:**

$$NO_2^- + H^+ \rightleftharpoons HNO_2$$

$$HNO_2 + H^+ \rightleftharpoons NO^+ + H_2O$$

$$NO^+ + NO_2^- \rightleftharpoons N_2O_3$$

$$N_2O_3 \rightleftharpoons NO + NO_2$$

Of these, NO^+ and N_2O_3 may act as typical nitrosating species, while NO_2 may induce nitrations. Moreover, NO_2 and nitrous acid itself may act as oxidants (E_0 = 0.996 V)[67]. Other sources of toxic nitrosating species include combustion, industrial

processes, environmental tobacco smoke and exhaust fumes from cars, which produce relatively high levels of nitrogen oxides.[68]

In living organisms an endogenous source of nitrosating species is nitrogen monoxide (commonly referred to as nitric oxide, NO), a most pervasive physiologic mediator. NO is synthesized in vivo by the action of nitric oxide synthase (NOS), which oxidizes L-arginine to yield NO and L-citrulline. Although NO subserves a variety of positive roles in human physiology, including control of vascular tone and neurotransmission,[69] its aberrant generation under oxidative stress conditions is associated with a series of adverse events, such as inflammation, atherosclerosis, apoptosis, neuronal degeneration and cancer.[70-72] These events are thought to be mediated by a range of NO-derived nitrogenous species including NO_2, N_2O_3, and peroxynitrite ($ONOO^-$), a highly reactive nitrating agent produced by coupling of NO with superoxide.[73, 74]

Nitrite and NO-derived nitrosating species and other reactive nitrogen species can induce the nitrosylation, nitrosation, nitration, and/or oxidation of metals,[75] proteins, 61, [74, 76-83] fatty acids[84-88] and DNA[89-92]. Interestingly, besides acting as a nitrating agent, peroxynitrite can react with secondary amines to give *N*-nitrosamines,[93] thus underscoring the role of peroxynitrite as a potential nitrosating agent. The nitrosative deamination of primary amine-containing purine and pyrimidine nucleobases is undoubtedly one of the major events implicated in mutagenesis and carcinogenesis[91,94,95] (Figure 4). Exposure of cytosine, adenine or guanine to nitrosating species results in the formation of uracil, hypoxanthine, and xanthine in that order. Conversion of cytosine can lead ultimately to a base pair substitution mutation, while deamination of adenine and guanine results in

transversion mutations. Moreover, the instability of hypoxanthine and xanthine in the DNA structure leads to rapid depurination and consequent single strand breaks.

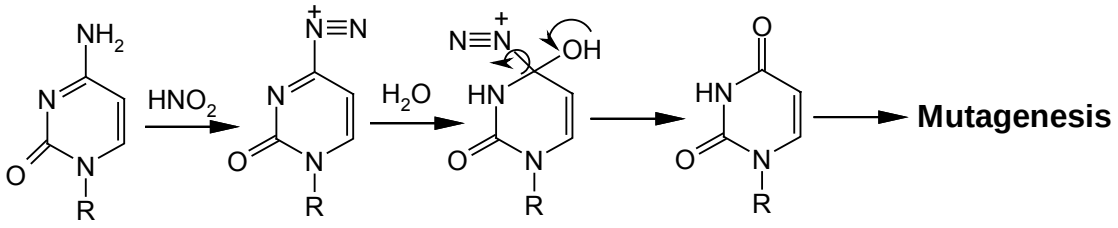

Figure 4. Nitrosative deamination of primary amine of nucleobases of DNA.

Another major mechanism of toxicity induced by reactive nitrogen species involves nitrosation of secondary aliphatic and aromatic amines leading to carcinogenic *N*-nitrosamines. Tertiary amines may also undergo nitrosation, even if the reaction rate is usually lower and occurs in mildly acidic conditions.[74,75] *N*-Nitroso compounds (NOC) have been found to produce tumors in 39 animal species.[61, 96] *N*-nitrosamines carcinogenesis depends primarily on a cytochrome P450-mediated metabolic activation step, which results in the generation of labile intermediates with DNA alkylating capabilities[97-99] (Figure 5). A substantial body of evidence links certain specific cancers, such as those of the stomach, esophagus, nasopharynx, urinary bladder in bilharzia, and colon, to nitroso compounds.[94] The main site of the endogenous synthesis of NOC is undoubtedly the stomach, where the presence of HCl favours nitrosation reactions. One of the major factors regulating the formation of NOC in the gastric environment is the concentration of nitrosating agents (N_2O_3, and NO^+). Two distinct mechanisms of endogenous formation of NOC have been identified. The first, a direct chemical reaction between secondary amino compounds

and nitrite, is strongly pH dependent, and does not proceed rapidly at neutral pH, even in the presence of chemical catalysts. The second mechanism depends on the direct bacterial catalysis of *N*-nitrosation and proceeds much more rapidly at neutral pH than the chemical reaction. The most rapid catalysis is associated with those bacteria capable of reducing nitrate and nitrite by the process of denitrification.[89] Large quantities of nitric oxide or NO^+-like species, however, were also found to be produced by non-denitrifying bacteria (Escherichia coli, and Proteus morgani).[90] The capacity to catalyse *N*-nitrosation is shared by microorganisms commonly present in human saliva and by bacteria isolated from the human gastrointestinal tract (Helicobacter pylori, E. coli, and Campylobacter jejuni) that possess nitrate reductase and/or nitrosating enzymes such as cytochrome-nitrite reductase.[91,92] In contrast with other groups of carcinogens, the activity of which is often restricted to a small number of species, nitrosamines are effective in many different species. For example, *N*-nitrosodimethylamine has been found to induce tumors in all of the many species in which has been tested, and *N*-nitrosodiethylamine in 25 species.[100] Humans can be exposed to preformed *N*-nitrosamines, e.g. through the diet, in certain occupational settings, and through the use of tobacco products, cosmetics, pharmaceutical products, and agricultural chemicals.[101] According to Preussmann,[102] the hypothesis of the irreversibility of the carcinogenic effects of NOC, and consequently of the impossibility of defining ‘‘thresholds’’or ‘‘no-effect levels’’ is valid; therefore even low doses could represent a low but definite health risk.

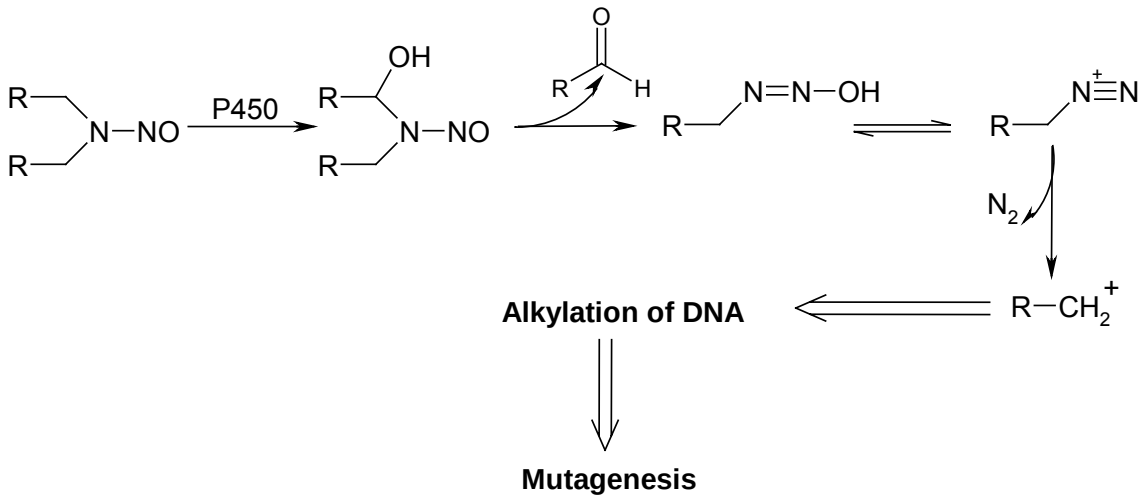

Figure 5. Generation of labile intermediates with DNA alkylating capabilities from *N*-nitrosamines trought cytochrome P450-mediated metabolic activation.

Among the potential chemopreventive agents acting against toxic nitrosation reactions and nitrosamine carcinogenesis, polyphenolic plant constituents widely distributed in food occupy a prominent position.[103-107] Indeed, the perspective of lowering the incidence of several forms of cancer through appropriate dietary regimens has spurred several campaigns in industrialized countries aimed at encouraging the public to increase the daily polyphenol intake by including more fruits and vegetables in their diet, and has incited research programs directed to evaluating extracts from edible plants or used in folk medicine as potential sources of antinitrosating agents. It should be emphasized, however, that epidemiologic studies do not produce hard experimental data that prove specific cancer-causative factors. Rather, they provide associative hypotheses or "risk factors" for further study.

1.3 Biological properties and occurence of dietary polyphenols.

1.3.1 Polyphenolics of olive oil. Hydroxytyrosol.

Hydroxytyrosol (2-(3,4-dihydroxyphenyl)ethanol, **1**) and related polyphenolic constituents of extra virgin olive oil are endowed with several biological properties that may contribute to the reduced risk of cardiovascular diseases and malignant neoplasms in the populations of Mediterranean countries.[108-110]

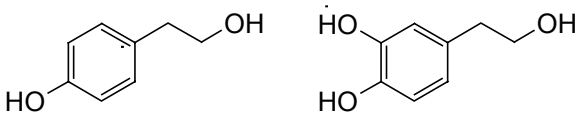

Tyrosol Hydroxytyrosol (**1**)

The beneficial role of olive phenols in cancer prevention is ascribed to their potent antioxidant properties enabling them to counteract the geno- and cytotoxic effects of reactive oxygen species generated in settings of oxidative stress.[111, 112] Extra virgin olive oil (EVOO) constituents can contribute to lower the incidence of coronary hearth diseases as well as of prostate and colon cancer.[108] **1** and related (poly)phenolic components can also inhibit the formation of carcinogenic and mutagenic heterocyclic amines.[113] The scavenging potential of **1** towards oxygen and nitrogen reactive species, including hydroxyl radical, peroxynitrite, superoxide radical, hydrogen peroxide and hypochlorous acid, has recently been determined.[114] The marked antioxidant properties of **1** are also exemplified by its ability to inhibit the copper sulphate induced oxidation of low density lipoproteins as shown by the reduced short chain aldehydes formation, sparing of vitamin E and decrease of the levels of malondialdehyde-lysine and 4-hydroxynonenal-lysine adducts indicating protection of the apoprotein layer.[115] Another mechanism by which **1** may exert its effects is metal chelation, particularly Cu^{2+} and Fe^{2+} ions which are able to promote peroxyl/hydroxyl

formation by decomposition of hydroperoxides by the Fenton and Haber-Weiss reactions. The ability of **1** to chelate ferric ions accounts for the marked inhibition of hydroperoxide formation promoted by enzymatic and non enzymatic process including lactoferrin and iron in liposomes and oil-in-water emulsions [116] or hemoglobin, enzymatic NADH-iron and non enzymatic ascorbate-iron[117]. Free iron sequestering by **1** may therefore represent an important route by which this compound exerts the documented beneficial effects towards those pathological conditions and chronic diseases associated with oxidative stress.[118]

The concentration of phenols in EVOO varies from 50 to 800 mg/Kg, with a mean value for commercial oil of 180 mg/kg;[100,112] a daily consumption of 50 g olive oil (a mean value in the Mediterranean countries) would therefore result in an intake of about 9 mg of olive oil phenols per day, of which it is estimated that 1 mg is derived from **1** and tyrosol and about 8 mg from the aglycones of oleuropein (2) and ligstroside (3) (decarboxymethyl dialdehydic forms). EVOO is also rich in the antioxidant compound α-tocopherol, whose concentration varies between a few ppm to 350 ppm.

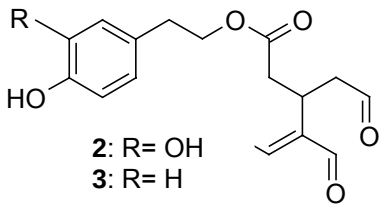

1 was reported to be absorbed by 66%: this would lead to a maximum concentration of 0.06 μM of this compound in plasma after a 50 g intake of olive oil.[100] A conjugate of **1** with glutathione was described as one of the biotrasformation product of dietary **1** formed in the gastrointestinal tract; yet this product, which was also obtained by mushroom tyrosinase oxidation of HTYR in the presence of

glutathione, was not fully characterized from a structural view point.[119] A glutathione-hydroxytyrosol adduct was also described as phase I metabolite found in the urine of women assuming dietary supplements containing Cimicifuga racemosa (Actaea racemosa; black cohosh). [120]

1.3.2 Red wine stilbenes.

Resveratrol (5-[2-(4-hydroxyphenyl)vinyl]benzene-1,3-diol, **4a**) is the most well-known and well-characterized stilbene. Primarily found in peanuts, red wine, and grapes,[120, 121] resveratrol is a polyphenolic phytoalexin produced by various plants in response to microbial attack, excessive ultraviolet exposure and disease.[122] Currently, has been shown how **4a** can act as a potent anti-inflammatory, anti-cancer and chemoprotective agent.

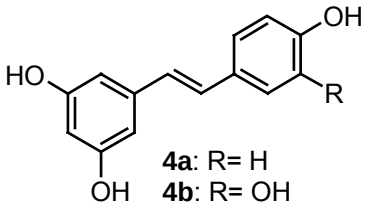

4a: R= H
4b: R= OH

Stilbenes exist as stereoisomers in *E* and *Z* forms, but naturally occurring stilbenes exist in the *E* (*trans*) form. Research has revealed the *E* form to exhibit more potent activity compared to the *Z* form across various anti-cancer and anti-oxidant assays. One such study demonstrated *trans*-resveratrol to be ten times more potent in its ability to induce apoptosis in the HL60 leukemia cell line compared to *cis*-resveratrol.[123]

4a showed that in vitro it could decrease the expression of vascular cell adhesion molecule-1 (VCAM-1), cyclooxygenase-2 (COX-2), and matrix metalloproteinase-9 (MMP-9) mRNA through suppression of activation of nuclear

factor AP-1. **4a** has been shown to be an efficient scavenger of cytotoxic oxygen and nitrogen species.[124-128] Studies of structure-activity relationships indicate that the antioxidant activity of **4a** stems from the peculiar oxygenation pattern on the planar stilbenic skeleton, featuring as a crucial determinant of the radical scavenger activity the 4'-OH group, synergistically supported by the 3- and 5-OH groups on the resorcin moiety. The efficiency of the 4'-OH group as a hydrogen donor is enhanced by the *trans* double bond, which increases both its acidity[129] and the resonance stabilization energy of the phenoxyl radical derived from H-atom abstraction, as confirmed by semiempirical (PM3)[130] and DFT[131-133] analysis.

Based on encouraging therapeutic evidence, resveratrol research has fueled a great deal of interest in characterizing structurally similar stilbene compounds and in synthesizing modified stilbenes substituted with various functional groups. Among these one of the best known is piceatannol (4-[2-(3,5-dihydroxyphenyl)vinyl]benzene-1,2-diol, **4b**).

First isolated and characterized from *Euphorbia lagascae* in 1984, **4b** is synthesized in response to fungal attack, ultraviolet exposure, and microbial infection. Induction of piceatannol synthesis is also evident during the ripening of grapes and increases during the fermentation process of wine production due to β-glucosidase activity of bacteria. Constitutive piceatannol has also been identified in the heartwood of *Cassia garrettiana*, a common plant family in Asian countries.[134] It has been reported to be found also on sugar cane, rhubarb, and some varieties of berries.[135]

One study employing human liver microsomes found that *trans*-resveratrol metabolism produces two main metabolites, with one being piceatannol. This biotransformation was dependent on the cytochrome P450 1A2 enzyme as evidenced through the investigator's use of enzyme specific inhibitors and protein antibodies.

The rate of resveratrol hydroxylation forming piceatannol was rapid, reporting a Km of 21μM with a Vmax of 86 $pmol^{-1}mg^{-1}$microsomal protein. These data have led investigators to postulate that resveratrol may act as a pro-drug for production of piceatannol and other stilbenes.

Piceatannol is an antagonist of the aryl-hydrocarbon (Ah) receptor, implicated in dioxin toxicity. Agonists of this receptor include halogenated aromatic compounds such as 2,3,7,8-tetrachlorodibenzo-*n*-dioxin (TCDD) and polycyclic aromatic carbohydrates such as benzo(a)pyrene. Depending on the extent of exposure, AhR agonists have the potential to involve extensive tissue damage and can induce tumor growth and progression in a number of organs through the activation of cytochrome P450 1A1 enzyme. Piceatannol and resveratrol compete inhibiting AhR binding sites, effectively displacing TCDD. In addition piceatannol also acts as a potent tyrosine kinase inhibitor. Due to its estrogen structural similarity piceatannol acts as a selective estrogen receptor modulator (SERM) in human breast cancer cell lines. A recent study found piceatannol to be a potent and selective inhibitor of the COX-2 pathway, even better than celecoxib, a selective COX-2 inhibitor currently utilized and available with a prescription. Further investigations have demonstrated that piceatannol was able to bind directly to the COX-1 and COX-2 enzyme isoforms, inhibiting their activity. The authors concluded that piceatannol is a potential therapeutic compound that inhibits COX-2 activity, which may have utility in various disease states associated with COX-2 activation.[136] One study determined piceatannol to be significantly more potent ininhibiting Cu^{2+} induced lipid peroxidation in low-density proteins compared to resveratrol. Further investigations revealed piceatannol to be a potent superoxide scavenger, suggesting a possible role in cardioprotection following ischemia. Recent research has shown piceatannol to be a more effective scavenger of nitric oxide and

hydrogen peroxide compared to resveratrol. Many investigators have hypothesized that the additional hydroxyl group of piceatannol makes it more reactive and is therefore a more potent free radical scavenger compared to resveratrol. Other investigators have reported that piceatannol induces apoptosis in a human prostate cancer cell line (NRP-154). It has been recently reported that piceatannol attenuates the proliferation rate in the human colon adenocarcinoma cell (Caco-2) model. The investigators concluded that piceatannol is an effective anti-cancer agent that inhibits proliferation and growth in colon cancer cell models *via* arresting the cell cycle at the S phase. Recent investigations of resveratrol and piceatannol have been conducted in BJAB Burkitt-like lymphoma cells and in an *ex vivo* model with leukemic lymphoblasts of 21 patients diagnosed with childhood lymphoblastic leukemia. Results suggest that both piceatannol and resveratrol are potent inducers of apoptosis in BJAB cells at an IC50 of 25 μM (6.1 μg/mL). Surprisingly, piceatannol, and not resveratrol was determined to effectively induce apoptosis in the *ex vivo* model. In the laboratory it has been determined that piceatannol is most active in HL60 leukemia and HCT-116 colon cancer cells with an IC50 of ~2-3μg/ml.[137] Resveratrol and piceatannol have been detected in red wine and have long been associated with cardioprotection. The "French paradox" was described in 1992 as an anomaly in which southern French citizens, who smoke regularly and enjoy a high-fat diet, boast a very low mortality rate of coronary heart disease. Scientists have attributed this unlikely relationship to moderate consumption of the anti-inflammatory and anti-oxidant polyphenolic compounds, such as piceatannol and resveratrol, in red wine.[138, 139] Piceatannol and resveratrol have been shown to elicit a number of cardioprotective activities including inhibition of low-density lipoprotein (LDL) oxidation, mediation

of cardiac cell function, suppression of platelet aggregation, and attenuation of myocardial tissue damage during ischemic events.

It has been estimated that the concentration of resveratrol in wine ranges from as little as 0.2 mg/L up to 10.6 mg/L, depending largely on grape type and environment while that of piceatannol is about 0.45 mg/L. Several studies have revealed that resveratrol is metabolized extensively *via* glucuronidation. Sulfation of resveratrol, yielding a sulfated metabolite, is also apparent, although it appears that glucuronidation is the predominant metabolic pathway.

1.3.3 Menthofuran.

(*R*)-Menthofuran (**5**), a minor terpenoid of peppermint (*Mentha piperita* L.), is better known as a mammalian metabolite and the proximate toxin of pulegone (**6**), the major constituent of pennyroyal oil.[140] This popular fragrance is also a potent hepatotoxin, and is obtained from *Mentha pulegium* L., a plant used in folk medicine as an abortifacient.[2] The metabolic conversion of **6** to **5** underlies the poisonous properties of pennyroyal oil.[1] Thus, oxidation of the allylic methyl of **6** triggers a cyclodehydration to **5**, eventually converted into a reactive epoxide that acts as an ultimate carcinogen because of its marked electrophilic properties.[140, 142]

Due to its unfavorable safety profile and bitter taste, **5** is an undesirable constituent of peppermint oil. On the other hand, **5** is also the precursor of menthofurolactone (**7**) and dehydromenthofurolactone (anhydro Woodward-Eastman lactone, **8**), two compounds whose sweet and persistent coumarinic odor is the hallmark

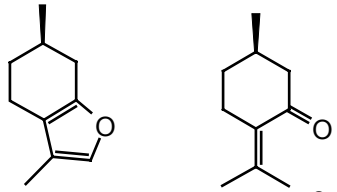

5

6

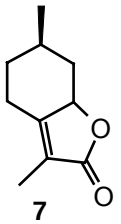

7

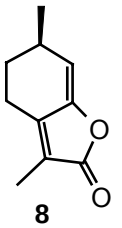

8

of premium-quality peppermint oils.[143] Accordingly, considerable efforts have been devoted to elucidate the genetic and epigenetic factors that affect the formation of **5** in mint plants,[144] and to develop chemical methods to remove it from peppermint oil while maintaining the sensory note of its oxidation products. These methods rely on the photosensitized oxygenation of the oil and its treatment with acids, and have been recently complemented by the reaction with dimethyldioxirane.[145] An additional issue of interest is the reaction of **5** with nitric acid in the presence of catalytic sulfuric acid,[146] which forms the basis of a popular color test for peppermint oil.

Despite the practical relevance of this reaction, little is known about the underlying chemistry, an unsurprising finding on account of the lack of information that currently exists on the chemistry of trisubstituted furans. These considerations prompted us to extend to menthofuran our studies on the behavior of bioactive natural products with nitrogenous mineral acids.[147]

1.3.3 Hydroxycinnamate compounds.

The total polyphenol intake has been reported to reach 1 g/d in people who eat several servings of fruit and vegetables per day. Hydroxycinnamate compounds, including *p*-coumaric acid (**9**), ferulic acid (**10**), caffeic acid (**11**) and its ester chlorogenic acid (5-caffeoyl-D-quinic acid) (**12**), are widely diffused at relatively

elevated levels in various agricultural products and contribute significantly to the total polyphenol intake: for example, **12** is present in quantities of 3.4-14 mg/100 g fresh weight in potatoes, 60 mg/kg in broccoli, 12-31 mg in 100 mL of apple juice, 89 mg/100 g in dry tea shoots, and 70-350 mg in a cup of coffee.[107, 148, 149] **11** is present in fruit such as pears (19 mg/g) and apples (1.3 mg/g), while **10** is the most abundant phenolic acid found in wheat grain (0.8-2 g/kg dry weight).

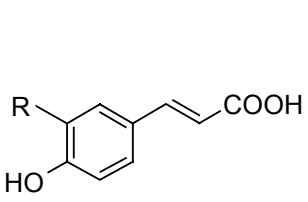

9: R= H
10: R=OCH_3
11: R=OH

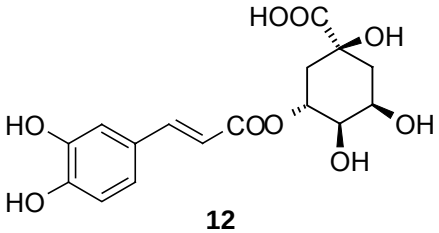

12

Hydroxycinnamic acids have been suggested to play a role in the apparent association between the regular consumption of polyphenol-rich foods and beverages and the prevention of inflammatory and proliferative diseases. In particular, **12** has been reported to exert inhibitory effects on carcinogenesis in the large intestine, liver, and tongue, and protective actions on oxidative stress *in vivo*. Hydroxycinnamic acids are rapidly absorbed from the small intestine and then glucuronidated. However, human tissues (intestinal mucosa and liver) and biological fluids (plasma, gastric juice) do not possess esterases capable of hydrolyzing **12** to **11**. Only the colon microflora is able to carry out this transformation, so the efficiency of absorption of hydrocycinnamates is markedly reduced when they are present in the esterified form. In fact an absorption of 33% and 95% was reported for **12** and **11**, respectively. Moreover, coffee administration resulted in increased total plasma concentration of **11**, with an absorption peak at 1 h (0.32-0.98 μM after β-glucuronidase treatment).

The inhibitory effects of naturally occurring *p*-hydroxycinnamic acid derivatives, such as **11** and its esters, namely **12** and caffeic acid phenethyl ester (CAPE), **9** and **10**, on nitrosamine formation have been recognized more than two decades ago and were confirmed in several *in vitro* studies. **10** and **11**, for example, react with nitrite *in vitro* and inhibit nitrosamine formation *in vivo*. They also inhibit tyrosine nitration mediated by peroxynitrite.

1.4 Endogenous polyphenols.

Besides plant-derived polyphenols which are endowed with peculiar bioactivities phenolic compounds biosynthesized by humans and other mammals have also been extensively investigated. Among these cysteinyldihydroxyphenylalanines (or cysteinyldopas), e.g. the 5*S* and 2*S* isomers (**13** and **14** respectively), which are produced by epidermal melanocytes and are involved in the biosynthesis of pheomelanins, the characteristic pigments of red-haired, fair-complexioned individuals.[150]

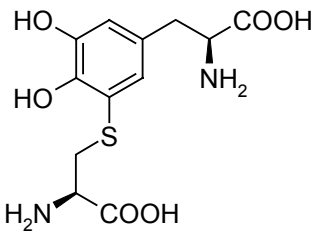

13

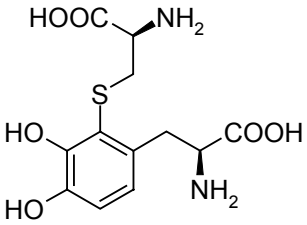

14

Current concepts of skin melanin photobiology are dominated by the notion that the black insoluble eumelanins are photoprotective whereas pheomelanins are phototoxic.[151, 152] However, in spite of extensive clinical data which have shown that red haired, fair-skinned people share increased UV-susceptibility with higher propensity for skin cancer[153] and a number of biochemical data supporting a

photosensitizing action of pheomelanins,[154] there is so far no clear-cut evidence demonstrating a direct causal link between the photochemical properties of pheomelanins and skin cancer. In fact, mounting genetic evidence points to MC1R mutations as the primary underlying factor in UV susceptibility,[155] whereby pheomelanin formation would only be the visible outcome of a metabolic switch and the consequent failure of active melanocytes to produce the "normal" eumelanin pigment pathway.

In this setting, a detailed understanding of the structural properties and mechanism of assembly of the pheomelanin pigment appears essential if the above and other pending issues concerning pheomelanin photochemistry and photobiology are to be settled. The persisting uncertainties that dominate the field are a direct consequence of the current lack of knowledge about the basic architecture of pheomelanins and their key structural features.

With this background, a critical assessment of the spectrophotometric properties of pheomelanins and the role of putative precursors prepared under biomimetic conditions is mandatory if the above uncertainties are to be tackled through an unambiguous experimental approach.

Besides being recruited for pheomelanin synthesis, cysteinyldopas are partly excreted into body fluids and are among the best diagnostic markers of disseminated malignant melanoma.[156] Moreover, their metal chelating[157] and antioxidant properties[158] point to important, though still unclear, functional roles.

Availability of cysteinyldopa isomers on a gram-scale is therefore central for addressing a number of chemical, biological and clinical issues relating e.g. to the structure and photoprotective/photosensitizing properties of pheomelanins, to the

functional significance of circulating melanogens, and to their role in the etiopathogenesis of malignant melanoma.

Current synthetic methodologies involve oxidative conjugation of cysteine with 3,4-dihydroxyphenylalanine (dopa) or a derivative mediated by a range of oxidizing systems, including cerium ammonium nitrate (CAN) in sulfuric acid,[159] silver oxide in methanol,[160] Fe^{2+}-EDTA/H_2O_2[161] or tyrosinase[162] in neutral aqueous buffers. As a rule, the 5-*S*-isomer **13**[163] is obtained as the major product (14-70% isolated yields), reflecting the dominant regiochemical course of the oxidative conjugation of 4-alkylcatechols with thiols,[164, 165] whereas the 2-*S* isomer **14** is formed in much lower amounts (<5% in our hands, despite slightly higher claims in the literature). To-date, separation from the reaction mixtures provides the only means of obtaining small amounts of **14** for biological studies and/or analytical purposes. This however requires a lengthy and cumbersome procedure involving repeated ion-exchange column chromatography with HCl gradients.[159-162] In fact, the regiochemical issue in catechol-thiol conjugation has so far prevented a gram-scale preparation of **14**, despite the importance of this isomer in pheomelanin build-up.[166]

The aims of this studies were on one side to discover a new method for the synthesys of **14** and on the other to provide a comparative description of the UV absorption properties of the main putative pheomelanin-related compounds that are generated in the oxidation of cysteinyldopas.

2. RESULTS AND DISCUSSION

2.1 Oxidative chemistry of hydroxytyrosol: hydrogen peroxide-dependent hydroxylation and hydroxyquinone/*o*-quinone coupling pathways.

Despite extensive studies on the antioxidant and free radical scavenging properties of **1**, its mechanism of action is still far from being completely elucidated, especially for what concerns the identity of the reactive oxygen species targeted and the nature of the products formed. Knowledge of the oxidative chemistry of **1** is yet of central relevance to an understanding of the fate of this *o*-diphenolic compound during its antioxidant action *in vivo* and for delineating the chemical processes underlying quality deterioration of olive oil.

The first insight came from a previous study[167] showing that autoxidation or tyrosinase-catalysed oxidation of **1** in phosphate buffer at pH 7.4 leads to the formation of two main regioisomeric products which could be isolated and identified as the novel methanooxocinobenzodioxinone derivatives **15a,b**. These products were suggested to arise by catechol-quinone coupling routes in which the *ortho* hydroxyl groups of **1** added onto the corresponding quinone.

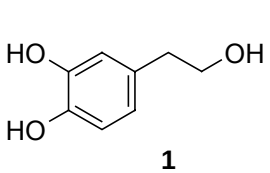

1

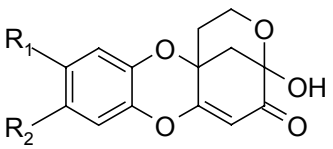

15a: R_1 = H, R_2 = $-CH_2CH_2OH$

15b: R_1 = $-CH_2CH_2OH$, R_2 = H

In another study[168] it was shown that **1** can act as an efficient scavenger of hydrogen peroxide produced by human neutrophils and may therefore provide a useful tool to analyse the role of hydrogen peroxide in pathological processes,

although no product arising from the scavenging action was identified. More recently, a mass spectrometric analysis of the species formed by 2,2'-azo-bis(2-amidinopropane) (AAPH)-induced oxidation of **1** was reported,[169] suggesting the formation of dimers with concomitant incorporation of a water molecule. It was proposed that *o*-quinones derived from **1** or tautomeric *p*-quinone methides undergo water addition before coupling with a second *o*-quinone molecule. The structures of the reaction products, however, were not supported by a complete spectral analysis.

The present study was aimed at gaining a deeper insight into the mechanism of the antioxidant action of **1** by providing a structural characterisation of the products formed upon exposure to peroxidase/H_2O_2, as a representative H_2O_2-containing oxidising system.

In a first series of experiments the reactivity of **1** with the oxidising system peroxidase/H_2O_2 was examined.

As a preliminary step a straightforward procedure for preparation of **1** was developed, which involved the use of the hypervalent iodine reagent 2-iodoxybenzoic acid (IBX),[170] an oxidant agent capable to promote the regioselective conversion of monophenols to *o*-diphenols. In a typical procedure, solid IBX (1.5 equiv.) was added to a solution of tyrosol (75 mM) in methanol at –25 °C, for the marked instability of *o*-quinone at room temperature. A yellow-to-orange colour developed and the mixture was stirred for 1h, followed by dithionite reduction and column chromatographic fractionation on silica gel of the organic extracts to give **1** in 30% yield.

A brief mechanistic description is illustrated in scheme 1. This involves as a first step reaction of tyrosol with IBX to generate the intermediate A, through elimination of water, followed by rearrangement to give B with the oxygenation of the *orto* position of the phenol. In this step iodine oxidation state changes from I(V) to

I(III). The subsequent tautomerization from B to C gives rise to the *o*-quinone and the 2-iodobenzoic acid, with the associated reduction of I(III) to I(I).

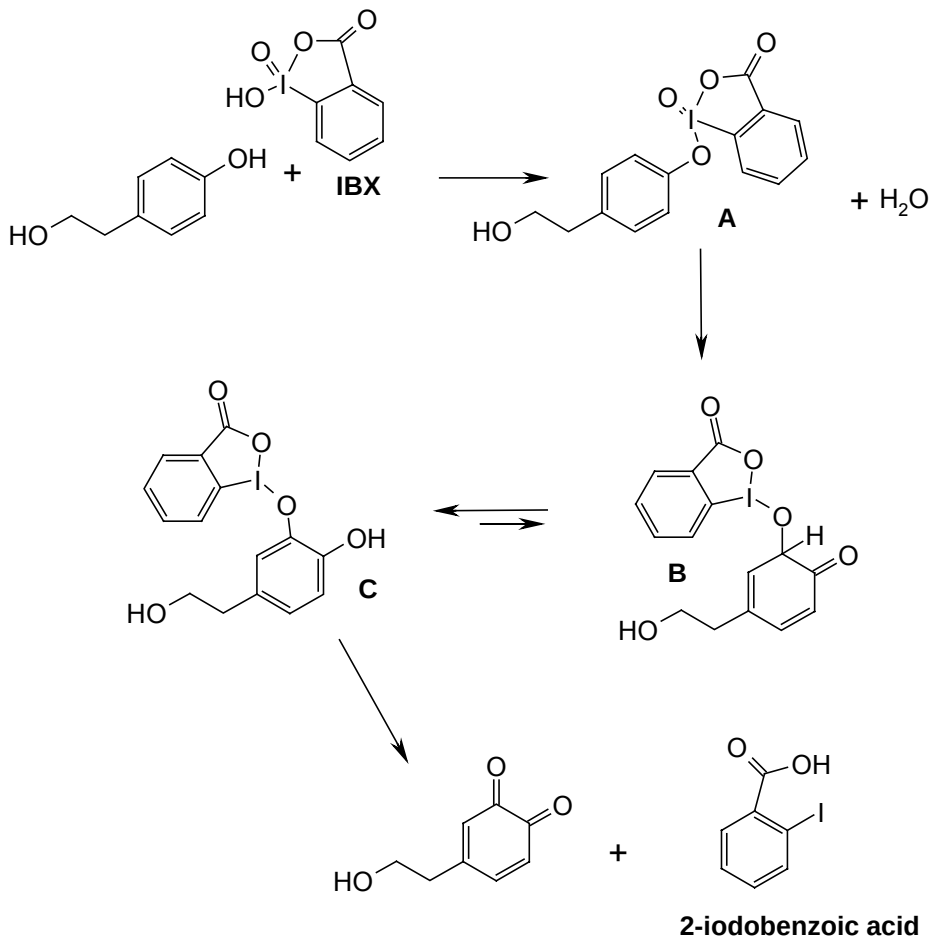

Scheme 1

Exposure of **1** (1 mM) to horseradish peroxidase (HRP, 3U/mL) and 4 mM H_2O_2 in 0.1 M phosphate buffer, pH 7.4, led to the rapid consumption of the substrate (about 90% after 1h) and the gradual development of a purple red colouration (absorption maximum at 490 nm). Attempts to isolate and characterise reaction products met with failure because of the apparent instability under conventional

chromatographic conditions. Accordingly, a procedure for product analysis was developed, which involves reduction of the reaction mixture with $NaBH_4$, acidification to pH 3, extraction with ethyl acetate and acetylation with Ac_2O/pyridine at room temperature. TLC analysis of the mixture thus obtained showed the presence of two main species eluted at R_f 0.47 (I) and 0.32 (II) (eluant cyclohexane-ethyl acetate 1:1). Small amounts of the acetylated derivatives of **15a,b** were also detected. Products I and II could be isolated in pure form from a large scale reaction and were subjected to complete spectral characterisation.

The ^{1}H NMR spectrum of product I displayed two 1H singlets at δ 7.01 and 7.09 showing direct correlation with carbon signals resonating at δ 116.1 and 123.0, respectively. In addition, two 2H triplets at δ 4.21 and 2.83 and four singlets for acetyl groups were distinguishable in the high field region, suggesting a tetraacetyl derivative. This latter conclusion was confirmed by the positive ion electrospray ionization (ESI+)/MS spectrum showing a pseudomolecular ion peak $[M+H]^+$ at *m/z* 339. On this basis, product I was formulated as the tetraacetyl derivative of 2-(2,4,5-trihydroxyphenyl)ethanol (**16**).

The ESI+/MS spectrum of product II exhibited pseudomolecular ion peaks $[M+H]^+$ and $[M+Na]^+$ at *m/z* 617 and 639, respectively, indicating a fully acetylated dimer of **1** bearing an additional acetoxyl group on one of the aromatic rings. Consistent with this conclusion was the ^{1}H NMR spectrum, showing seven singlets for the acetyl groups and four 2H triplets in the high field region, and three 1H singlets at δ 6.89, 7.17 and 7.21 in the aromatic proton region. The compound was therefore identified as the heptaacetyl derivative of 2,3,3',4',6-pentahydroxy-5,6'-bis(2-hydroxyethyl)biphenyl (**17**), arising evidently by oxidative coupling of **1** with **16**. The mode of linkage of the units was deduced from the presence of distinct NOE

contacts in the $^{1}H,^{1}H$ ROESY spectrum between the triplet at δ 2.86 and the singlet at δ 7.21 indicating that the 6-position of the 2,4,5-trihydroxyphenylethanol unit was unsubstituted.

NMR assignments for the acetylated derivatives of **16** and **17** are reported in Table 1.

Table 1. NMR spectral data of the acetylated derivatives of **16** and **17** ($CDCl_3$).

	16		**17**	
	^{1}H (*J*, Hz)	^{13}C	^{1}H (*J*, Hz)	^{13}C
1[c]	-	126.4	-	128.4
2	-	144.8	-	140.8[d]
3	7.01 (s)	116.1	-	139.5
4	-	138.0[e]	7.21 (s)	124.3
5	-	139.1[e]	-	129.4
6	7.09 (s)	123.0	-	145.1
α	2.83 (t, 7.0)	27.6	2.86 (t, 6.8)	29.6
β	4.21 (t, 7.0)	61.5	4.27 (t, 6.8)	63.1
1’			-	129.7
2’			6.89 (s)	125.7
3’			-	140.2[d]
4’			-	142.1
5’			7.17 (s)	123.8
6’			-	135.9
α’			2.71 (t, 7.2)	31.4
β’			4.20 (t, 7.2)	63.3

[a]Acetyl groups: ^{1}H NMR δ (ppm) 2.02 (s, 3H), 2.26 (s, 3H), 2.27 (s, 3H), 2.32 (s, 3H); ^{13}C NMR δ (ppm) 18.9 (2 × CH_3), 19.1 (CH_3), 19.2 (CH_3).

[b] Acetyl groups: ^{1}H NMR δ (ppm) 1.92 (s, 3H), 1.96 (s, 3H), 2.02 (s, 3H), 2.04 (s, 3H), 2.25 (s, 3H), 2.28 (s, 3H), 2.29 (s, 3H); ^{13}C NMR δ (ppm): 19.8 (CH_3), 19.9 (CH_3), 20.4 (CH_3), 20.6 (2 × CH_3), 20.9 (2 × CH_3).

[c] Numbering as shown in structural formulas **16** and **17**.

[d,e] Interchangeable.

The formation yields of the acetylated derivatives of **16** (t_R 28.5 min, eluant II) and **17** (t_R 39.9 min, eluant II) were 31% and 3%, respectively, as estimated by HPLC analysis of the reaction mixture after the acetylation treatment.

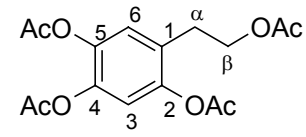

16 (tetraacetyl derivative)

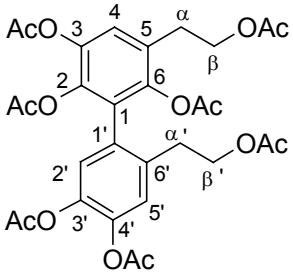

17 (heptaacetyl derivative)

When the oxidation of **1** was carried out under an argon atmosphere no appreciable change in product distribution was observed, ruling out a significant role of oxygen in the oxidation process.

To test if the additional hydroxyl group of **16** derives from H_2O_2, the oxidation of **1** was carried out with equimolar amounts of $K_3Fe(CN)_6$ in 0.1 M phosphate buffer, pH 7.4, in the presence and in the absence of variable amounts of H_2O_2. As expected, no trace of **16** and **17** was found in the absence of H_2O_2, dimers **15a,b** being the main identifiable species. However, a pattern of products matching that formed in the HRP/H_2O_2 catalysed reaction was produced in the presence of H_2O_2.

To estimate the effect of H_2O_2 the reaction of **1** with HRP/H_2O_2 was carried out with increasing amounts of H_2O_2 (in the range 4-10 molar eqs). Under these conditions the yields of **16** varied from 25% to 93%.

In another series of experiments, the mechanism of formation of **17** was investigated using 4-methylcatechol as a model compound. The oxidation reaction, carried out in 0.1 M phosphate buffer, pH 7.4, with the substrate at 1 mM concentration and HRP (3 U/mL)/H_2O_2 (4 mM), led to the formation of two main

acetylated products eluting on TLC at R_f 0.46 and 0.61 (eluant cyclohexane-ethyl acetate 6:4). These were isolated and identified as the triacetyl derivative of 1,2,4-trihydroxy-5-methylbenzene (**18**) (14% yield) and the pentaacetyl derivative of 2,3,3',4',6-pentahydroxy-5,6'-dimethylbiphenyl (**19**) (21% yield), suggesting an oxidative pathway of 4-methylcatechol akin to that of **1**.

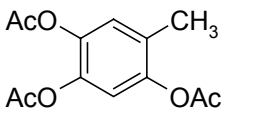

18 (triacetyl derivative)

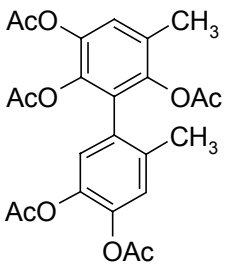

19 (pentaacetyl derivative)

Since formation of **19** was evidently the result of the oxidative coupling of 4-methylcatechol with **18**, it seemed of interest to inquire whether the two partners reacted both in their quinonoid forms or in different oxidative states. In an *ad hoc* experiment 2-hydroxy-5-methyl-1,4-benzoquinone, produced by periodate oxidation of **18**, was allowed to react with 4-methyl-1,2-benzoquinone[171] in phosphate buffer, pH 7.4, under an argon atmosphere and was found to give, after the usual work up, the acetylated dimer **19** in good yield.

A plausible mechanism to account for the formation of products **16/17** and **18/19** is depicted in Scheme 2.

In the proposed scheme, interaction of the catechol with the HRP/H_2O_2 system generates the corresponding *o*-quinone which may be trapped by H_2O_2 to give hydroxyquinone intermediates *via* a carbonyl-forming fission of the hydroperoxy initial adduct.[172]

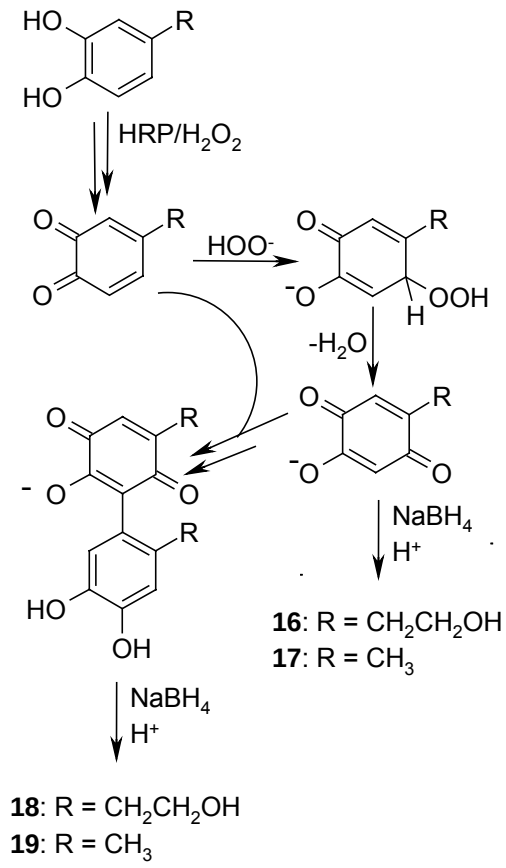

Scheme 2

Nucleophilic attack of H_2O_2 to *o*-quinones substituted at the 4-position is an efficient process which proceeds regioselectively at the 6-position[173-175] and appears to compete favourably with alternative reaction routes, including nucleophilic attack by the *o*-diphenolic substrate to give benzodioxinone adducts, an event that becomes significant only when H_2O_2 is low or absent. The observation of a purple red colouration in the early phases of the oxidation provides support for the generation of hydroxyquinone species.[176]

Just formed, the hydroxyquinones, which are vinylogous carboxylic acids (pK_a= 2.90)[177], are expected to be partially ionised at neutral pH and are competent to couple with the primary *o*-quinones to give the pentahydroxybiphenyl dimers.

The regiochemistry of the coupling reaction reflects the enolate-like character of the 3-position of hydroxyquinones. Consistent with this view, DFT analysis of 2-

hydroxy-5-methyl-1,4-benzoquinone in the ionised form revealed a relatively large HOMO coefficient on the 3-position (Figure 6).

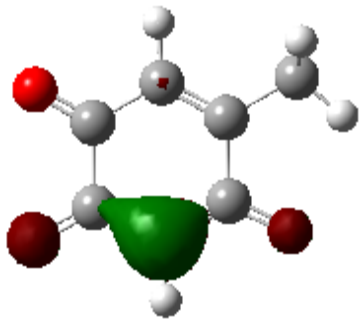

Figure 6. HOMO of 2-hydroxy-5-methyl-1,4-benzoquinone calculated at the HF/6-31+ G(d,p) level using PCM to model the effects of the solvent medium.

Although the proposed quinone-quinone coupling mechanism might seem unusual, it is reminiscent of the early steps of purpurogallin formation by oxidation of pyrogallol[178]and of the previously reported generation of pentahydroxybiphenyl dimers by tyrosinase-catalysed oxidation of hydroquinone *via* hydroxybenzoquinone.[179]

2.2 Acid-Promoted Reaction of the Stilbene Resveratrol with Nitrite Ions.

Assessing the susceptibility of resveratrol (**4a)** to react with acidic NO_2^- and characterizing the reaction products is of particular interest to predict the possible transformations and fate of the compound in the stomach in the presence of high NO_2^- levels. Studies of the nitr(os)ation chemistry of **4a** are also expected to provide a convenient entry to novel stilbene derivatives of potential synthetic and pharmacological interest, *e.g.* in the field of cyclooxygenase inhibitors and antiestrogenic compounds.[180-182]

This study describes the isolation and structural characterization of the main products formed by acid-promoted reaction of **4a** with NO_2^- under mild conditions, with the view to filling a major gap in the chemistry of this bioactive stilbene, and to gaining an improved background for further studies of the biological activity of this phytoalexin. Further interest of this study stems from the potential bioactivity of the oxidation/nitration products of **4a** against phytopathogenic fungi which is currently under scrutiny.

In a first series of experiments **4a** (1×10^{-3} M) was reacted with NO_2^- (5 molar equivalents) in 0.1 M phosphate buffer, pH 3.0. Reverse phase HPLC analysis of the reaction mixture after 3 h indicated complete substrate consumption and the presence of a complex pattern of products (Figure 7, plot A), two of which (t_R 29.2, product *V*, and t_R 37.9 min, product *VII*) displayed intense UV absorption at 320 nm.

The complexity of the reaction mixture was confirmed by TLC analysis of the ethyl acetate extractable fraction which showed seven bands at R_f 0.36, 0.40, 0.48, 0.55, 0.69, 0.78 and 0.84, two of which (R_f 0.36 and 0.55) exhibited a marked bathochromic shift on exposure to alkali. At lower concentrations of both **4a** (2.5×10^{-5} M) and NO_2^- (8 molar equivalents added with stirring over 2 h at 15 min intervals

of time), that is under conditions aimed to model interactions that may occur in the gastric compartment during digestion following continuous elevated nitrite intake, the product pattern was slightly different (Figure 7, plot B). In particular, formation of *VII* and the product at t_R 24.2 min (*IV*) was enhanced, while an abatement of those at t_R 12.2 (*I*), 15.5 (*II*), 20.9 (*III*) and 32.3 (*VI*) min was observed; moreover, novel species, for example that eluted at t_R 38.7 min (*VIII*), were present. Under such conditions (2.5×10^{-5} M **4a**, 1 mM NO_2^-), a pseudo-first order rate constant of $9.9 \pm 0.5 \times 10^{-3}$ s^{-1} for **4a** decay was determined.

For products isolation, the reaction of **4a** (1×10^{-3} M) with NO_2^- (5 molar equivalents) was run on preparative scale and the ethyl acetate extractable fraction was subjected to careful TLC fractionation.

The compound at R_f 0.40 (*VI*) was identified as the dimer **20**, previously isolated from *Smilax bracteata* rhizomes,[183] while products at R_f 0.69 and 0.84, corresponding to *II* and *III* in the elutogram in that order, were identified as 4-hydroxybenzaldehyde (4%) and 4-hydroxy-3-nitrobenzaldehyde (1%), respectively, by comparison with authentic samples.

The product at R_f 0.36 (*V*) gave a pseudomolecular ion peak $[M-H]^-$ in the ESI-/MS spectrum at *m/z* 272, suggesting a nitrated derivative of **4a**. The ^1H NMR spectrum featured the expected resonances for unchanged resorcin and 4-substituted phenol moieties, but lacked the pair of doublets for the *trans* protons on the stilbene double bond. These were replaced by a 1H singlet appearing downfield at δ 8.14, suggesting a strong deshielding effect caused by a spatially close nitro group. A distinct cross-peak in the ^1H, ^{13}C HMBC spectrum between the resorcin proton resonances at δ 6.36 and a deshielded carbon signal at δ 147.7 supported nitration on

the α-position of the stilbene system. On this basis, the product was formulated as (*E)*-3,4',5-trihydroxy-α-nitrostilbene (**21a**). Isolated yield of **21a** was 4%.

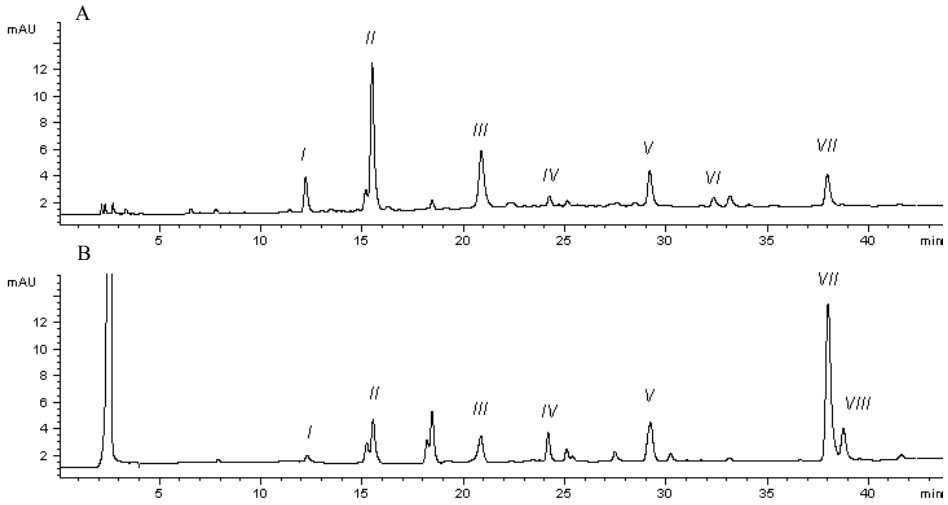

Figure 7. HPLC elution profile of the reaction mixture of **4a** with NO_2^- in 0.1 M phosphate buffer, pH 3.0, at 37 °C, at 3 h reaction time at different concentrations. Plot A: 1.0×10^{-3} M **4a**, 5.0×10^{-3} M NO_2^-; plot B: 2.5×10^{-5} M **4a**, 2.0×10^{-4} M NO_2^-. Elution conditions: eluant A, detection at 280 nm.

The band eluting at R_f 0.48 proved positive to the Griess reagent for nitroso compounds or nitrite-releasing species.[184] On NMR analysis it was shown to consist of an intimate mixture of two products at a 2:1 ratio. The major product was identified as 3,5-dihydroxybenzaldehyde (compound eluting under peak *I* in the elutogram of Figure 7) by comparison of the spectral features with those of an authentic sample. The signals of the ^{1}H NMR spectrum pertaining to the minor component included those typical of a resorcin moiety and a 2H singlet at δ 5.48 for a methylene group apparently linked to a nitro group (^{13}C NMR: δ 81.8). Accordingly, the compound was assigned the structure of 3,5-dihydroxyphenylnitromethane. LC/ESI+/MS

analysis of the R_f 0.48 band showed, in addition to a peak due to 3,5-dihydroxybenzaldehyde (t_R 15.1 min), a peak at t_R 13.9 min displaying a pseudo-molecular ion peak $[M+Na]^+$ at *m/z* 192.

The product at R_f 0.55 (*VII*) was evidently an isomer of **21a**, as inferred from the pseudomolecular ion peak $[M-H]^-$ in the ESI-/MS spectrum at *m/z* 272. Inspection of the ^1H NMR spectrum revealed the characteristic signals for the *trans* double bond (2H singlet at δ 7.14 in $(CD_3)_2CO$, appearing as a couple of doublets (J= 16.4 Hz) at δ 6.96 and 7.01 in CD_3OD) and the resorcin ring, but indicated a substituted phenol ring, as denoted by an ABX spin system (doublet at δ 7.20, double doublet at δ 7.97 and deshielded doublet at δ 8.23). These data, along with 2D NMR analysis, allowed formulation of the product as (*E*)-3,4',5-trihydroxy-3'-nitrostilbene (**22**).[185] The product was isolated in 1% yield. Notably, **22** was also obtained in 45% formation yield by reaction of **4a** (3.5×10^{-2} M) with NO_2^- (0.35 M) in acetonitrile containing 2.5% acetic acid. In this conditions no detectable formation of **21a** was observed.

The compound at R_f 0.78 was characterized as a dinitro compound (ESI+/MS: pseudomolecular ion peaks $[M+H]^+$ and $[M+Na]^+$ at *m/z* 319 and 341, respectively). The ^1H NMR spectrum showed the signals for a *trans* double bond, a substituted phenol ring (doublet at δ 7.25, double doublet at δ 8.00 and deshielded doublet at δ 8.27) and two doublets (J= 2.0 Hz) at δ 6.53 and 6.79. On this basis the product was formulated as (*E*)-3,4',5-trihydroxy-2,3'-dinitrostilbene (**23**) (1% yield). NMR data assignments for **21a**, **22** and **23** are reported in Table 2.

With the attempt to isolate the products *IV* and *VIII*, the reaction of **4a** (2.5×10^{-5} M) and NO_2^- (8 molar equivalents) was run on preparative scale. TLC fractionation of the ethyl acetate extracts allowed isolation of four main bands at R_f 0.09, 0.36, 0.55 and 0.69. The product at R_f 0.09, corresponding to *VIII*, was identified

as the resveratrol (*E*)-dehydrodimer **24** (4% yield) by comparison with literature data,[186, 187] whereas the species at R_f 0.36, 0.55, and 0.69 were identified as **21a** (3%), **22** (5%) and 4-hydroxybenzaldehyde (4%), in that order.

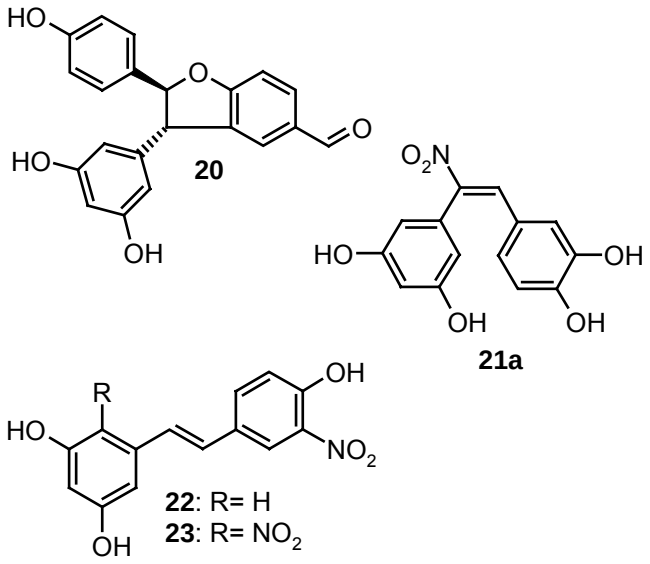

Table 2. NMR spectral data of **21a**, **22** and **23** ($(CD_3)_2CO$).

	21a		**22**		**23**	
	^{1}H (*J*, Hz)	^{13}C	^{1}H (*J*, Hz)	^{13}C	^{1}H (*J*, Hz)	^{13}C
1	-	133.9	-	139.8	-	136.8
2	6.36(d, 2.0)	109.3	6.61 (d, 2.0)	106.0	-	130.5
3	-	160.1	-	159.6	-	156.0
4	6.53 (t, 2.0)	104.6	6.33 (t, 2.0)	103.4	6.53 (d, 2.0)	103.0
5	-	160.1	-	159.6	-	162.0
6	6.36(d, 2.0)	109.3	6.61 (d, 2.0)	106.0	6.79 (d, 2.0)	107.5
α	-	147.7	7.14 (s)	130.5	7.42 (d, 16.0)	125.5
β	8.14 (s)	134.8	7.14 (s)	126.4	7.15 (d, 16.0)	130.0
1	-	123.3	-	131.3	-	129.8
2	7.21(d, 8.8)	134.3	8.23 (d, 2.4)	123.3	8.27 (d, 2.0)	123.5
3	6.79(d, 8.8)	116.4	-	135.3	-	135.0
4	-	160.9	-	154.5	-	154.0
5	6.79(d, 8.8)	116.4	7.20 (d, 8.8)	121.0	7.25 (d, 8.0)	120.5
6	7.21(d, 8.8)	134.3	7.97(dd,8.8, 2.4)	135.5	-	134.8

Because of the difficulties to isolate product *IV* by the above procedure, an alternative approach was pursued, involving column chromatography of the ethyl

HPLC. This methodology allowed isolation of the product, that could be identified as restrytisol B[188] (**25**) (1%) by NMR analysis and comparison with literature data. The stereochemical features of **25** were deduced from the ^{1}H NMR spectrum: in particular, the splitting patterns of the aliphatic protons at δ 3.40 (t, *J*= 9.2 Hz), 3.96 (t, *J*= 9.2 Hz), 5.00 (d, *J*= 9.6 Hz) and 5.50 (d, *J*= 8.6 Hz) were in agreement with those reported for a *cis*-*trans*-*trans* configuration[188] as illustrated in structure **25**.

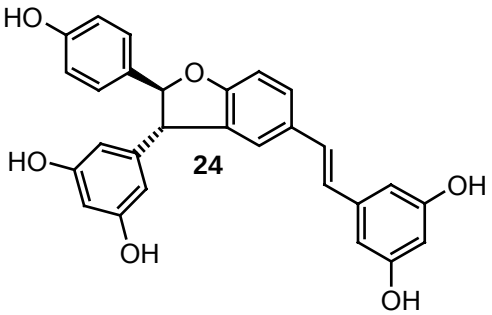

24

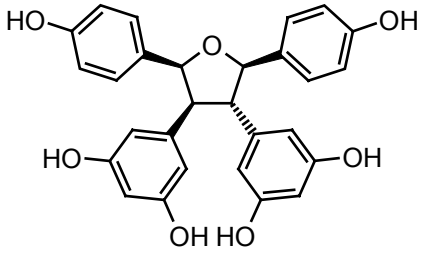

25

At 3 × 10^{-6} M concentration, **4a** reacted with NO_2^- (0.2 × 10^{-3} M, added in eight portions at 15 min intervals) to give mainly the two nitration products **21a** and **22** and 3,5-dihydroxybenzaldehyde and 4-hydroxybenxaldehyde, with little or no detectable dimers formation (HPLC evidence).

Close inspection of the aqueous phase after extraction and work up revealed the presence in all cases of chromatographically ill-defined materials, presumably oligomers and polymers, which could not be identified. Whether other dimers, e.g. restrytisols A and C,[188] are produced in the mixture remains uncertain, although, if present, they would be only minor constituents. In no case, however, could *trans*-ε-

viniferin[189,190] be detected (HPLC evidence in mixtures spiked with an authentic sample).

No significant change in product distribution was observed when the reaction of 1×10^{-3} M **4a** with NO_2^- was run under an oxygen-depleted atmosphere, care being taken to avoid contact with air prior to work up. Furthermore, the reaction of **4a** with NO_2^- was also run under an $^{18}O_2$ atmosphere and products were analyzed for incorporation of the label. LC/ESI+/MS analysis of the reaction mixture confirmed the expected lack of incorporation of ^{18}O within the main reaction products, including notably the aldehyde derivatives. Taken together, these observations ruled out any significant involvement of O_2 in the nitration, dimerization and aldehyde-forming pathways.

To gain some insights into the mechanism of dimerization and oxidative cleavage, the behavior of **4a** to one-electron oxidants at acidic pH was investigated. Oxidation of 0.25×10^{-3} M **4a** with 0.25×10^{-3} M CAN in 0.1 M phosphate buffer, pH 3.0, resulted in the formation of **24** and **25** as the main products as well as of 4-hydroxybenzaldehyde and 3,5-dihydroxybenzaldehyde in comparable amounts, but in much lower yields than in the reaction with NO_2^-. Interestingly, oxidation of **4a** with $K_3Fe(CN)_6$ at pH 7.0 led to the formation of both aldehyde products and the dimer **24** but no detectable **25**, suggesting that the latter reflects a specific acid-mediated oxidation pathway of **4a**.

To establish possible relationships between reaction products, additional experiments were directed to investigate the fate of isolated aldehydes, nitrated derivatives and dimers on exposure to NO_2^- under the usual reaction conditions. Careful monitoring of the reaction course by HPLC or TLC at various intervals of time showed that 4-hydroxybenzaldehyde, 3,5-dihydroxybenzaldehyde and 3,5-

dihydroxyphenylnitromethane in the R_f 0.48 band remained unchanged in 0.1 M phosphate buffer, pH 3.0, at 37°C, with or without added NO_2^-, after 24 h. Conversely, under the typical reaction conditions, **22** smoothly decayed to give 4-hydroxy-3-nitrobenzaldehyde and 3,5-dihydroxyphenylnitromethane, while **21a** gave rise to 4-hydroxybenzaldehyde as the main product. In the same conditions **24** gave the cleaved dimer **20**.

The products obtained by exposure of **4a** to acidic NO_2^- suggest competing reaction channels that lead to nitration, dimerization and cleavage of the stilbene double bond.

To distinguish between several possible mechanistic pathways, the *O,O,O*-trimethyl derivative of **4a**, prepared by a reported procedure,[191] was allowed to react with acidic NO_2^- under the same conditions used for **4a** and HPLC analysis did not reveal appreciable conversion to products. This observation would suggest that reaction of **4a** with acidic NO_2^- proceeds via an initial oxidative step (probably via H-atom transfer,[192-93] though electron transfer has also been proposed[194]) leading to the delocalized 4'-phenoxyl radical as a common intermediate from which the nitration, dimerization and aldehyde forming paths depart. Oxidation of **4a** (E^{ox}_p= +1.14 V *vs* saturated calomel electrode in CH_3CN)[195] may be brought about by HNO_2 (the reduction potential for the equation $HNO_2 + H^+ + e^- = NO + H_2O$ is +0.996 V at pH = 0),[196] or by the NO_2 produced by decomposition of HNO_2 (the reduction potential for $NO_2 + e^- = NO_2^-$ is 0.99 V).

Formation of nitration products would involve coupling of the phenoxyl radical with NO_2 at the 3'- and α-positions[197-98] (Scheme 3). According to this scheme, double bond nitration to give **21a** follows from a nitro quinone methide intermediate and is in line with the reactivity of the 4'-phenoxyl radical at the α-

position predicted by computational studies at the semiempirical and the DFT levels. This mechanism reflects again the dominant role of the 4-OH group in directing the reactivity of phenolic stilbenes toward the double bond.

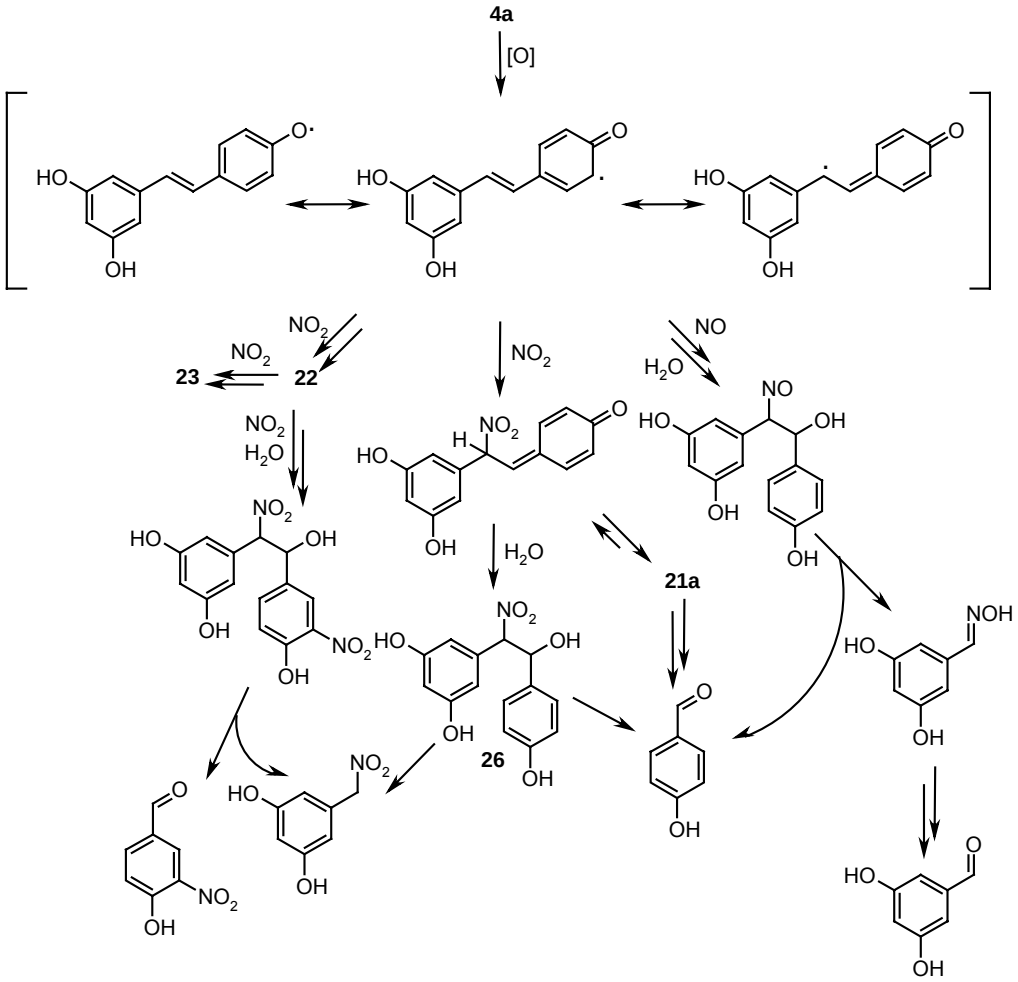

Scheme 3

Oxygen-independent formation of aldehydes by oxidative fission of the double bond of **4a** and related natural stilbene antioxidants under mild conditions of physiological relevance has apparently escaped the attention of previous workers.. To the best of our knowledge, formation of 4-hydroxybenzaldehyde and 3,5-dihydroxybenzaldehyde (as *O*-methyl derivatives) was reported only by harsh

ozonolytic splitting of the double bond of the *O,O,O*-trimethyl derivative of **4a**.[199] It is also noteworthy that aldehyde formation is enhanced in the NO_2^- -induced reaction compared to the CAN oxidation at pH 3.0, suggesting a specific NO_2^--dependent mechanism. The identification of 3,5-dihydroxyphenylnitromethane among the products argues strongly for an oxidative fission pathway involving nucleophilic attack of water to the nitro quinone methide intermediate in Scheme 2 to give 3,4',5,β-tetrahydroxy-α-nitro-α,β-dihydrostilbene (**26**), which would undergo fragmentation to give 4-hydroxybenzaldehyde and 3,5-dihydroxyphenylnitromethane. Unfortunately, all attempts to isolate the postulated hydroxynitro derivative **26** proved unsuccessful, due to the apparent instability of this species during chromatographic separation and work-up. In an attempt to demonstrate its formation, the reaction was carried out with 2.5×10^{-5} M **4a** and ^{15}N-labeled NO_2^- under the usual reaction conditions. Direct analysis of the crude ethyl-acetate extractable fraction by ^{1}H, ^{15}N HMBC revealed, as expected, two significant series of cross peaks, correlating the proton resonances of **22** at δ 8.23 (appearing as a triplet (J= 2.4 Hz) because of the further splitting by coupling with ^{15}N) and δ 7.20 with a nitrogen signal at δ 373, and the proton signals of **21a** at δ 8.14 (doublet, J= 4.0 Hz) and δ 6.36 with a nitrogen resonance at δ 378 (Figure 8). Another cross peak correlating a proton signal at δ 6.95 with a nitrogen signal at δ 383 (Figure 8, region A) was considered to be indicative of the presence of the *Z* isomer of **21a**.[200]

In addition, two intense ^{15}N resonances were detectable at δ 388 and 392 (Figure 8, region B), denoting nitro groups linked to sp^3 carbons.[200,201] These resonances (cross peaks with proton signals in the range δ 5.4-5.6) may be attributed to the nitrogens of 3,5-dihydroxyphenylnitromethane and **26** (mixture of diastereoisomers).

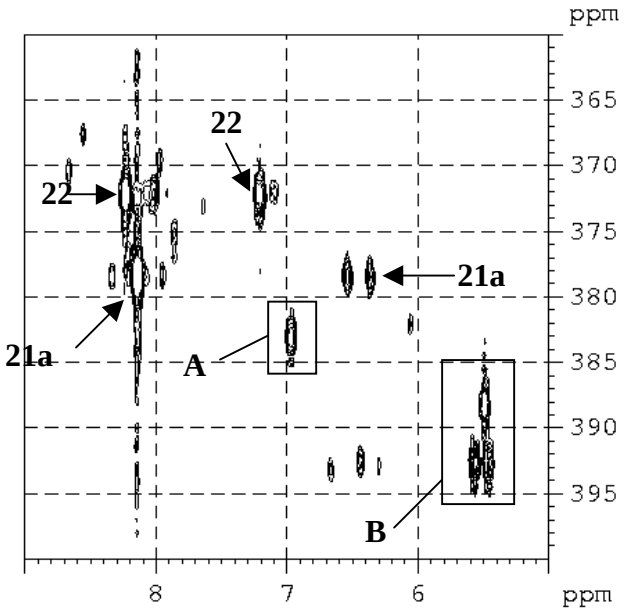

Figure 8. ^{1}H, ^{15}N HMBC spectrum of the ethyl acetate extractable fraction of the reaction mixture of **4a** with [^{15}N]$NaNO_2$ at pH 3.0. Arrows indicate cross-peaks of identified products (see text).

Consistent with this interpretation, LC/ESI+/MS analysis of two separate mixtures obtained from reaction of **4a** with ^{15}N-labeled and unlabeled NO_2^- indicated in both cases a species eluted at t_R 14.1 min giving a pseudomolecular ion peak $[M+Na]^+$ at *m/z* 315 and 314, respectively, confirming the presence of **26** (Figure 9). Label incorporation was observed also in the case of **21a** (t_R 31.8 min) and **22** (t_R 46.5 min), showing pseudomolecular ion peaks $[M+H]^+$ and $[M+Na]^+$ at *m/z* 275 and 297, respectively.

Cleavage of a nitrohydroxy derivative akin to **26** from **22** could account for the formation of 4-hydroxy-3-nitrobenzaldehyde.

Formation of 3,5-dihydroxybenzaldehyde is however incompatible with reaction pathways involving **26**, since it does not seem to arise from 3,5-dihydroxyphenylnitromethane. A plausible route would be through hydrolysis of an

oxime intermediate[202] produced by cleavage of a nitrosohydroxy species akin to **26**, arising by coupling of NO with the 4'-phenoxyl radical of **4a**.

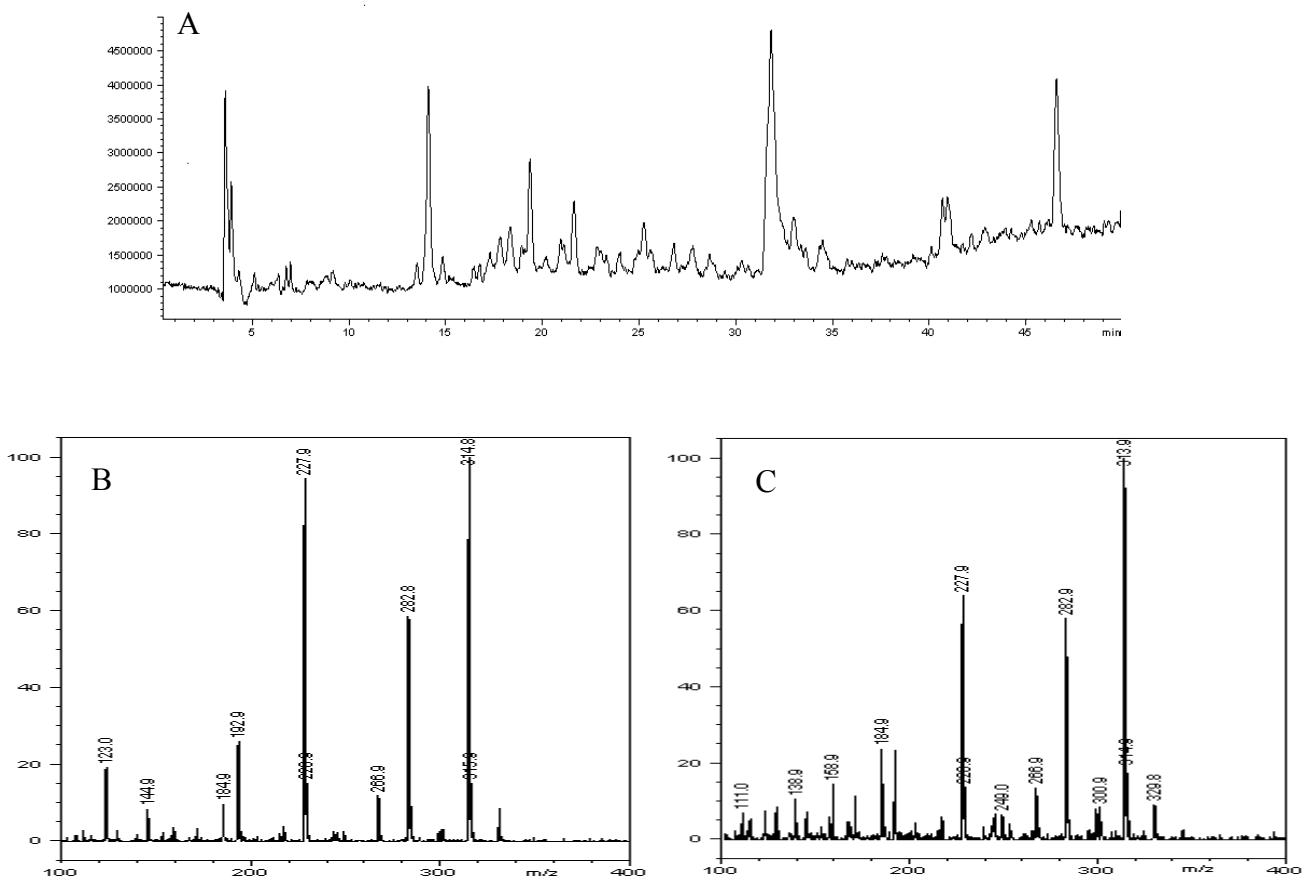

Figure 9. (A) LC/ESI+/MS elution profile of the ethyl acetate extractable fraction of the reaction mixture of **4a** with ^{15}N-labeled NO_2^- at pH 3.0. (B) ESI+/MS spectrum of the species eluting at t_R 14.1 min in the ethyl acetate extractable fraction of the reaction mixture of **4a** with ^{15}N-labeled NO_2^-at pH 3.0. (C) ESI+/MS spectrum of the species eluting at t_R 14.1 min in the ethyl acetate extractable fraction of the reaction mixture of **4a** with unlabeled NO_2^- at pH 3.0.

To test the proposed route, 3,5-dihydroxybenzaldoxime was prepared by reaction of 3,5-dihydroxybenzaldehyde with NH_2OH in 1.2 M sodium acetate at 80 °C[203] and exposed to NO_2^- under the usual reaction conditions: HPLC analysis of the

reaction mixture showed a ca. 50% consumption of the oxime after 2 h, with concomitant formation of 3,5-dihydroxybenzaldehyde. 3,5-Dihydroxybenzaldoxime was also detected in trace amounts by careful HPLC analysis (t_R 11.4 min, eluant A) in the reaction mixture of **4a** (1×10^{-3} M) with NO_2^- (5×10^{-3} M).

Dimerization of **4a** is well documented, and occurs *via* coupling of the resulting phenoxyl radical. Formation of **25** in small amounts by NO_2^--induced oxidation of **4a** is however noteworthy, since this dimer was previously described only by enzymatic oxidation produced by a fungal grapevine pathogen, but was never obtained by chemical oxidation under mild conditions. Present data indicate that one-electron oxidants, like CAN, can induce formation of **25** and that the heterocyclic oxygen derives from H_2O rather than O_2, because of the apparent formation of this dimer under O_2-depleted atmosphere. A possible mechanism is depicted in Scheme 4.

This mechanism is akin to that proposed for the biogenesis of tricuspitadol A, a diastereoisomer of **25** isolated from *Parthenocissus Tricuspidata*,[204] and for the formation of related tetrahydrofuran derivatives by chemical oxidation of caffeic acid under acidic conditions.[205] Formation of **25** in acidic but not in neutral medium is in line with previous observations and indicates that H_2O can act as a nucleophile toward the quinone methide only when acidic catalysis is provided.

Cleaved dimer **20** may derive at least in part by NO_2^- -induced oxidation of **24**. The likely mechanism would involve free radical addition of NO_2 to the double bond followed by recombination of the β-nitroalkyl radical with another molecule of NO_2 to give a nitronitrito adduct, which would suffer subsequent cleavage. This mechanism, which does not require a phenolic oxidation step, would become operative under forcing conditions like those leading to the formation of **20**.

The reaction pathways illustrated in Schemes 2 and 3 entail that product distribution mirrors the relative concentrations of reacting free radical species in the medium. The incomplete mass balance, due to the presence of other ill-defined species that escaped isolation and characterization, prevents a more detailed mechanistic analysis, so it is possible that other reaction pathways of **4a** are operative. However, the above schemes establish the central role of the 4'-OH group in directing the main reaction pathways of **4a** with acidic NO_2^- toward the double bond, which is a most significant outcome of this study.

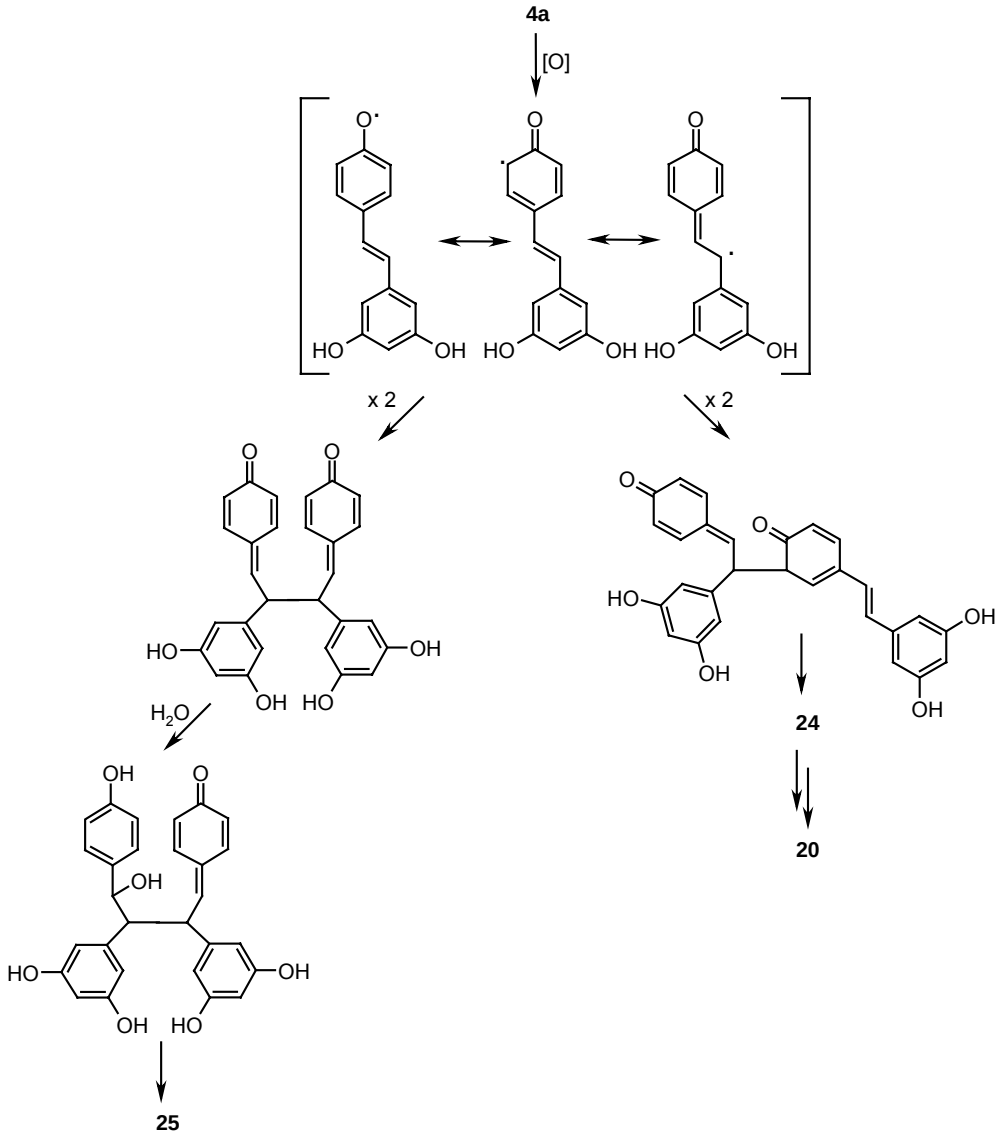

Scheme 4

2.3 Acid-Promoted Reaction of the Stilbene Piceatannol with Nitrite Ions.

The reactivity of stilbenes toward the reactive nitrogen species formed in the decomposition of nitrite in acidic medium was further investigated addressing piceatannol (**4b**). Studies of the chemistry and bioactivity of **4b** have indeed underscored its remarkable antioxidant, anti-inflammatory, anti-proliferative and cancer chemopreventive activities, but little is known about its potential nitrite scavenging and antinitrosaminic properties.

4b was easily obtained from resveratrol by an expedient procedure involving oxidation with IBX. In brief, a solution of **4a** in methanol was treated with IBX (2.5 equiv.) under vigorous stirring at –78 °C. After 70 min the reaction mixture was reduced with a dithionite solution, acidified to pH 3 and extracted with chloroform first and then with ethyl acetate to give **4b** in 58% yield.

In a first series of experiments the potential nitrite scavenging and antinitrosaminic properties of **4b** were explored using a standard assay for evaluating the potential of antinitrosating agent, known as the 2,3-diaminonaphthalene (DAN) assay.[107] The ability of the test compound of inhibiting the reaction of 2,3-diaminonaphthalene (DAN) with nitrous acid leading to fluorescent naphtho[2,3-d]triazole formation is evaluated by spectrofulorimetric measurements. For comparative purposes, caffeic acid (**11**), an established inhibitor of DAN nitrosation,[107] was also investigated.

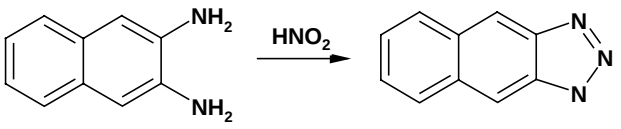

DAN Naphto[2,3-d]triazole

The results in Figure **10** show that, under the typical conditions of the assay, **4b** was more effective than **11** in inhibiting fluorophore development over the whole concentration range examined. From fluorescence measurements, the ratio of the kinetic constants $k_{\mathbf{4b}}/k_{11}$ for the reactions of **4b** and **11** with nitrite could be calculated as 1.7 ± 0.5 using the equation below:[107]

$$f/F = 1 - k_{In}[In]/k_{DAN}[DAN]$$

where f and F are the fluorescence intensities determined in the presence and in the absence of the inhibitor (In), respectively. For the reaction of DAN with nitrite the reported rate constant of 8.6×10^9 M^{-1} s^{-1} was used.[107]

Based on this observation, the reaction of **4b** with nitrite ions was then investigated under conditions mimicking at best those found in human gastric fluid during a regular intake of physiological levels of nitrite.

At 20 μM concentration, **4b** reacted with sodium nitrite (4 molar equivalents added in four portions at 30 min intervals of time) in 0.1 M phosphate buffer (pH 3.0) at 37°C to give two species, of which one was isolated and identified as 3,4-dihydroxybenzaldehyde (19%) while the other was identified as 3,5-dihydroxybenzaldehyde by comparison of chromatographic properties with an authentic sample, and a major product which was isolated in pure form in 68% yield from a preparative scale reaction by preparative HPLC of the ethyl acetate extractable fraction.

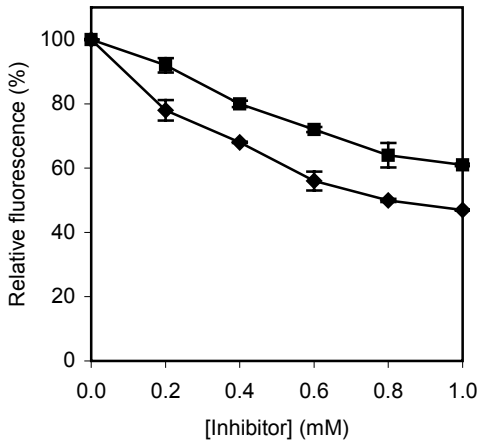

Figure 10. Inhibition of *N*-nitrosation of DAN by **4b** (♦) and **11** (■) measured as fluorescence emission at 450 nm of naphtho[2,3-d]triazole. Relative fluorescence represents the ratio of fluorescence values measured in the presence *vs* that determined in the absence of the inhibitor. Shown are the mean ± SD values for two separate experiments.

The product displayed absorption maxima at 256, 277 and 373 nm (CH_3OH), shifting to 285 and 472 nm in CH_3OH/0.1 M $NaHCO_3$ solution (pH 8). It gave pseudomolecular ion peaks at *m/z* 312 $[M+Na]^+$ and at *m/z* 288 $[M-H]^-$ in the ESI(+) and ESI(-)/MS spectrum, respectively, suggesting a nitrated derivative. The ^1H NMR spectrum showed a set of aromatic/olefinic proton resonances which lacked the expected 1H doublets for the *trans* H-α and H-β protons. Besides the resonances of the resorcin moiety, appearing as a doublet (2H, *J*= 2.0 Hz) at δ 6.25 and a triplet (1H, *J*= 2.0 Hz) at δ 6.44, showing one-bond correlation with two carbon resonances at δ 109.9 and 105.1, respectively, and those of the catechol ring (broad 3H singlet at δ 6.71 due to three overlapped proton resonances correlating with three carbon signals at δ 116.6, 119.5 and 126.5), a diagnostic feature was a down-field 1H singlet at δ 8.07 correlating with a carbon signal at δ 136.1. These data allowed unambiguous identification of the product as the unexpected (*E*)-3,3',4,5'-tetrahydroxy-*β*-

nitrostilbene (**21b**).

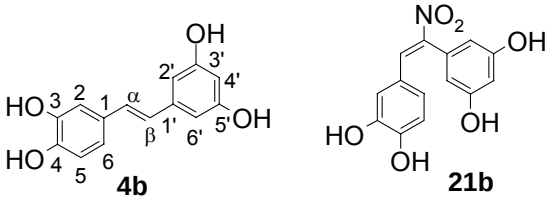

This structural assignment was deduced from extensive 2D NMR analysis: in particular, the position of the nitro group was determined by distinct cross-peaks in the $^{1}H,^{13}C$ HMBC spectrum between the signal at δ 8.07 and the carbon resonances at δ 119.5 and 126.5 due to the catechol moiety. The *E* configuration at the double bond was inferred from the characteristic chemical shift of the H-α proton experiencing the magnetic anisotropy effect of the adjacent nitro group,[206] and was confirmed by a correlation in the ROESY spectrum between the resorcin doublet at δ 6.25 and the overlapped catechol signals at δ 6.71.

The geometrical features of **21b** were examined by DFT optimizations,[207] using the hybrid PBE0 functional[208] in combination with a medium-size basis set of the Pople series, namely 6-31+G(d,p).[209] Absolute NMR shielding tensors were computed within the Gauge-Including Atomic Orbitals (GIAO) ansatz[210] at the PBE0/6-311+G(d,p) level, which has proven reliable in similar applications,[211] and were converted to isotropic chemical shifts using as reference the values obtained at the same level for benzene. Since the experimental NMR data have been collected in acetone, the polarizable continuum model (PCM)[212] was used throughout to simulate the solvent, in combination with the United Atom for Hartree-Fock (UAHF) parametrization for atomic radii.[213] A few asymmetric conformers that were energy minimized initially evolved to structures of C_s symmetry, with the resorcinol ring

perpendicular to a plane containing the whole nitrostyrene moiety. Several additional optimizations were performed on symmetric conformers, differing by a 180° rotation of the catechol ring and/or in the orientation of the phenolic hydroxyl groups, and NMR calculations were carried out on the main minima (Figure 11).

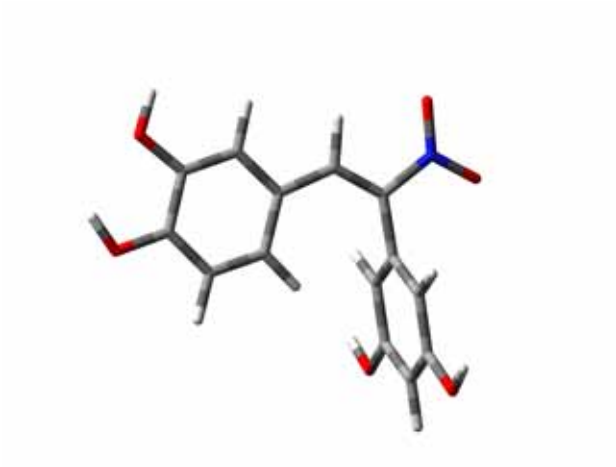

Figure 11. Energy minimized structure of **21b** (C_s symmetry conformer).

The computed isotropic shielding were Boltzmann averaged, and are compared to the experimental values in Table 3. The data indicate a satisfactory agreement, with a noteworthy simulation of the unexpectedly similar proton shifts of the catechol ring. Careful HPLC analysis of the reaction mixture failed to show the presence of additional nitration products (UV evidence). Notably, when the reaction was run at pH 1.0, a marked decrease in the yield of **21b** (less than 1%) was observed. This was shown to be due to the instability of **21b** which was converted to unidentified species. A greater stability of **21b** was observed, however, at pH 3.0.

The observed site specific nitration of **4b** on the double bond was unexpected, since *o*-diphenols bearing a conjugated double bond, such as chlorogenic acid (**12**) and other caffeic acid esters, usually react with acidic nitrite to give ring nitrated products, e.g. 6-nitrochlorogenic acid.[214,215]

Table 3. NMR spectral data of **21b** (acetone-d_6).

	^{1}H (J, Hz)		^{13}C	
	Experimental	Calcd.	Experimental	Calcd.
1	-	-	125.0	122.7
2	6.71 (br s)	6.56	119.5	119.1
3	-	-	147.0	143.0
4	-	-	151.0	148.2
5	6.71 (br s)	6.53	116.6	113.9
6	6.71 (br s)	6.40	126.5	127.5
α	8.07 (s)	8.28	136.1	140.4
β	-	-	148.5	144.6
1’	-	-	134.2	135.5
2’/6’	6.25 (d, 2.0)	5.92	109.9	106.2
3’/5’	-	-	161.0	159.9
4’	6.44 (t, 2.0)	6.28	105.1	100.3

To gain some mechanistic insights, in separate experiments it was found that the tetra-*O*-methyl derivative of **4b** (prepared with methyl iodide following a reported procedure),[130] to which phenolic oxidation is precluded, does not react with acidic nitrite under the usual reaction conditions. This observation points to an oxidation step as a necessary requisite for nitration of **4b**. This would be carried out by HNO_2 or NO_2 (E_0= 0.99 V) derived by decomposition of HNO_2. As a result, one-electron oxidation of **4b** would lead to the corresponding semiquinone. This may disproportionate to give the *o*-quinone which may undergo nucleophilic attack by nitrite ions, as previously suggested in the case of caffeic acid derivatives, including **12**.[215,215] This route, however, was ruled out in the light of separate experiments, in which the *o*-quinone of **4b** was generated *in situ* under different conditions, i.e. by tyrosinase-catalyzed or ferricyanide-promoted oxidation of **4b** at pH 7, in the presence of excess NO_2^- (5 molar equivalents) without detectable conversion to **21b**. Moreover, from inspection of the LUMO[216] of the putative *o*-quinone of **4b** shown in Figure 12, the β position did not appear as the most reactive electrophilic site with respect to the

other conceivably reactive positions.

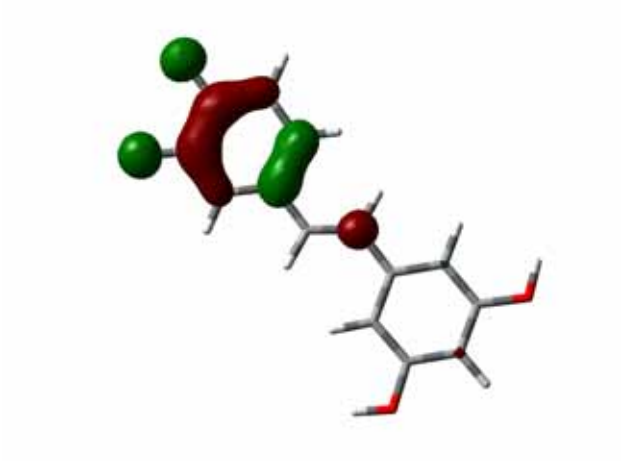

Figure 12. LUMO of the *o*-quinone of **4b**.

Accordingly, a free radical coupling mechanism for the nitrous acid-induced nitration and oxidative cleavage of **4b** was proposed, with a mechanisms similar to those described above for **4a**. In the proposed mechanism, one-electron oxidation of **4b** at the 4-OH group gives a highly delocalized radical (semiquinone), akin to that from **4a**.[217] Semiquinone intermediates are known to be formed by oxidation of stilbene catechols and have been detected under neutral conditions in the presence of Mg^{2+} or Zn^{2+} as spin stabilizing agents.[218] Homolytic coupling of the semiquinone with NO_2 at the β-position would then give **21b**.

The results of a DFT investigation of the 4-phenoxyl radical of **4b** are consistent with the proposed free radical mechanism.[219] Figure 13 depicts the singly occupied molecular orbital (SOMO) of one conformer of the 4-phenoxyl radical of **4b** in aqueous solution. The orbital is π in character, and has an appreciably larger coefficient on the β position, *i.e.* the one involved in nitration, than on the other conceivably reactive site, namely C-5. The overall picture is essentially unchanged for the other conformer of the radical, both *in vacuo* and in aqueous solution.

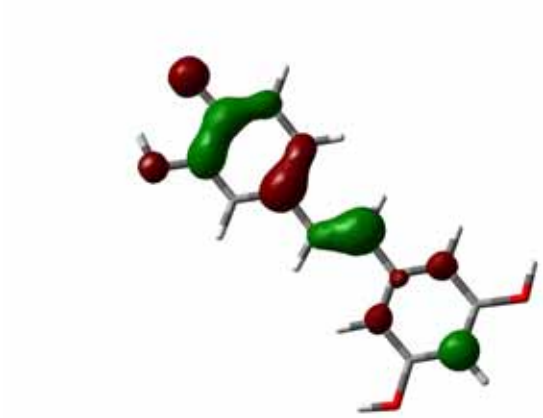

Figure 13. SOMO of the 4-phenoxyl radical of **4b** (conformer #1).

To allow for a more quantitative comparison, the Mulliken atomic spin densities on the relevant double bond and ring positions were determined. Data in Table 4 indicate that the spin density on C-β is much higher than on the C-5 ring position. Appreciable spin density is also present on the 2', 4' and 6' positions of the resorcinol ring.

Table 4. Selected Mulliken atomic spin densities of the 4-phenoxyl radical of 4b.

	conf. #1	conf. #2	conf. #1	conf. #2
	in vacuo		aqueous solution	
Relative energy (kcal/mol)	0.0	0.0	0.0	0.2
C-β	0.297	0.332	0.300	0..333
C-5	0.194	0.239	0.163	0.204
C-2'	0.099	0.106	0.102	0.109
C-4'	0.110	0.119	0.118	0.127
C-6'	0.087	0.094	0.091	0.098

Despite the 3,4-dihydroxystiryl moiety in common with caffeic acid esters, e.g. **12**, only **4b** reacts with acidic nitrite *via* coupling of the 4-phenoxyl radical with

NO_2. This may reflect an additional stabilization of this radical by the resorcin ring, as shown by the significant SOMO coefficient at the 4'-position of **4b** denoting extensive spin delocalization (Figure 13) as well as by spin density data (Table 4). In the case of **12** and other caffeic acid esters, the 4-phenoxyl radicals would expectedly be less stable, escaping trapping by NO_2. They would preferentially disproportionate to give the *o*-quinones,[214, 215] which are amenable to nucleophilic attack by nitrite ions to give ring nitration products.

2.4. Antinitrosating properties of catecholic compounds and of their *S*-glutathionyl conjugates.

Chemical investigations of the reaction products of polyphenolic compounds with acidic nitrite indicated unexpectedly different nitrosation/nitration patterns of reactivity depending not only on the structural features of the polyphenolic scavenger but also on the specific reaction conditions.[147] This is well apparent by comparing the reaction behavior of catechol derivatives. For example, **11** undergoes mainly nitrosation at the propenyl sector whereas its ester **12** is nitrated at the catechol moiety.[214, 215] To add to this complex scenario, **4b**, despite structural analogies with **11** and its esters, suffers mainly nitration at the double bond.[220] The structures of the catechol compounds previously investigated and their reaction products with acidic nitrite are shown in Figure 14.

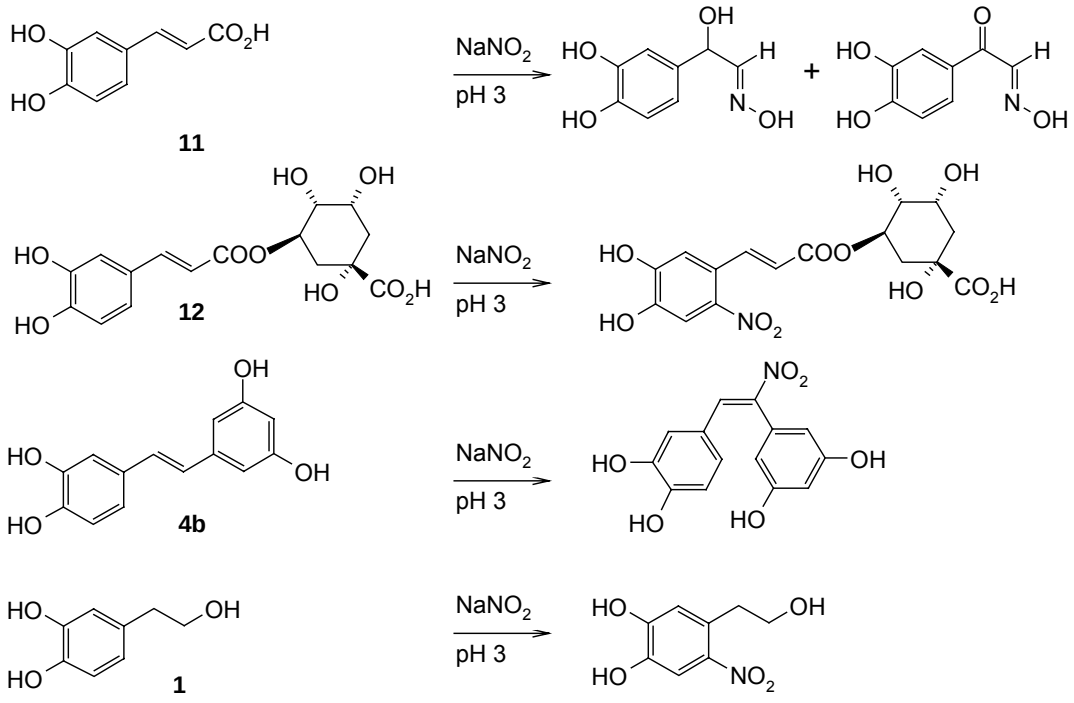

Figure 14. Products formed by reaction of **11**, **12**, **4b** and **1** with nitrite at acidic pH.

At a more general level, marked differences in the nature of reaction products with acidic nitrite are also observed with other polyphenolic compounds, which appear to depend on the structural characteristics of the reactive sites.[200,220,221] Although the chemistry of these interactions suggests differential inhibitory effects on the various nitrite-derived RNS via a broad range of mechanisms, very little is presently known as to the structural features imparting specific RNS scavenging abilities under different experimental conditions. An interesting related issue is the existence of any relationships between the RNS scavenging properties, with the underlying reactivity patterns, and the antioxidant/hydrogen donor properties of these phenols.

In these series of experiments the relative RNS scavenging abilities of some representative catechol compounds of plant origin, namely **11**, **12**, **4b** and **1** was also assessed. These catechols were selected because of their simple and closely related structures, which allowed to compare the effects of variously substituted conjugated double bonds versus an alkyl group (**1**) on the RNS scavenging properties of the catechol system. For each phenolic compound examined, the effects were compared with those of the corresponding *S*-glutathionyl (GSH) conjugate because of the biological relevance of these derivatives, e.g. to phase II metabolic transformations.[119,222-224] These latter experiments were also prompted by recent reports showing that sulfur substituents can affect the antioxidant properties of monophenols[225] and green tea catechins[226], whereby it seemed of interest to extend the investigation to the RNS scavenging properties of catechols.

Glutathionyl conjugates of **11** and **12**, **27** and **28**, were obtained in good yields by tyrosinase-catalyzed oxidation of **11** and **12** in the presence of GSH.

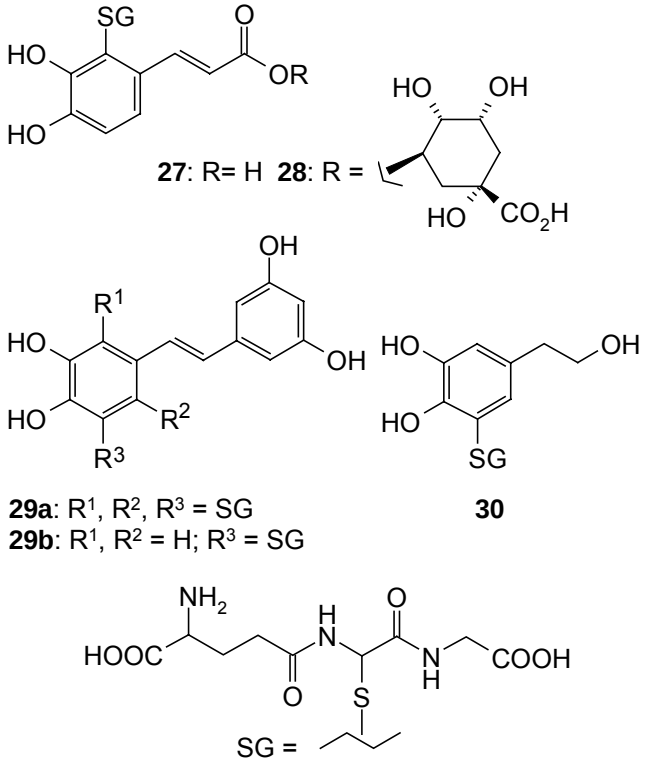

Attempts to extend the procedure to the synthesis of the GSH adduct of **4b** met with failure, due to unexpected difficulties in arresting the reaction at the monoadduct stage, and the triadduct **29a** was usually the prevalent species, with only little **29b**. Accordingly, an alternate procedure was developed, involving oxidation of resveratrol with IBX to give the corresponding *o*-quinone, which was then reacted with GSH. By this method, the desired monoadduct **29b** was obtained in pure form in 43% isolated yield (Scheme 5). NMR spectral data of 29a and 29b are reported in Table 5.

A similar IBX-based procedure was conveniently employed to prepare the GSH adduct of **1**, **30**, from tyrosol. The advantage of this procedure lies not only in the control exerted over the reaction course, preventing repeated coupling with GSH, but also in the possibility of using as substrates the easily accessible monophenols in the place of the more expensive catechols. It is noted that whereas **11** and its ester 1**2** give the 2-*S* adduct, catechols **4b** and **1** give the corresponding 5-*S* adducts. The

different regiochemistry of the conjugation process does not depend on the oxidation procedure but reflects the intrinsic positional reactivity of the quinones, as discussed recently.[223]

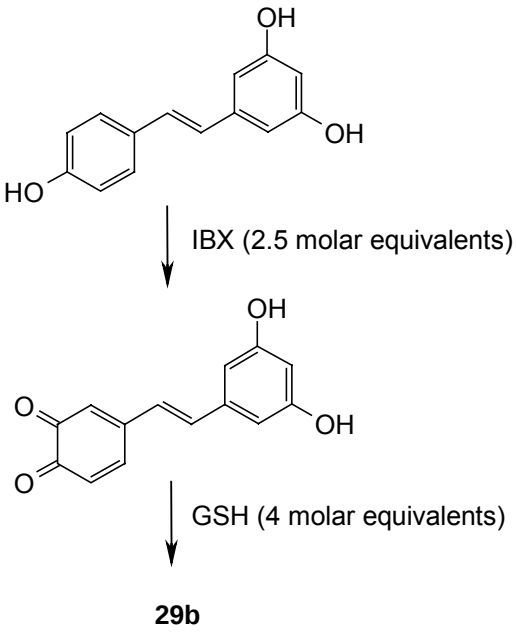

29b

Scheme 5.

To assess the relative scavenging properties of compounds under exam and their GSH conjugates on nitrite-derived RNS, two different assays were used, namely the DAN nitrosation assay and the tyrosine nitration assay. The DAN assay, as seen above, involves determination of fluorescent naphtho[2,3-*d*]triazole generated by *N*-nitrosation of DAN in 50 mM acetate buffer at pH 4.0 in the presence of excess nitrite.[107] The assay allows selective monitoring of the levels of nitrosating species, such as NO^+ or N_2O_3, that are produced by decomposition of nitrite in acidic media and that specifically account for fluorescence development. The tyrosine nitration assay is based on the HPLC quantitation of the 3-nitrotyrosine produced by reaction of tyrosine (400 μM) and equimolar nitrite in 0.5 M HCl at 37 °C.[103] The reaction is complete after about 4.5 h and leads to 3-nitrotyrosine in an acid-dependent reaction,

due to the generation in the strongly acidic medium of efficient nitrating species.

Table 5. NMR spectral data of **29a** and **29b** (D_2O).

	29a[a]		**29b**	
	^{1}H (*J*, Hz)	^{13}C	^{1}H (*J*, Hz)	^{13}C
1	-	141.3	-	131.3
2	-	121.1	6.98 (d, 2.0)	115.1
3	-	149.4[b]	-	145.5[c]
4	-	149.8[b]	-	145.9[c]
5	-	127.4	-	120.4
6	-	129.4	6.96 (d, 2.0)	125.8
A	7.30 (d, 16.4)	128.6	6.83 (d, 16.4)	129.2
B	6.61 (d, 16.4)	137.5	6.73 (d, 16.4)	127.7
1’	-	142.2	-	141.1
2’/6’	6.66 (br s)	107.5	6.52 (br s)	106.9
3’/5’	-	159.4	-	158.2
4’	6.38 (br s)	104.7	6.27 (br s)	103.2
CH cys			4.47 (m)	54.8
CH_2 cys			3.18 (dd, 14.8, 8.0)	36.5
			3.23 (dd, 14.8, 4.8)	
CO cys			-	173.4
CH glu			3.82 (m)	55.4
β-CH_2 glu			2.11 (m)	27.4
γ-CH_2 glu			2.44 (m)	32.7
CO glu			-	175.9
CH_2 gly			3.84 (s)	43.5
COOH glu			-	175.3[d]
COOH gly				175.6[d]

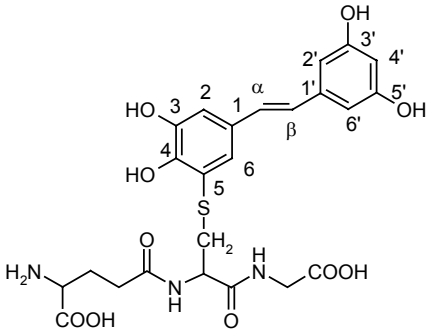

29b

a: resonances for the glutathione residues: 2.01 (m, 4H), 2.18 (m, 4H), 2.34 (m, 2H), 2.57 (m, 2H), 2.96 (m, 1H), 3.07 (m, 1H), 3.21 (m, 3H), 3.52 (m, 1H), 3.79 (s, 2H), 3.81 (s, 2H), 3.83 (m, 4H), 4.06 (m, 2H), 4.17 (m, 1H), 4.32 (m, 1H).

b, *c*, *d*: interchangeable.

These assays were well suited for the comparative purposes of the present study because of their different experimental conditions and predictive significance, allowing to distinguish selective effects of potential inhibitors in the nitrosation and nitration processes.

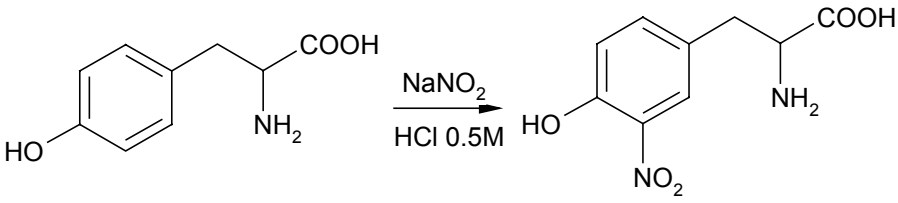

The relative effects of the various catechols and their GSH conjugates on DAN nitrosation were compared using 0.2 mM DAN, 20 mM $NaNO_2$ and varying concentrations of the catechols. Relative fluorescence values determined in the presence and in the absence of the inhibitor are shown in Figure 15.

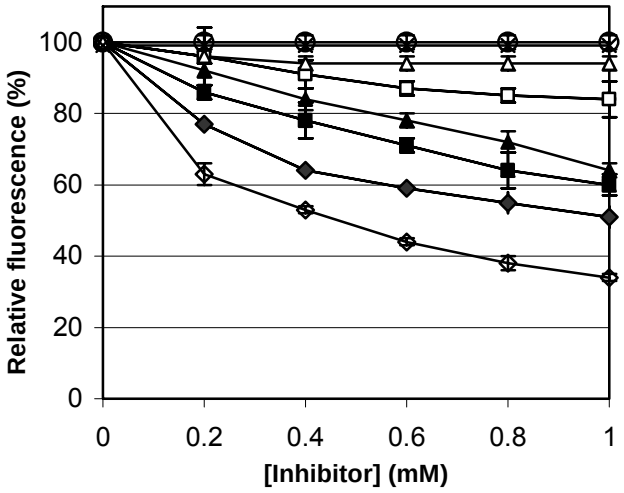

Figure 15. Inhibition of *N*-nitrosation of DAN by **11** (■), **12** (▲), **4b** (◆), **1** (×), **27** (□), **28** (△), **29b** (◇) and **30** (○) measured as fluorescence emission at 450 nm of naphtho[2,3-*d*]triazole. Relative fluorescence represents the ratio of fluorescence values measured in the presence and in the absence of the inhibitor. Shown are the mean ± SD values for two separate experiments.

A noticeable finding is that adduct **29b** proved more effective than **4b** in inhibiting fluorophore development over the whole concentration range examined. From fluorescence measurements, the ratio of the kinetic constants $k_{\mathbf{29b}}/k_{\mathbf{4b}}$ for the reactions of **29b** and **4b** with nitrite could be calculated as 1.7 ± 0.5**.** By contrast, triadduct **29a** was devoid of activity. Moreover, and quite unexpectedly, adduct **27** was much less active than **11**, indicating that the glutathionyl residue can exert opposite effects on the inhibitory properties of catechol compounds.

To gain an insight into the origin of these effects, competition experiments were performed in which the rates of decay of each catechol against its GSH conjugate were determined under the typical conditions of the assay but in the absence of DAN, with the compounds 0.4 mM each and nitrite ions at 0.4 mM concentration in acetate buffer at pH 4.0. HPLC analysis indicated that **29b** was consumed at a faster rate than **4b** and that all the conjugates were more reactive than the corresponding catechols, with the exception of the **11/27** couple, for which no significant difference in the rates of decay was observed.

In a related competition experiment, catechols at 0.4 mM concentration each were mixed together with 0.4 mM nitrite in acetate buffer at pH 4.0, both in the presence and in the absence of oxygen (argon flushed mixture). After 2 h incubation, the extent of decay was **4b>11** while 1**2** and **1** were little consumed, and no difference was noted under oxygen-depleted atmosphere (Figure 16). These data confirmed the higher reactivity toward acidic nitrite displayed by the catechol ring incorporated into a stilbene scaffold, as in **4b**.

In subsequent experiments the nature of the products formed by exposure of the catechols to nitrite was briefly investigated. All attempts at isolating reaction products from **4b** were unsuccessful, due to their fast degradation to very polar and ill-defined materials eluding chromatography. Detectable amounts of ring nitration products were formed from **12**[214, 215] and **1**[200], whereas **11** gave as main product a previously reported hydroxyoxime,[215] as determined by HPLC analysis in comparison with authentic standards.

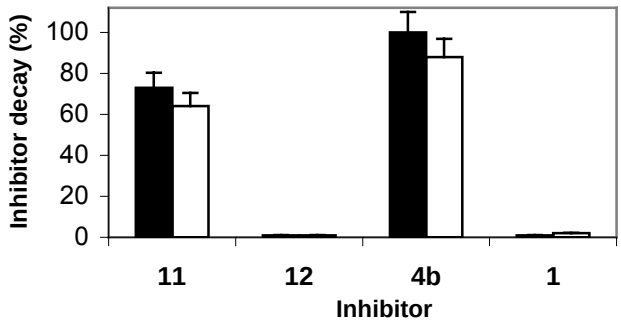

Figure 16. Decay of compound **11**, **12**, **4b** and **1** (400 M each) in the reaction mixture with nitrite ions (400 M) in 0.05 M sodium acetate buffer at pH 4.0 in the presence (black bars) or in the absence (open bars) of oxygen at 2 h after addition of nitrite. Shown are the mean ± SD values for two separate experiments.

The effect of catechols on tyrosine nitration was assessed as reported, measuring 3-nitrotyrosine formation by reaction of 0.4 mM tyrosine with equimolar nitrite in 0.5 M HCl in the presence and in the absence of the inhibitor (25-150 μM). 3-Nitrotyrosine detection was carried out by HPLC with analytical wavelength set at 275 nm, under conditions in which no interference by the catechols and reaction products was observed. Typically, 3-nitrotyrosine yield in the absence of inhibitor was 8 μM.

Data in Figure 17 indicated that 1**2** was the most effective inhibitor of nitrotyrosine formation (>95% inhibition at 100 μM concentration) followed by **11**, **1** and **4b**, in that order. Conjugation with GSH caused a marked drop in the inhibitory activity in all catechols examined: in particular, adduct **28** was about 60% less active than 1**2**.

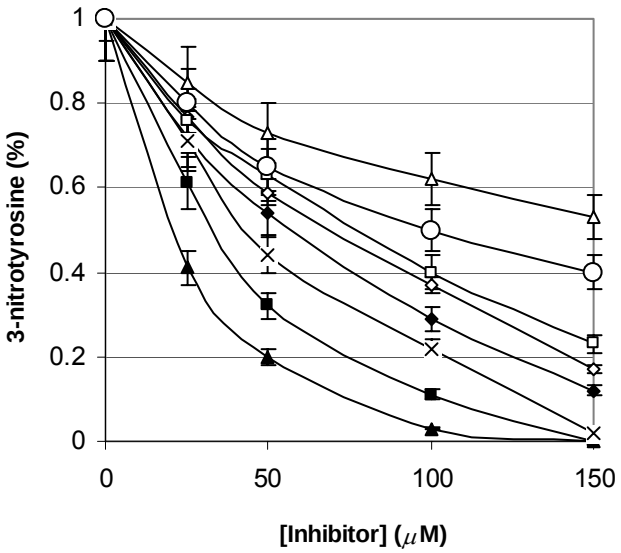

Figure 17. Inhibition of 3-nitrotyrosine formation by **11** (■), 1**2** (▲), **4b** (◆), **1** (×), **27** (□), **28** (△), **29b** (◇) and **30** (○) in the reaction mixture of tyrosine (400 M) with nitrite ions (400 M) in 0.5 M HCl, 37 °C, at 4 h 30 min after addition of nitrite. Shown are the mean ± SD values for two separate experiments.

To inquire into the factors determining the different rank order of activity of the various catechols in the two assays, the decay rates of the catechols at 0.4 mM concentration each were investigated under the specific conditions of the tyrosine nitration assay but without tyrosine, *i.e.* with 0.4 mM nitrite in 0.5 M HCl. Figure 18 shows that after 2 h incubation the more reactive catechols were again **4b** and **11** as in the previous experiment (see Figure 16), but under more acidic conditions also **1** decayed to an appreciable extent. Consumption of 1**2** was relatively low and the rates of catechol decay were significantly lower in the oxygen-depleted mixtures.

Overall, these results were suggestive of prevalent oxidative processes contributing to catechol reactions with nitrite ions under strongly acidic conditions.

To support this conclusion, the products formed by reaction of the catechols

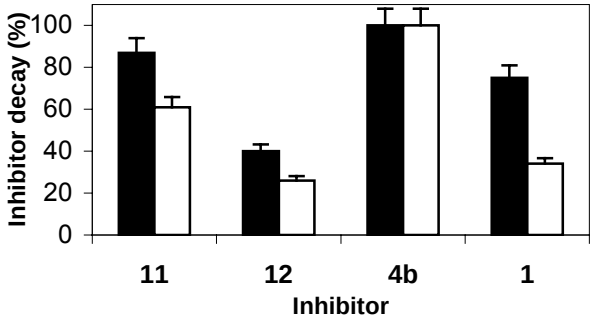

Figure 18. Decay of compound **11**, **12**, **4b** and **1** (400 M each) in the reaction mixture with nitrite ions (400 M) in 0.5 M HCl in the presence (black bars) or in the absence (open bars) of oxygen at 2 h after addition of nitrite. Shown are the mean ± SD values for two separate experiments.

with nitrite ions in 0.5 M HCl were investigated. Although HPLC analysis of the reaction mixtures from **11**, **12** and **4b** was little informative, spectrophotometric monitoring showed in the case of **11** the development of a chromophore similar to that attributed to the *o*-quinone.[227] HPLC analysis of the mixture from **1** showed after 2 min the formation of a main product (Figure 19, trace a) whose chromatographic properties were superimposable to those of a synthetic sample of the *o*-quinone of **1** prepared by the IBX-based methodology (trace b). Accordingly, reductive treatment of the mixture showed conversion of the product back to **1** (trace c).

The UV spectrum of the reaction mixture at that time showed a species with a maximum at 390 nm in good agreement with that of a 4-alkyl-*o*-quinone.[173] No detectable formation of nitrosation/nitration products was observed by HPLC analysis.

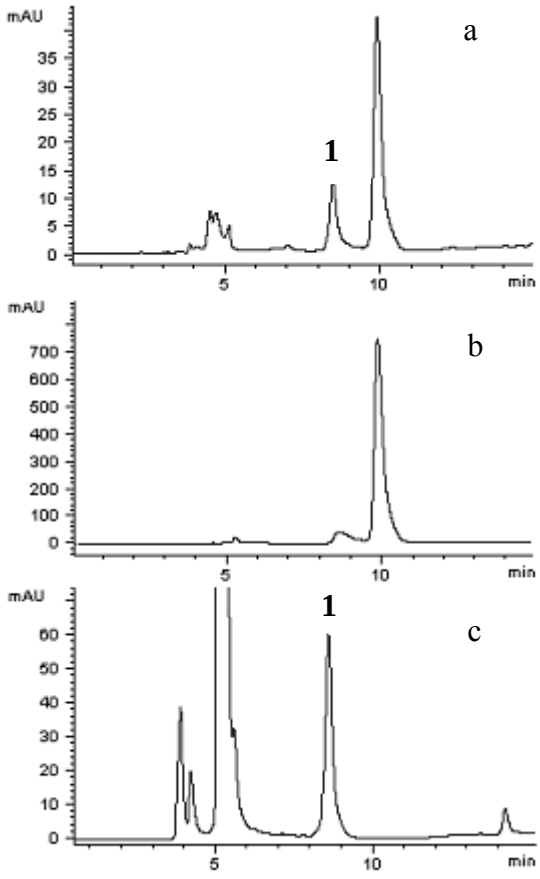

Figure 19. HPLC elution profiles of the reaction mixture of (trace a) **1** (400 M) with nitrite ions (400 M) in 0.5 M HCl at 2 min reaction time; (trace b) tyrosol with IBX in methanol at –25 °C after 1h; (trace c) **1** with nitrite ions as in trace a but after reduction treatment. Elution condition: 3% trifluoroacetic acid, solvent A; acetonitrile, solvent B; 5% B, 5 min; from 5 to 90% B, 5-45 min; flow rate 0.7 mL/min; detection at 280 nm.

The DAN assay represents a model system of *N*-nitrosation processes, because under the conditions of low acidity and excess nitrite a significant formation of N_2O_3 can be expected. Under these conditions the *S*-glutathionyl derivative **29b** was found to be one of the most effective inhibitors so far tested, even more potent than the parent **4b**.

This finding is of significant interest also in the light of the opposite effect of the sulfur substituent on the inhibitory activity of **11**, which was unexpectedly blunted in **27**. Previous studies [215,216] suggested that the scavenging effects of **4b** and **11** may be due to free radical nitration of the double bond, and to nitrosation/decarboxylation of the propenoate side chain, respectively. Thus, the potent inhibitory activity of **29b** may be due to the stabilizing effect of the GSH moiety on the phenoxyl radical intermediate crucial to the inhibition mechanism. On the contrary, the same *S*-glutathionyl group would decrease the reactivity of the propenoate chain of **27** relative to **11**, due possibly to the bulky GSH group forcing the side chain double bond out of coplanarity with the catechol ring and hindering efficient electron delocalization over the phenylpropenoate π-framework. In this line is the lack of activity of the triglutathionyl derivative of **4b**, **29a**, whose absorption maxima are hypsochromically shifted with respect to those of the parent catechol.

Another interesting outcome of the DAN assay is the identification of a conjugated double bond as an important structural feature in defining the antinitrosating potential of catechol compounds, considering the higher potency of **11**, **12** and **4b** relative to **1**.

A different mechanistic scenario can be envisaged in the tyrosine nitration assay, in which **4b** and its conjugate **29b**, the most active compounds in the DAN nitrosation assay, were found to be the least efficient inhibitors. The efficient inhibitory effects of **12** on tyrosine nitration were likewise unpredicted, since **12** was a very poor inhibitor in the DAN assay and was consumed at relatively slower rate with respect to the other catechols tested. In 0.5 M HCl, the nitrite protonation equilibrium is completely shifted toward nitrous acid formation, and an increase in the pseudo-first order rate constant for nitrite decomposition is anticipated with decreasing pH.[228]

It follows that nitration of tyrosine occurs probably via oxidation to a tyrosyl radical by HNO_2 (E_0= 0.996 V) and subsequent radical coupling with NO_2. The apparent prevalence of catechol oxidation over nitrosation/nitration processes under these conditions was suggested also by HPLC analysis of the reaction mixtures. The lack of correlation between catechol consumption and the inhibitory effects suggests that oxidizability *per se* is not a requisite for inhibition of tyrosine nitration at strongly acidic pH, consistent with the observation that reducing agents such as ascorbic acid (E_0 = 0.28 V)[229] are inactive in the tyrosine nitration assay. This can be explained considering that the nitrogenous species formed by redox interaction of nitrite-derived RNS with catechols, e.g. NO, can be reoxidized in the mixture. On this basis, it can be speculated that the inhibitory effects of **12** are due to conversion to polymeric species acting as more efficient scavengers via covalent reactions.

2.5. Antioxidant properties of a new derivative of hydroxytyrosol with α-lipoic acid.

In the field of antioxidants research, development of new antioxidants with enhanced activity and lower toxicity is highly desirable for the prevention and/or treatment of a number of diseases and, in food chemistry, for better food preservation.

All naturally occurring antioxidant are strongly hydrophilic and this makes their incorporation into fat and oil matrices difficult. To overcome this problem in recent years preparation of lipophilic antioxidants from natural sources, as clovamide derivatives, poly(lauroyl(+)-catechin)s or hydroxytyrosol fatty acid esters, as the hydroxytyrosol acetate, palmitate, oleate and linoleate has largely been pursued.[230-232] Yet, improvement of the antioxidant activity of **1** through modification of the catecholic nucleus has never been attempted, the only derivatives so far prepared being esters at the phenolic or alcoholic functionality .

With this in mind new experiments were directed to the synthesis a new derivative of **1** derived by conjugation with dihydrolipoic acid (DHLA) and evaluation of its antioxidant properties.

These experiments were also prompted as illustrated above for glutathionyl derivatives by recent reports showing that sulfur substituents can affect the antioxidant properties of monophenols [225] and green tea catechins.[226]

Lipoic acid (1,2-dithiolane-3-pentenoic acid, LA) and its reduced form dihydrolipoic acid (DHLA) are naturally occurring compounds.

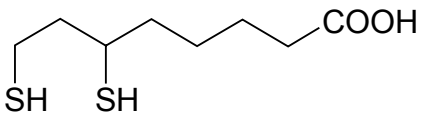

DHLA

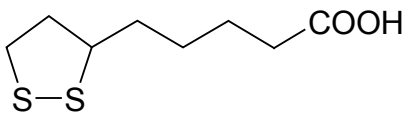

LA

LA has long been known as a coenzyme of multienzymatic mitochondrial complexes catalyzing oxidative decarboxylation of α-ketoacids.[233] Therapeutic action of LA is based on unique antioxidant properties of LA/DHLA system, which possesses one of the lowest standard biological redox potentials (E^0=-0.29 V). Thus, DHLA is able to reduce not only ROS but also the oxidized forms of other antioxidant.[234] It is worth remembering that LA has antioxidant properties as well. Owning to its easy absorption from the gastrointestinal tract and ability to cross the blood-brain barrier, exogenous LA can reach the majority of tissues. Moreover, LA and DHLA are easily soluble both in fats and water, which is a unique features among antioxidants, and are therefore active both at membrane level and in aqueous phases of cytoplasm.

Due to its unique properties, LA has also been administered in the treatment of various oxidative stress related diseases such as alcoholic liver disease, heavy metal poisoning, mushroom poisoning, diabetes, glaucoma, ischemia/reperfusion injury of heart and neurodegenerative disorders.[235] The most important exogenous source of LA are potatoes, spinach and red meats.

Examples of conjugate of DHLA with polyphenols have been reported in literature e.g. the 5-*S*-lipoyl-DOPA, obtained by the reaction of DHLA with L-3,4-dihydroxyphenylalanine (L-DOPA), which was found to act as inhibitor of DOPAchrome formation. [236]

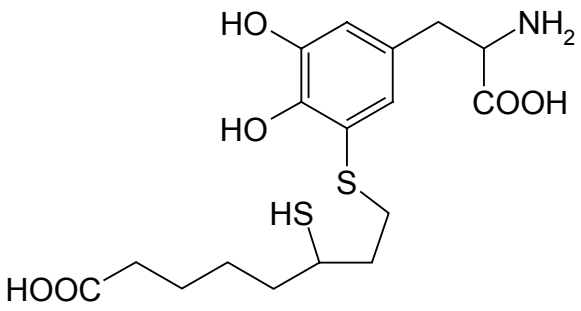

5-*S*-lipoyl-DOPA

A first series of experiment was aimed to the preparation of DHLA by reduction of LA with $NaBH_4$, following a procedure reported in the literature.[237]

In brief, to an aqueous solution of LA (0.25 M) in 0.25M $NaHCO_3$, $NaBH_4$ (1.0 M) at 0°C was added. After 2h the mixture was acidified to pH 1 and extracted with toluene.

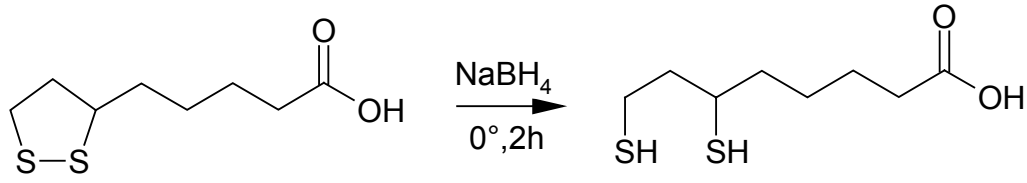

LA **DHLA**

The organic layer was analyzed by NMR (Figure 20). The ^1H NMR spectrum of the extract showed signals only in the region between 1.4-2.9δ and no one around 2.9-3.6δ, suggesting that a quantitative conversion of LA in DHLA has happened to give DHLA in 70 % yield.

DHLA was used for the synthesis of the lipoyl derivative of **1**, using the same procedure seen above for the preparation of **30**, but with DHLA as the nucleophile.

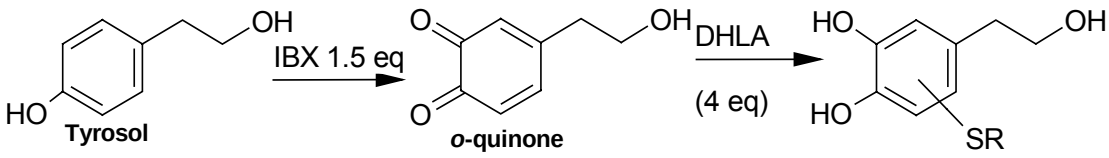

Tyrosol ***o*-quinone**

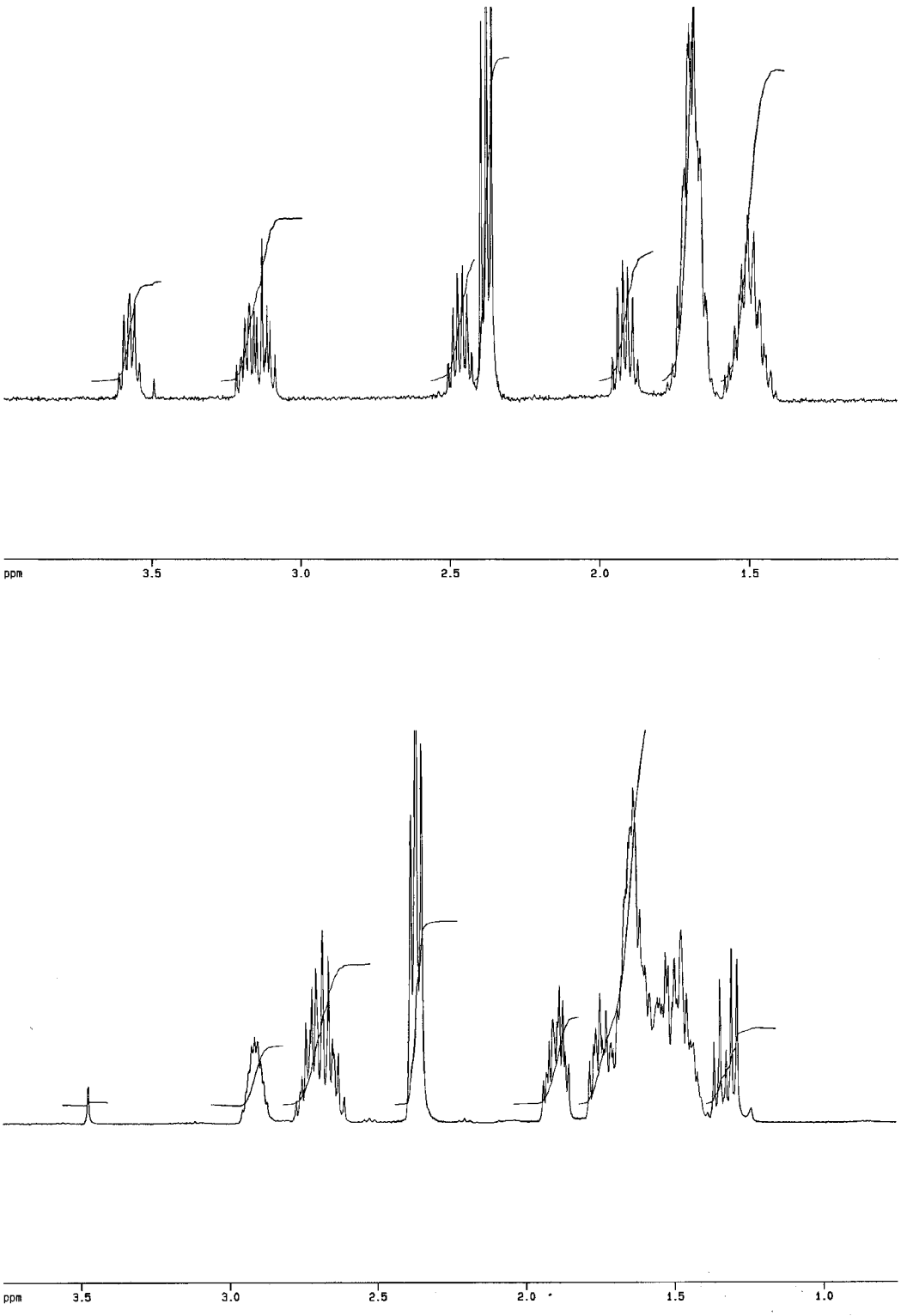

Figure 20. ^{1}H NMR spectrum in $CDCl_3$ of LA (upper spectrum) and DHLA (lower spectrum).

In detail, solid IBX (1.5 equiv.) was added to a solution of tyrosol (75 mM) in methanol at –25 °C and after 1h DHLA (4 equiv.) was added. After 15 min the reaction mixture was acidified until pH 3, extracted with ethyl acetate and than the organic layers were fractionated on silica gel chromatography to give the compound in a pure form and in 12% yield.

The ESI+/MS spectrum of product exhibited pseudomolecular ion peaks $[M+H]^+$ at *m/z* 361.1, indicative of the addition of one DHLA unit to one moiety of **1**. Consistent with this conclusion was the ^1H NMR spectrum in CD_3OD, showing in the aliphatic region resonances typical of DHLA and two triplets at δ2.65 e 3.67 characteristic of the hydroxyethyl chain of **1**. On the contrary the protons of the catecholic nucleus displayed as two doublets at δ 6.62 and 6.71 with a *J* of 2.0 Hz typical of a meta relation. On this basis, the product was formulated as 5-*S*-lipoylhydroxytyrosol (**31**).

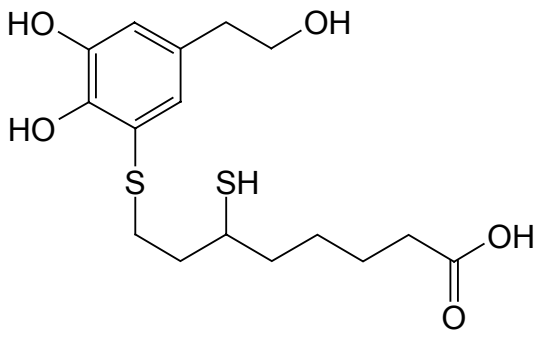

5-*S*-lipoylhydroxytyrosol (**31**)

The regiochemistry of the addition was similar to that seen for **4b** and for 4-alkyl *o*-quinones, as for example dopa and dopamine, while is different from that of cinnamic acid, as **11** or **12**, that undergoes nucleophilic addition at 2 position because of the coniugation of the propenoate chain with the acyl group. [223]

In a further series of experiments the antioxidant properties of **31** were tested.

Initially, the antioxidant efficiency of **31** in inhibiting the processes of lipid peroxidation was assessed. To this aim a spectrophotometric test was used based on recording the accumulation of the lipid hydroperoxides LOOH (λmax = 234 nm) from linoleic acid in a model system consisting of micelles of sodium dodecyl sulfate (SDS).[238] In heterogenous systems water-soluble initiators are generally employed to provide a constant flux of radicals production to mimic the natural radicals present in biological system. One of the most used water-soluble azo initiator is 2,2'-azobis-2-amidinopropane (ABAP), initially designed for aqueous emulsion polymerization and introduced in autoxidation studies in 1984. At 37°C and at pH 7, ABAP slowly decomposes and in the presence of oxygen a constant flux of peroxyl radicals is provided to initiate the processes of initiation and propagation of lipid peroxidation at a constant rate.

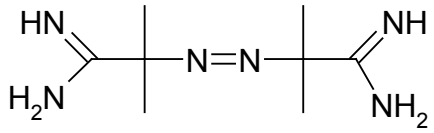

ABAP

Initiation:

$RN = NR \rightarrow 2R^{\cdot} + N_2$

$R^{\cdot} + O_2 \rightarrow ROO^{\cdot}$

$ROO^{\cdot} + LH \rightarrow LOO^{\cdot}$

Propagation:

$L^{\cdot} + O_2 \rightarrow LOO^{\cdot}$

$LOO^{\cdot} + LH \rightarrow LOOH + L^{\cdot}$

Measuring the autoxidation rate of linoleic acid in the presence and in the absence of a selected inhibitor is possible to determine the ability of the tested compound to act as a chain breaking antioxidant. **1** And α-tocopherol. were used as reference compounds

The results obtained are reported in Figure 21.

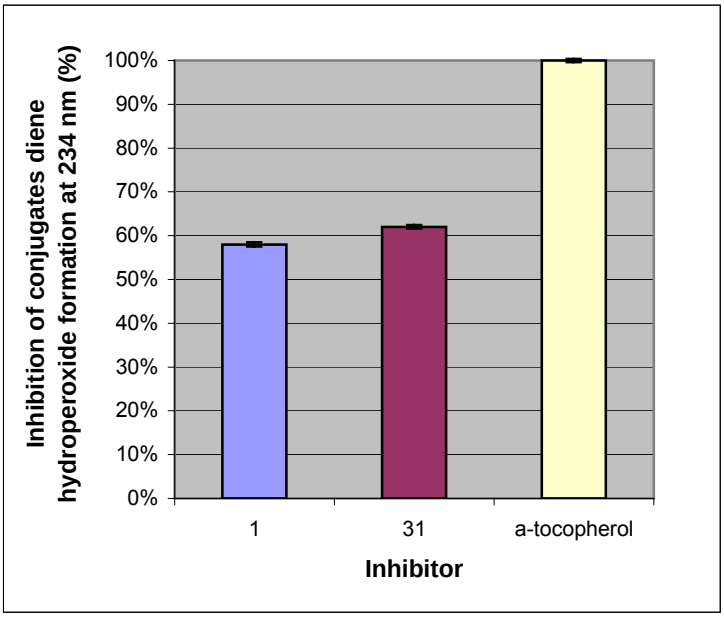

Figure 21. Inhibition of linoleic acid autoxidation by **1**, **31** and α-tocopherol in aqueous micelles of SDS.

As shown above, although **31** was a better inhibitor than **1,** both were much less active than α-tocopherol, typically an amphiphilic chain breaking antioxidant, probably due to its better partitioning in the micellar phase.

In a second series of experiments the antioxidant activity of **31** was tested by the DPPH assay.[169]

DPPH is a stable nitrogen-centered free radical. A quantitative analysis of the H-atom transfer reaction from a given phenol to DPPH provides a very simple and straightforward way to characterize the phenol by a set of parameters (*i.e.*, rate

constants and stoichiometry) tightly related to its intrinsic antioxidant activity. The H-transfer reactions are monitored by UV/VIS spectroscopy by recording the decay of the DPPH visible absorption band (λmax = 515 nm in MeOH) that reflects the conversion of the DPPH radical into the corresponding colorless hydrazine (DPPH–H) by the antioxidant. The experiments are run at a DPPH to antioxidant molar ratio of four in order to exhaust the H-donating ability of the antioxidant. With potent antioxidants, the visible absorbance quickly decays over 1–3 min as a result of the transfer of the most labile H-atoms of the antioxidant (fast step, monitored over 250 s). This step may be followed by a much slower decrease of the visible absorbance featuring the residual H-donating ability of the antioxidant degradation products (slow step). Only the fast step is kinetically analyzed. Experiments extending over 10 min are used for determination of the total stoichiometry n_{tot} of the antioxidant, according to: $n_{tot} = (A_0 - A_f)/(eC)$ (A_f : final absorbance, A_0: initial absorbance, C: initial antioxidant concentration).

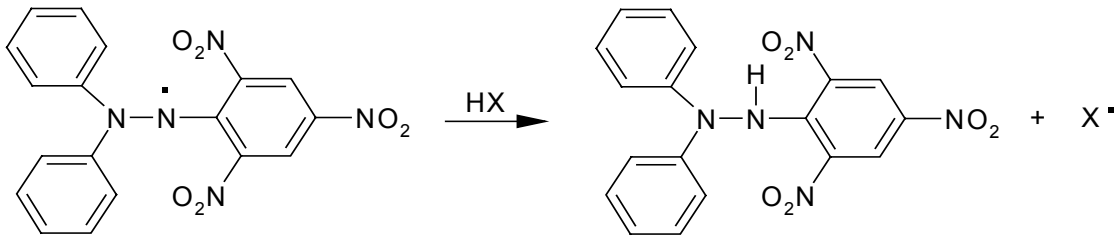

DPPH

The general kinetic model used for analyzing the H-atom transfer reaction between DPPH and a given antioxidant during the fast step (50–300 s) does not allow to draw conclusions about the mechanism of antioxidant degradation. An antioxidant of stoichiometry n is simply regarded as n independent antioxidant subunits (AH) which all transfer a single H-atom to DPPH with the same second-order rate constant k. Hence, the curve fitting of the absorbance *vs* time plots can be carried out using

simple second-order kinetics, the initial AH concentration being set at *nC*. Moreover, rate constant *k* can be identified with *k*1/*n*, *k*1 being the rate constant for the first (most labile) H-atom abstraction from the antioxidant.

The results of the test obtained for the compound under investigation are reported in table 6.

Table 6. H-atom transfer reactions from **31, 1**, DHLA and α-tocopherol to DPPH.

Antioxidant	**1**	**31**	α-tocopherol	DHLA
% inhibition	50 ± 3	67 ± 3	34 ± 4	55 ± 2
Δt/s	20	20	20	20
k/ M^{-1} s^{-1}	345 ± 26	512 ± 64	349 ± 49	531 ± 38
N	1.23	1.82	1.24	1.89
K_1/ M^{-1} s^{-1}	424	932	433	1003
n_{tot}	1.77	2.42	1.50	2.15

For experimental details see Experimental Section.

In this assay **31** showed to be more effective than **1** and α-tocopherol with regard to either kinetic parameters or total inhibition. As far as DHLA is concerned although this in the first seconds revealed an activity higher than **31**, after some minutes reduced its efficacy and the value of total inhibition was lower than **31**.

2.6 Nitration *vs.* Nitrosation Chemistry of Menthofuran: Remarkable Fragmentation and Dimerization Pathways and Expeditious Entry into Dehydromenthofurolactone.

To integrate this study, was extended to menthofuran this work on the behavior of bioactive natural products with nitrogenous mineral acids.[147]

Treatment of **5** with 40% nitric acid and catalytic sulfuric acid led to the instantaneous development of a purple color, while TLC analysis evidenced the complete conversion of **5** into two colorless, UV-absorbing compounds. Gravity column chromatography afforded the least polar compound as colorless crystals and the more polar reaction product as an amorphous white powder. The NMR spectra of the more polar product ($C_{23}H_{32}O_3$, HRMS) showed the presence of a pair of 2-menthofuranyl moieties and a three-carbon fragment. The two menthofuranyl moieties exhibited apparent chemical shift equivalence except for the signals of the pseudobenzylic methyl protons ($\Delta\delta$= 0.02 ppm) and carbon ($\Delta\delta$= 0.04) and the signal of C-3 ($\Delta\delta$= 0.06 ppm). The three-carbon fragment was identified as a 2-hydroxy-1-methylethylidene moiety by multiplicity considerations, and by HMBC correlations between the methyl protons at δ 1.68 and the signals of the –CH< and $HOCH_2$- carbons (δ 44.3 and 69.2, respectively). Diagnostic HMBC correlations between the hydroxymethyl and the methyl protons of the three-carbon moiety (δ 3.94 and 1.68, respectively) and C-2 (δ 148.8) of the menthofuranyl residue eventually allowed identification of the compound as the bis-(2-menthofuranyl) adduct of hydroxyacetone **32** (28% yield after crystallization).

The less polar compound ($C_{27}H_{38}O_2$, HRMS) resembled **32** in that NMR analysis showed the presence of two 2-menthofuranyl residues bound to a seven carbon moiety which was identified as a cyclohexane ring bearing three substituents,

two of which in a geminal relationship. Given the duplication of all the menthofuranyl protons, an extensive overlapping was present in the ^{1}H NMR spectrum, and the relative location of the substituents around the cyclohexane ring was not immediately apparent. However, the detection of six distinct ^{13}C NMR resonances for the cyclohexane core ruled out a symmetric 1,4-relationship between the two substituted carbons, while the lack of any detectable ROESY correlations between the methyl of the cyclohexane core (δ 0.82) and the furanyl methyls (δ 1.34 and 1.84), concurred to suggest a 1,3 rather than a 1,2-relationship between the substituted cyclohexane carbons. Accordingly, the product was formulated as 1,1-(bis-2-menthofuranyl)-3-methylcyclohexane (**33**) (39% yield after crystallization). These structures were supported by literature precedents for the formation of alkylidene-*bis*-furanyl structures from the reactions of furans with carbonyl compounds, and by the observation that, in the presence of catalytic amounts of strong acids, **5** reacted quickly with hydroxyacetone to afford a compound having ^{1}H and ^{13}C NMR spectra corresponding to those of **32**, and with *rac*-3 methylcyclohexanone to afford the known **33**.[239b,240,241]

When the reaction of **5** with nitric acid was run under conditions of lower acidity (20% HNO_3, cat. H_2SO_4), the nitro derivative **34** was obtained as the major reaction product (18% yield), along with minor amounts of the adducts **32** and **33** (5% and 7%, respectively). Interestingly, formation of **32** and **33** did not occur with a variety of other mineral acids (H_2SO_4, HCl, H_3PO_4), while with 40% HNO_3 alone the reaction was sluggish. In order to evidence a possible oxidative role for nitric acid, **5** was treated with a variety of oxidants, but formation of **32** and **33** could not be evidenced. Incidentally, during investigation of the reaction of **5** with different oxidizing systems, we noticed that while transition metal-based oxidants (PCC, PDC,

tetrapropyl ammonium perruthenate (TPAP)) and oxone® gave messy reaction mixtures, DDQ cleanly and reproducibly (*ca* 40-45% yield) afforded the important fragrant monoterpenoid dehydromenthofurolactone (anhydro Woodward-Eastman lactone) **8**.[142] Surprisingly, this reaction has gone unreported in the abundant scientific and proprietary literature of **5**, and is worth considering for further development on account of the relevance of **8** in perfumery and its metal-free conditions.[142] Lactone **8** is endowed with a pleasant and tenacious coumarinic smell, and could also be obtained, albeit in lower yield (13%), by treatment of **5** with IBX (*o*-iodoxybenzoic acid).

Overall, available evidence indicates that nitric acid plays a specific role in the formation of **32** and **33,** which, however, does not involve the nitro derivative **34**, a compound stable under the reaction conditions. A tentative mechanism for sulfuric acid-catalyzed, nitric acid-dependent formation of **32** and **33** is depicted in Scheme 6. According to this scheme, compounds **32** and **33** arise from the electrophilic trapping of the two carbonyl fragments, hydroxyacetone (**35**) and 3-methylcyclohexanone (**36**), by **5**. The observation that the ten carbons of **5** are complementarily distributed between the alkylidene moieties of **32** and **33** suggests that the formation of **35** and **36** is mechanistically coupled.

The fragmentation step might be a relatively unsurprising acid-promoted retaldol cleavage of the β-hydroxycarbonyl derivative **37**, whose formation raises, however, interesting mechanistic issues. **37** might be formed from **5** by conjugated addition of nitric acid or water to the heterocyclic ring. Under these reaction conditions, α–protonation of the furan ring seemingly prevails over electrophilic addition of nitronium ion, generating a nitrate ester (or water addition product, **38**) that next affords, through a series of water (nitric acid) addition and eliminations steps

(**39** and **40**), the seco-aldol **37,** eventually trapped as a bis-furanyl adduct by unprotonated starting material. With strong mineral acids (H_2SO_4, HCl, and $HClO_4$) or concentrated nitric acid, protonation of the furan moiety might be essentially quantitative, preventing nucleophilic trapping of the fragmentation products, a step that might well act as a steering sink for what is essentially a complex equilibrium between alternative reaction pathways. Conversely, with H_3PO_4 the conjugate addition product is apparently formed too slowly or, alternatively, reaction pathways different from the conversion to aldol **37** are preferentially activated, leading to a plethora of compounds that could not be characterized. This view is supported by the strong dependence of the reaction course from the concentration of HNO_3,with 40% (along with cat. H_2SO_4) being optimal for the formation of the bis-menthofuranylidene adducts.

Exposure of **5** (5 mM in the organic phase) to $NaNO_2$ (3 mM) in a biphasic system consisting of 0.1 M phosphate buffer (pH 3.0)/CH_2Cl_2 4:1 v/v for 2.5 h resulted in the smooth conversion of the substrate to a complex mixture of products, three of which could be characterized. The least polar one was the Woodward-Eastman lactone **41**, while a nitrogen-containing more polar compound was identified as the lactam **42**, a new compound that we have named anhydro mentholactam. The structural assignment of **42** was backed up by MS (pseudomolecular ion peak at *m/z* 164 ($[M + H]^+$), corresponding to the molecular formula $C_{10}H_{13}NO$ (HRMS)), and NMR data (olefin proton resonances at δ 5.77 (H-7), and amide-like carbon resonance at δ 173.1 (C-2)).

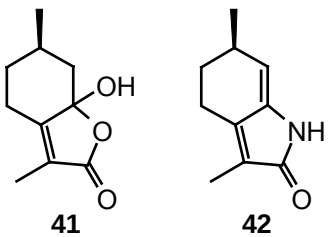

41 **42**

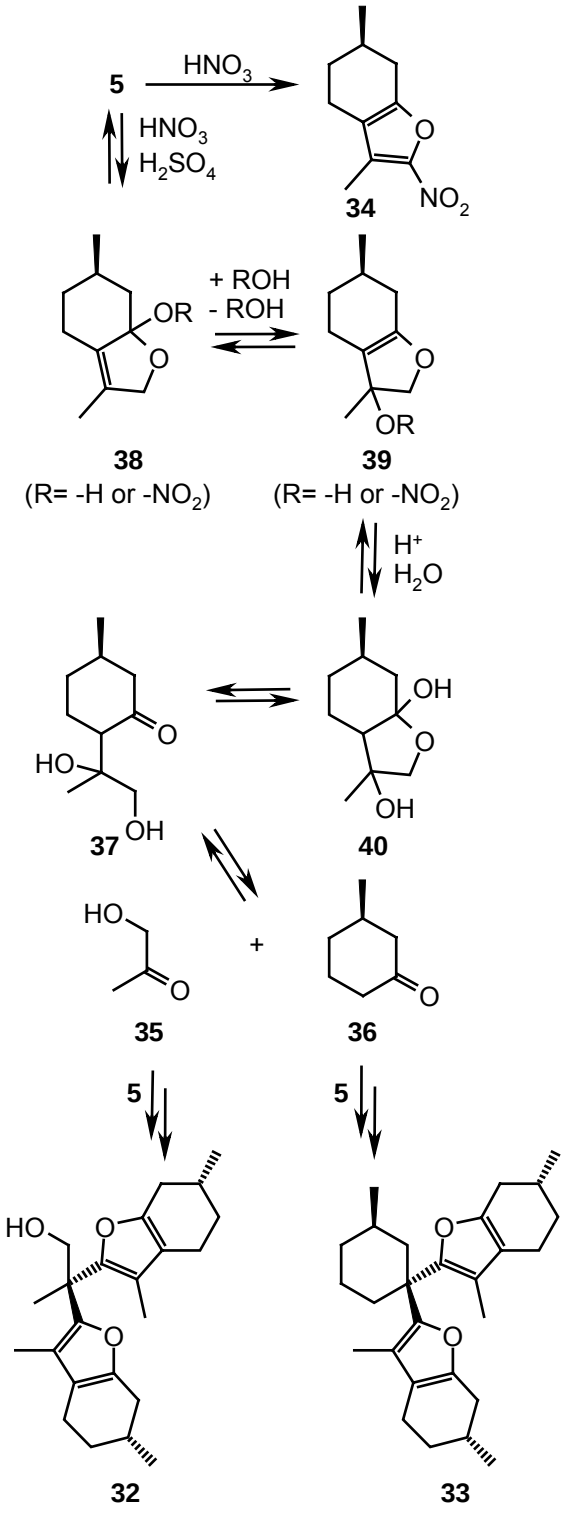

Scheme 6. Reactions of **5** with nitric acid. **32**, **33** and **34** are isolated compounds whereas the remainder are postulated intermediates.

The third compound displayed intense absorption maxima at 249 and 285 nm and a weak maximum at 364 nm, a pseudomolecular ion peak $[M + H]^+$ at *m/z* 422, and a molecular formula of $C_{20}H_{27}N_3O_7$ (HRMS), consistent with a menthofuran dimer bearing three nitrogen atoms.

The ^1H NMR spectrum exhibited two distinct sets of signals, corresponding to two substructures of the dimeric scaffold. One substructure showed a proton resonance at δ 5.08 (d, *J*= 4.0 Hz) cross-peak related (HSQC-DEPT spectrum) with a carbon resonance at δ 90.4. This proton resonance was coupled to a multiplet at δ 2.67, correlating in turn with a carbon signal at δ 33.1 and scalarly coupled to a methyl resonance at δ 1.08. Another diagnostic feature was the presence of two pairs of diastereotopic methylene protons, one pair (δ 3.07 and 2.67) correlating with a carbon resonance at δ 22.2, and the other (δ 1.75 and 1.84) giving one-bond correlations with a carbon resonance at δ 27.5 and cross-peaks in the $^1H,^{13}C$ HMBC spectrum with four quaternary carbon resonances (δ 110.2, 127.3, 140.3 and 158.7).

The most prominent features of the second substructure were a deshielded methylene resonance at δ 45.0 in the ^{13}C NMR spectrum, and a set of three quaternary carbon resonances at δ 173.0, 158.2, and δ 87.6, pointing to a substantial structural deviation from the menthofuran basic motif.

Since the proton- and carbon NMR data could not provide conclusive insights into the nature of the nitrogen functionalities of the dimer, the reaction was carried out under identical conditions but using $Na^{15}NO_2$ as the nitrous acid source. The ESI+/MS spectrum of the dimer prepared in this way gave a pseudomolecular ion peak at *m/z* 425, consistent with the incorporation of three ^{15}N atoms. The $^1H,^{15}N$ HMBC spectrum revealed three nitrogen resonances at δ 195, 280 and 380. The upfield resonance, suggestive of an amide-type nitrogen, was assigned to the second

structural unit based on the detection of a cross-peak with the allylic methyl of that unit. The other two nitrogen resonances were attributed to the first substructure on the basis of the following evidence: the signal at δ 380, typical of a nitro group, gave a cross-peak with the proton resonance at δ 5.08, whereas that at δ 280, compatible with an oxime-type functionality, correlated with the allylic CH_3 group of that moiety at δ 1.87. These spectroscopic data could be translated into a nitro-substituted 2-oximinofuran structure (**A**) for the first substructure, and an *O*-substituted 1,7a-dihydroxy-2-pyrrolinone system for the second moiety, with both partial structures **B** and **C** being compatible with the NMR data.

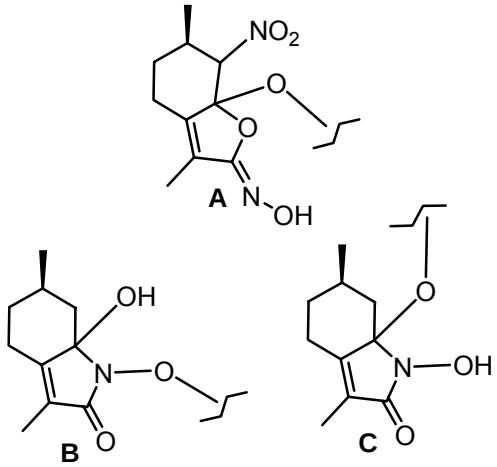

These substructures would exhibit different acidities since B is a hemi-aminal and C a hydroxamic acid and could be, in principle, distinguishable by methylation experiments with diazomethane. Thus, a compound made up of substructures **A** and **B** should give a monomethyl derivative, whereas a dimer built on **A** and **C** would instead afford a dimethyl derivative. LC-MS analysis indicated reaction product consistent with a monomethyl derivative, pointing to substructure **B** for the second moiety of the dimer.

To support this conclusion and select among the possible configurational options, a systematic computational effort aimed at simulating the NMR spectra for all possible model structures was carried out, using validated protocols based on DFT to calculate energies, geometries, and NMR chemical shifts.[211,212] Candidate structural models were geometry optimized at the DFT level, using the "hybrid" PBE0 functional,[208] which has been shown to provide quite satisfactory energies and geometries for a wide range of organic and biological systems,[211] as well as an accurate description of NMR parameters.[212] Solvent effects were considered in some test calculations using the polarizable continuum model (PCM, see experimental) and were found to exert a marginal influence on computed carbon shifts, so that use of in vacuo calculations is justified.

The relatively large molecular size of the product and the number of diastereomers/conformers to be explored combine to make the quantum-mechanical characterization computationally expensive. Therefore, a factorization of the problem was devised by analyzing the product into its two different moieties, and using a methoxy group to mimic the inter-moiety link. For the **A** moiety the configuration depicted in **I** corresponds to the best fulfillment of two criteria adopted to sort out the different structural possibilities, namely the correlation coefficients between computed and experimental carbon shifts, and the maximum chemical shift deviation from a linear correlation (Experimental Part-Computational details). Moreover, the predicted value (55°) for the H6-C6-C7-H7 dihedral angle is compatible with the small scalar coupling (4.0 Hz) observed between H-6 and H-7. As far as the **B** moiety is concerned, a satisfactory agreement between experimental and theoretical NMR data was obtained with the *O*-substituted 1-hydroxy-2-pyrrolinone ring **II**.

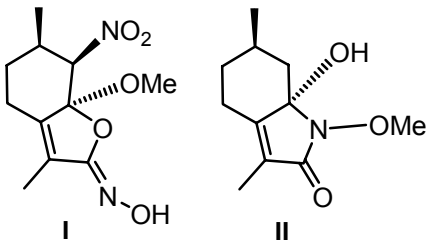

The combination of the two moieties led to structure **43** for the dimeric compound. A full conformational exploration of **43** was then performed at the same PBE0/6-31+G(d,p) level. A linear correlation plot between computed and experimental carbon chemical shifts for the entire structure gave a correlation coefficient of 0.9996. Furthermore, the constitution and configuration of **43** were further validated by the detection of ROESY contacts between the H-7 methine (δ 5.08) and the H-7' methylenes (δ 1.10 and 2.38), a finding computationally predicted for **43** but not for its 7a*R* diastereoisomer. A similar exploration was carried out for two other different diastereoisomers of **43**, and comparison with the available experimental information allowed to dispel both alternatives (Experimental part-Computational details).

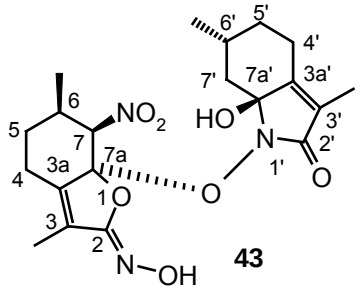

NMR data assignments for **42** and **43** are reported in Table 7.

Interestingly, on exposure to aqueous NaOH, the chromophore of **43** underwent an irreversible bathochromic shift to 440 nm, suggesting a base-induced degradation, presumably expressed as a β-elimination reaction that generates, along with the hydroxamate **44**, the extensively conjugated nitroderivative **45** (Scheme 7).

This view is consistent with the detection of two peaks with molecular weights corresponding to those of **44** and **45** in the LC-MS analysis of an UV bathochromically-shifted alkaline solution of **43**.

Table 7. NMR spectral data of **42** and **43** ($CDCl_3$).

	42			**43**			
	^{1}H (*J*,Hz)	^{13}C	^{15}N	^{1}H (*J*,Hz)	^{13}C	^{15}N	^{13}C, computed
1	-	-	126	-	-	-	
2	-	173.1	-	-	158.7	-	161.7
2-N	-	-	-	-		280	
3	-	136.6	-	-	127.3	-	132.1
3a	-	155.5	-	-	140.3	-	146.7
4	2.45 (m), 2.75	21.5	-	2.67 (d, 3.2),	22.2	-	24.0
5	1.40 (m), 2.00	31.8	-	1.75 (m), 1.84	27.5	-	26.9
6	2.60 (m)	30.1	-	2.67 (m)	33.1	-	33.2
7	5.77 (d, 4.0)	115.8	-	5.08 (d, 4.0)	90.4		92.0
7-N	-	-	-	-	-	380	
7a	-	141.5	-	-	110.2	-	110.6
3-	1.87 (s)	8.1	-	1.87 (s)	8.5	-	7.5
6-	1.14 (d, 6.8)	21.4	-	1.08 (d, 6.8)	17.8	-	16.3
1’				-	-	195	
2’				-	173.0	-	175.3
3’				-	122.8	-	127.3
3a’				-	158.2	-	165.2
4’				2.37 (m), 2.57	24.2	-	24.8
5’				0.97 (m), 1.97	36.2	-	37.2
6’				2.06 (m)	28.0	-	28.6
7’				1.10 (m), 2.38	45.0	-	45.1
7a’				-	87.6	-	87.1
3’-				1.74 (s)	7.9	-	7.3
6’-				0.98 (d, 6.8)	21.0	-	19.9

A possible mechanism for the formation of **43** is outlined in Scheme 8. Attack of nitrosonium ion to the unsubstituted α-position of the furan ring could afford a sigma intermediate (**46**) susceptible of pseudo-benzylic deprotonation or, alternatively, water trapping, affording eventually, after tautomerization of the nitroso group, the 2-oximinofuran derivatives **47** and **48**. The former can undergo further addition of nitrosonium ion to its enol moiety, generating, after nitroso-to-nitro oxidation and restoration of the double bond, the nitro-olefin **49**. Conversely, the hemiketal **48** could

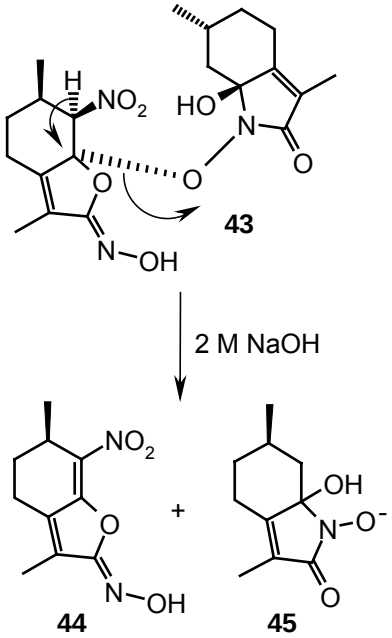

Scheme 7

generate an open ketohydroxamic acid (**50**), in equilibrium with its cyclic *N*-hydroxylactam tautomer (**51**). This might then add to the nitroolefin moiety of **49** in a Michael fashion, eventually affording **43**.

This reaction sequence could also accommodate the formation of the lactone **41** from intermediate **50**, since hydroxamic acids are hydrolyzed to carboxylic acids following exposure to nitrosating agents.[242] Lactam **42** might result from a more complex process involving dehydration of **51** and a deoxygenation step, possibly by redox exchange with some reaction intermediates, but this mechanism escaped elucidation.

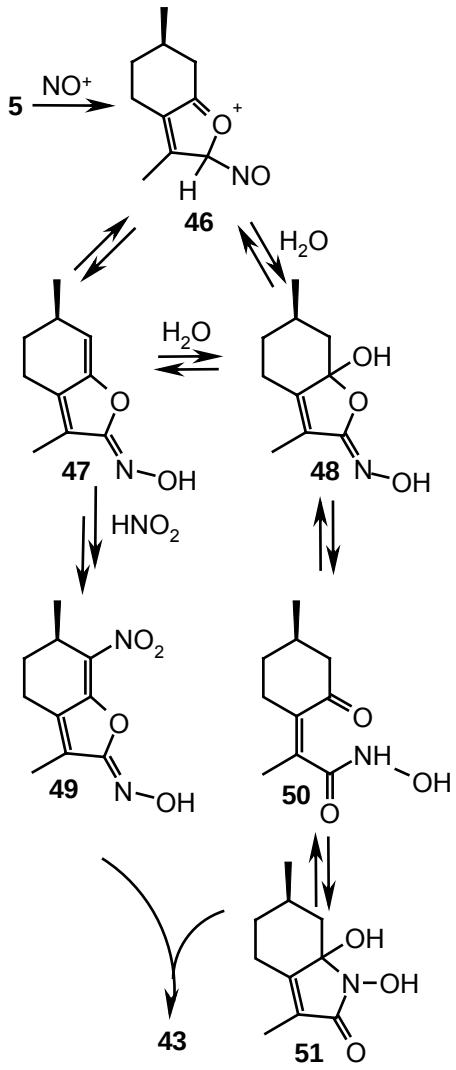

Scheme 8

2.7. New synthetic approach to the endogenous antioxidant 2-*S*-cysteinyldopa.

The observation that **11** and related 3,4-dihydroxyphenylpropenoic acid derivatives react with thiol compounds under oxidative conditions to give mainly 2-*S*-conjugates, instead of the usual 5-*S*-conjugates that are formed with simple 4-alkylcatechols, such as dopa, dopamine, and 4-methylcatechol, has proved the basis for a new synthetic approach to 2-*S*-cysteinyldopa (**14**) which revolves around an amino-substituted 3,4-dihydroxyphenylpropenoic acid which would expectedly form a 2-*S*-adduct by oxidative conjugation with L-cysteine. Stereoselective reduction of the propenoate moiety would then afford the desired product **14** with both amino acids in the natural L-configurations.

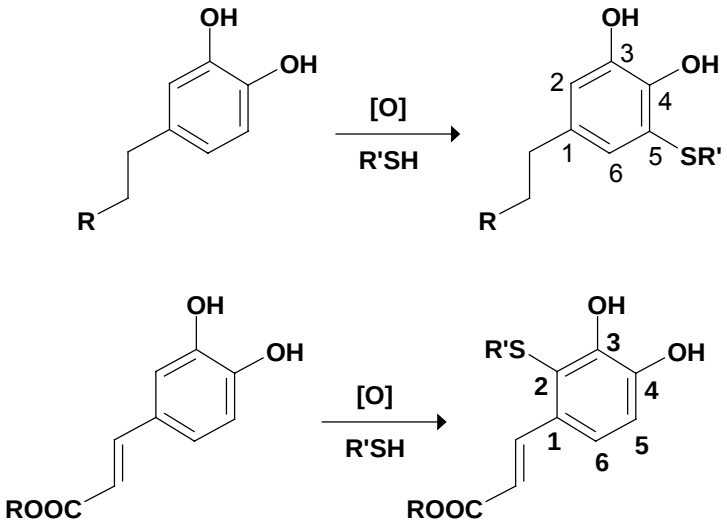

Accordingly, 2-acetylamino-3-(3,4-dihydroxyphenyl)propenoic acid (**52**) was prepared by a Knoevenagel-type condensation of 3,4-dihydroxybenzaldehyde with *N*-acetylglycine in acetic anhydride at 120 °C followed by hydrolysis of the ethyl acetate extracts containing the oxazolone intermediate (Scheme 9).[243] After removal of some unreacted starting material by ethyl ether extraction, product **52** (> 95% purity) was isolated in 60% yield.

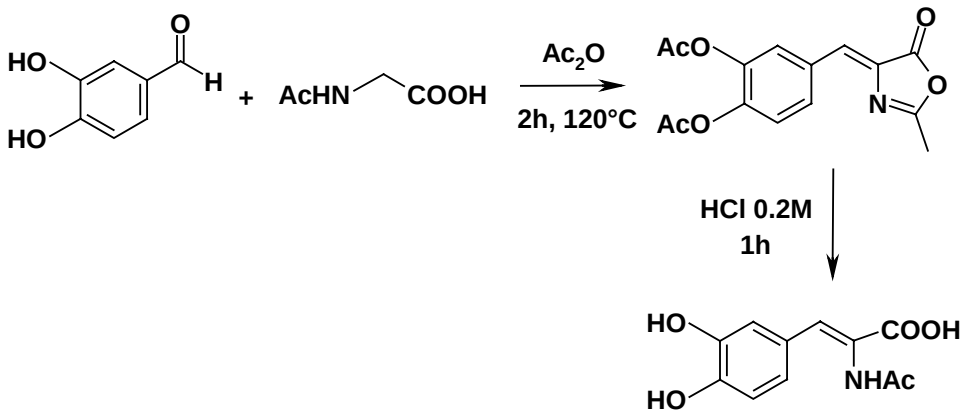

Scheme 9 **52**

Several oxidants were then screened to install the cysteinyl moiety onto the desired position of **52**. To this aim, *N*-acetylcysteine was preferably used in the place of cysteine to prevent intramolecular cyclization of the amino group on the quinone produced by oxidation of **52**. Under a variety of conditions, however, di- and tri-cysteinyl adducts were invariably obtained as main products because of the increased ease to oxidation of the initial *S*-conjugate with respect to the starting material. This difficulty was overcome by using commercially available mushroom tyrosinase as the oxidant. Thus, in line with our expectations, enzyme-promoted oxidation of **52** in the presence of 2 molar equivalents of *N*-acetylcysteine in aqueous buffer at pH 7.4 resulted in a complete consumption of the starting material after 2 h with formation of the desired (*Z*)-2-*S*-cysteinyl-3-(3,4-dihydroxyphenyl)-2-acetylaminopropenoic acid (**53**), isolated in 55% yields by preparative HPLC (Scheme 10).

Asymmetric hydrogenation of the *Z*-double bond in **53** was achieved in the presence of a rhodium chiral biphosphine catalyst[244] in a Parr apparatus. Purity of the starting material with respect to residual cysteine contamination proved critical because of catalyst poisoning, and hence a chromatographic purification prior to hydrogenation proved necessary.

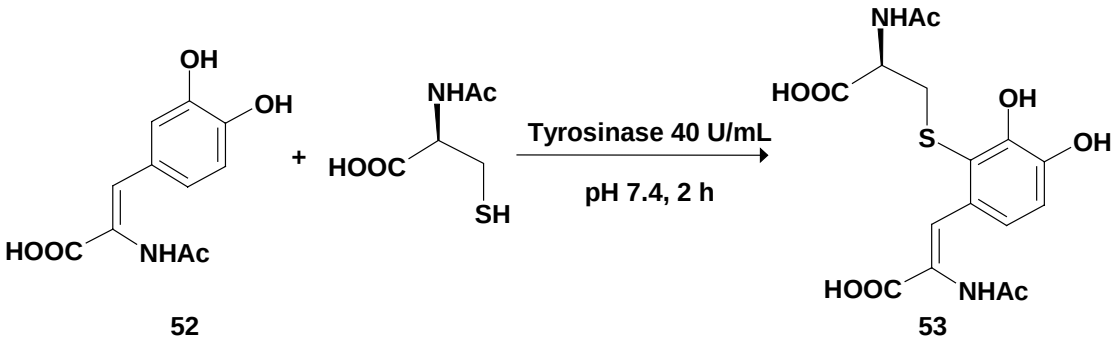

Scheme 10

Under 50 atm hydrogen pressure, with a 3 mol% catalyst loading and methanol as the solvent, the reaction was complete within 72 h (Scheme 11). Acid hydrolysis of the hydrogenation mixture under reflux eventually afforded **14** in 90%yield with a diastereoisomeric excess of 90% by HPLC analysis. Product identity was secured by comparison with an authentic sample, while purity was checked by NMR analysis.

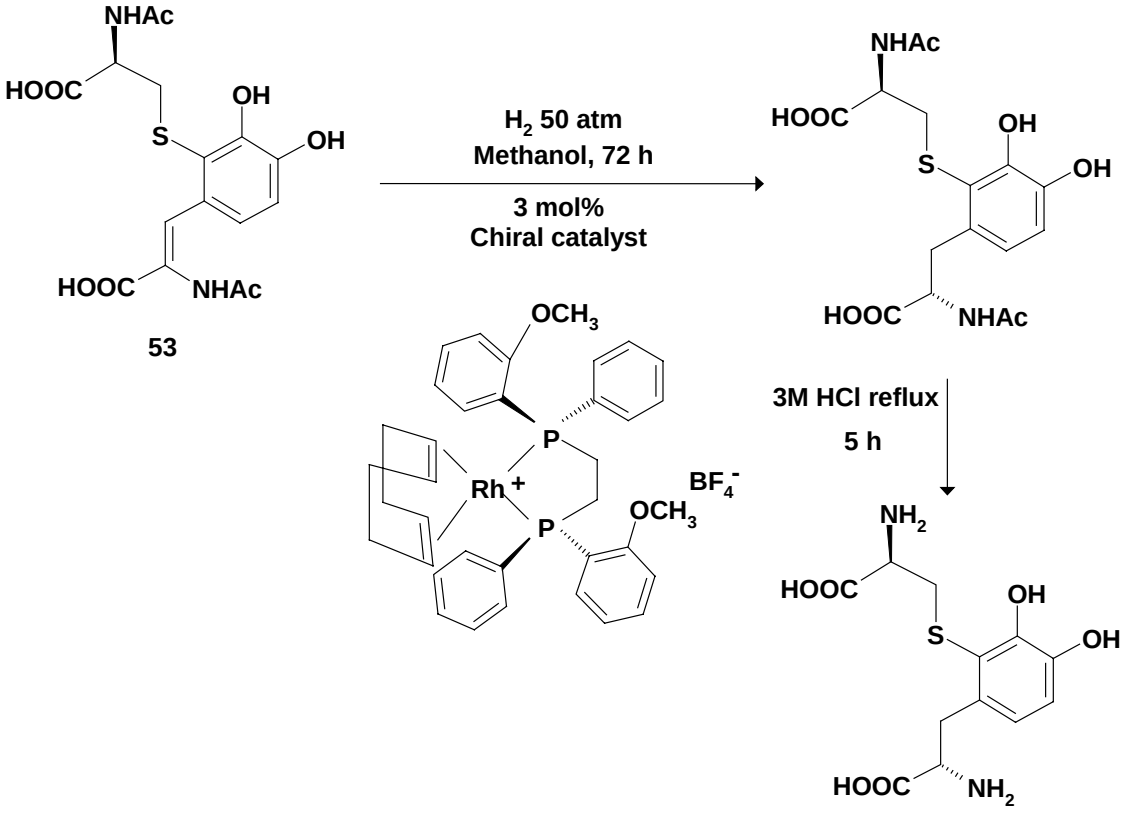

Scheme 11

2.8. The "Benzothiazine" Chromophore of Pheomelanins: a Reassessment.

Recently, the first ultrafast absorption spectroscopy measurements for synthetic pheomelanin have been reported, and have highlighted the fast generation of a transient species with an absorption maximum centered at 780 nm.[245] This species has been attributed to a photoexcitation product whose action spectrum peaks in the range between 350-360 nm, thus resembling the reported absorption spectrum of benzothiazines. It was argued that the reactive chromophore of pheomelanins is of low molecular weight but is present and exhibits similar photophysics in the aggregated state, and may be adequately described in terms of "benzothiazine" structural motifs which are biogenetically derived from the key pigment precursor, 5-*S*-cysteinyldopa.[246] It must be noted, however, that the occurrence of benzothiazine units in the pheomelanin backbone is largely a matter of surmise, and has so far lacked direct and unambiguous experimental support. Moreover, the term "benzothiazine" which surfaces in many reports is chemically little informative, due to the broad range of structural motifs that may fall under this category and the associated variety of chromophoric features. Nonetheless, this notion has become a central axiom in pheomelanin research and has in part been built upon the identification many decades ago in pheomelanin-containing tissues of a peculiar group of low molecular weight compounds, the trichochromes, featuring the peculiar $\Delta^{2,2'}$-bi(2*H*-1,4-benzothiazine) skeleton. [247,248]

On this basis, a critical assessment of the spectrophotometric properties of pheomelanins and of the putative precursors that are generated in the oxidation of cysteinyldopas is mandatory to provide a comparative description of the UV absorption properties of these compounds with a view of determining whether and to

what extent each of them can be included among the primary determinants of the pheomelanin "chromophore".

The electronic absorption spectra of natural and synthetic pheomelanins obtained under conditions ensuring minimal structural alterations have been recorded in 0.1 M phosphate buffer pH 7.4 (Figure 22). Selected pigments included a natural sample from red human hair, that was freed from the proteic matrix by a reported enzymatic procedure[249,250] and two standard synthetic pheomelanins produced by peroxidase/H_2O_2 oxidation of **13** in the presence and in the absence of Zn^{2+}. The peroxidase/H_2O_2 couple was chosen as the oxidizing system since it ensured an efficient oxidation of **13** with substantial and rapid consumption of the substrate as shown in previous studies.[251,252] Under different reaction conditions including aerial or tyrosinase catalyzed oxidation the kinetic of the process is much lower, and the yields of the final pigment are rather poor.[251] Inclusion of Zn^{2+} in the oxidation mixture was suggested by the high levels of the metal in human red hair[253] and by its established stabilizing effect on the course of pheomelanogenesis *in vitro*,[249] allowing for a more clear-cut detection of intermediate species and more defined chromatographic profiles.

Inspection of the absorption profiles in Figure 22 showed a gross similarity between the natural and synthetic pigment samples. A salient common feature includes a flat maximum around 305 nm with barely detectable inflections at shorter and longer wavelengths, and in all cases a low featureless absorption above 500 nm, indicating limited scattering effects compared e.g. to eumelanins. Despite such similarities, however, some differences emerged relating to the shapes of the traces, and the presence/positions of inflections.

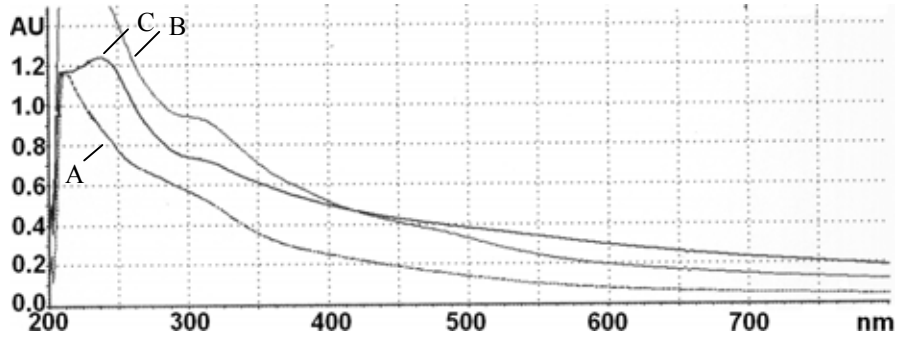

Figure 22. Absorption spectra at pH 7.4 of natural pheomelanin from human hair (A) and synthetic pheomelanin from 5-*S*-cysteinildopa prepared in the presence (B) and in the absence (C) of Zn^{2+}.

To inquire into the nature of the species responsible for the basic chromophoric features of the pheomelanin pigments, the spectrophotometric changes accompanying the oxidative conversion of 5-*S*-cysteinyldopa in the presence and in the absence of Zn^{2+} were investigated. Data in Figure 23 indicated a profound effect of Zn^{2+} which markedly slowed down the kinetic course of the reaction and allowed for detection of well defined chromophoric phases. Comparison of traces in Figure 23a *vs* 23b indicated in the latter case the fast development within 30 s of two absorption maxima, one at 309 nm, which survived after 2 h, and the other at 339 nm, which decayed within few minutes.

By contrast, in the presence of Zn^{2+} (Figure 23a) a well defined chromophore with a maximum centered at 390 nm developed within the first minutes. Following addition of ethylenediaminetetraacetic acid (EDTA), this chromophore underwent ipsochromic shift to 337 nm suggesting a Zn^{2+}-chelate (not shown). Gradually, the 390 nm chromophore was replaced by two bands at 302 and 356 nm but, after 24 h, only the band at 302 nm was detectable. Centrifugation of the mixture at this stage allowed separation of the pheomelanin pigment which, taken up in phosphate buffer,

gave the absorption spectrum in Figure 1. UV analysis of the supernatant revealed a chromophore with an absorption maximum at 302 nm contributing to a significant extent to the absorption properties of the whole mixture (not shown).

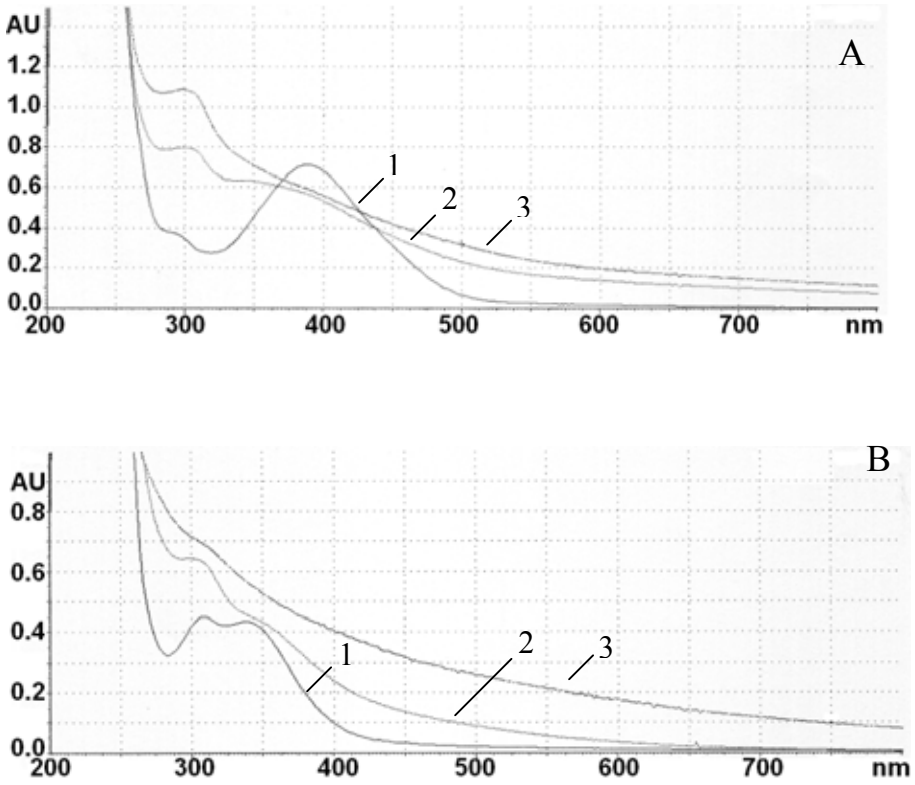

Figure 23. Spectral changes during oxidation of 5-S-cysteinyldopa in the presence (a) and in the absence (b) of Zn^{2+}. Plot a: trace 1, 15 min; trace 2, 3 h; trace 3, 24 h. Plot b: trace 1, 30 s; trace 2, 5 min; trace 3, 2 h.

Based on these preliminary data, the species formed at the various chromophoric phases in Figure 23 were investigated by HPLC analysis with UV and ESI+/MS detection (Figure 24).

The HPLC elution trace of the oxidation mixture carried out in the presence of Zn^{2+} at 15 min reaction time (Figure 24, panel a) indicated a single major species (R_T

9.5 min) exhibiting higher absorption at 340 than at 280 nm, which gave a pseudomolecular ion peak $[M+H]^+$ at *m/z* 297 (panel b).

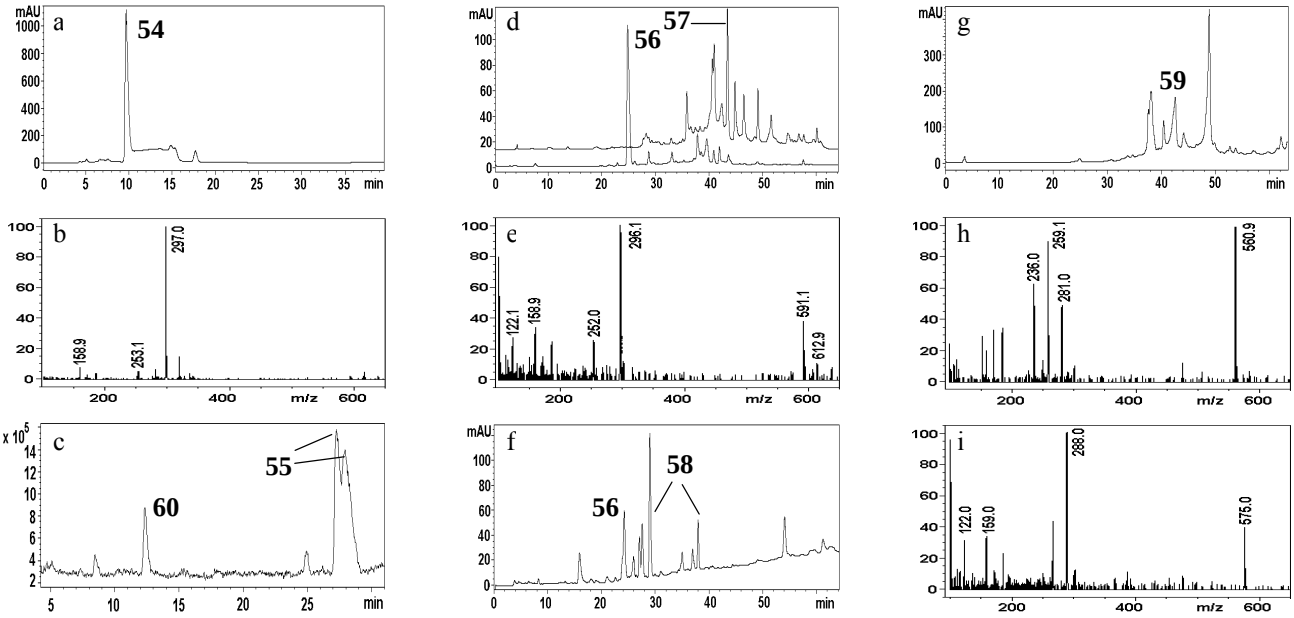

Figure 24. HPLC elution profiles and ESI+/MS spectra of the mixtures obtained by oxidation of **13** in the presence of Zn^{2+}: (a) elution profile of the mixture at 15 min reaction time (eluant II, detection at 340 nm); (b) ESI+/MS spectrum of the species eluting at 9.5 min; (c) LC/ ESI+/MS elution profile of the mixture at 15 min reaction time after reduction with NaBH4 (eluant I); (d) elution profile of the mixture at 3 h reaction time (eluant I, lower trace, detection at 280; upper trace detection at 340 nm); (e) ESI+/MS spectrum of the species eluting at 40.6, 40.9 and 43.4 min; (f) elution profile of the mixture at 3 h reaction time after reduction with $NaBH_4$ (eluant I, detection at 280 nm); (g) elution profiles of the mixture at 5 h reaction time (eluant I, detection at 460 nm); (h) ESI+/MS spectrum of the species eluting at 42.9 min; (i) ESI+ /MS spectrum of the species eluting at 49.2 min. Elutographic peaks corresponding to identified compounds are marked with structural numbers.

Reduction of the mixture with sodium borohydride resulted in formation of a 1:1 mixture of two related compounds (panel c, R_T 27.3 and 27.9 min) with absorption maxima at 290 nm and pseudomolecular ion peaks $[M+H]^+$ at *m/z* 299. On this basis, it was concluded that the first formed species was the benzothiazine carboxylic acid **54**. This forms a stable Zn^{2+} complex, giving the maximum at 390 nm, that can be reduced to give diastereoisomeric 3-carboxy dihydrobenzothiazines (**55**).

HPLC analysis of the mixture after 3 h (panel d) revealed complete conversion of the benzothiazine **54** into a number of species including the 3-oxo-3,4-dihydrobenzothiazine derivative **56** (lower trace at 280 nm, R_T 25.1 min, $[M+H]^+$ *m/z* 269) and the diastereoisomeric 2,2'-bi(2*H*-1,4-benzothiazine) dimers **57** eluted at R_T 40.6, 40.9, 43.4 min (upper trace at 340 nm, $[M+H]^+$ *m/z* 591, panel e). The above structural assignments were supported by the different behavior to sodium borohydride reduction: whereas the amide **56** resisted the treatment (panel f) as confirmed also in separate experiments on standard samples, the dimers **57** gave the reduction products ($[M+H]^+$ *m/z* 595) corresponding to the gross structure **58** two of which were identified as the species eluting under peaks at R_T 29.0 min and 37.9 min (panel f) with absorption maxima in fairly good agreement with literature data.[249] Most of the products shown in the profile taken at 340 nm were converted by the reduction treatment and were well detectable at 280 nm.

After 5 h chromatographic analysis showed gradual conversion of the dimers **57** into a collection of unidentified species exhibiting intense absorption at 460 nm (panel g) among which a peak eluting at R_T 42.9 min ($[M+H]^+$ at *m/z* 561, panel h) was identified as trichochrome C (**59**)[254] by comparison of the chromatographic behavior and chromophoric features with those of an authentic sample.[249] Panel i shows the mass spectrum of the species eluting at R_T 49.2 min with a pseudomeolecular ion peak

$[M+H]^+$ at *m/z* 575, suggesting a trichochrome-related structure. Structural elucidation of this species and the other major components of the oxidation mixture of 5-*S*-cysteinyldopa at this stage is the focus of ongoing studies. At 24 h reaction time, when the oxidation process was apparently come to an end and no further chromophoric change was detectable, HPLC analysis indicated loss of dimers **57** and trichochromes, but persisting quantities of the amide **56** and substantial amounts of more polar species eluding isolation and characterization.

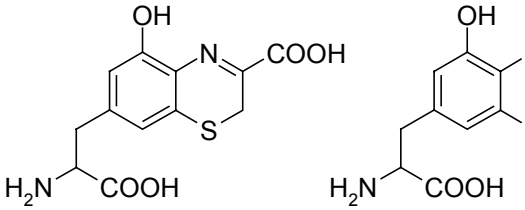

54

55

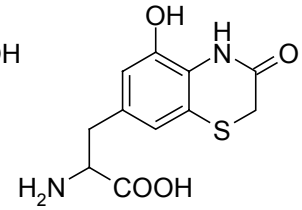

56

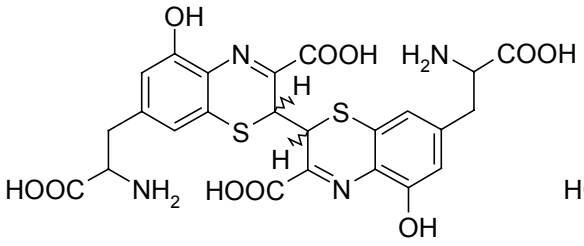

57

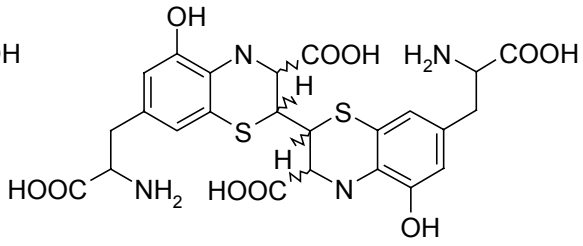

58

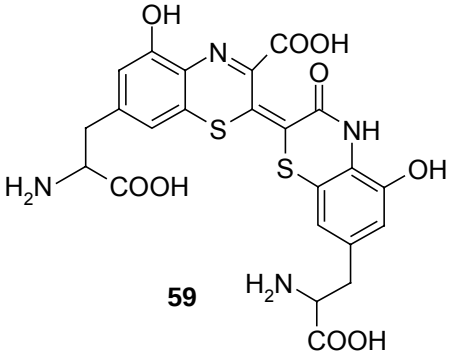

59

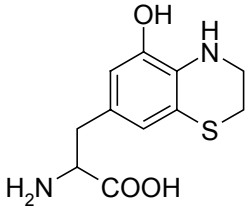

60

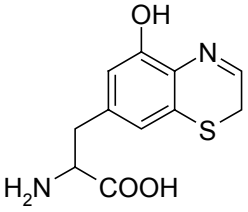

61

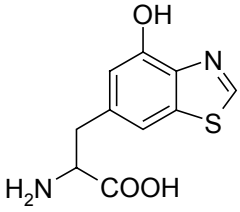

62

HPLC analysis of the reaction mixture obtained in the absence of Zn^{2+} at 5 min showed a poorly defined chromatographic pattern. However after reduction with sodium borohydride distinct species were apparent, which could be identified as the dihydrobenzothiazine **60** (R_T 12.0 min, $[M+H]^+$ *m/z* 255) and the diastereoisomeric dihydrobenzothiazine-3-carboxylic acids **55** at 3:1 ratio (Figure 4, panel a, b). This indicated the formation in the very early phases of the reaction of decarboxylated derivative **61** along with very small amounts of the benzothiazine carboxylic acid **54**. The ratio of the diastereoisomeric dihydrobenzothiazines **55** different from the 1:1 expected by sodium borohydride reduction of **54** suggests that the isomer of **55** having configuration at C-3 related to L-cysteine was present in the reaction mixture prior to reduction, as a result of a redox exchange process between the *o*-quinonimine generated by cyclization of the cysteine chain of 5-*S*-cysteinyldopa with 5-*S*-cysteinyldopa itself.[255] After 1 h the dihydrobenzothiazine **60** had decayed (panel c) and the major components of the reduced mixture were the 3-oxo-3,4-dihydrobenzothiazine **56** and a compound at R_T 20.3 min ($[M+H]^+$ *m/z* 239, panel d), identified as the benzothiazole **62** by comparison with an authentic sample.[256] In separate experiments it was shown that, similarly to **56**, the benzothiazole **62** resisted sodium borohydride reduction.

Given the different behavior of the various benzothiazine intermediates to sodium borohydride reduction, it was reasoned that the treatment of pheomelanins with sodium borohydride might yield important clues as to the nature of the main structural units. Thus, in a final experiment it was assessed whether exposure to sodium borohydride caused any detectable change of the pheomelanin chromophore, and it was found that under the conditions in which the benzothiazine carboxylic acid

54 is efficiently reduced, the pheomelanin chromophore (both natural and synthetic samples) is unaffected (not shown).

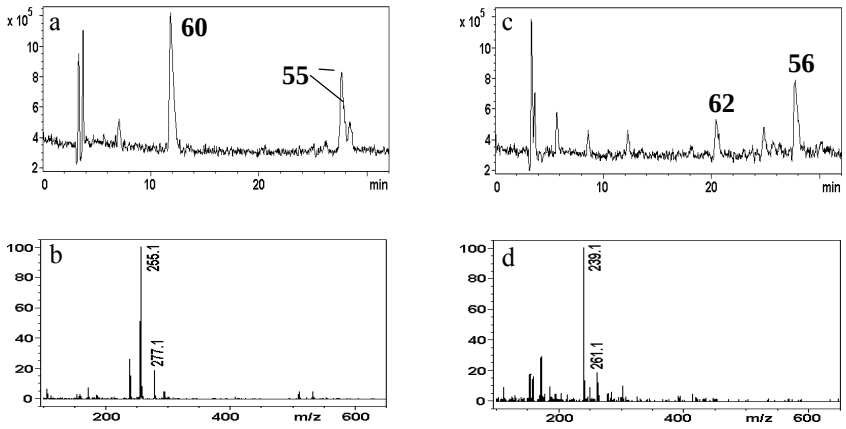

Figure 24. LC/ESI+/MS elution profiles and ESI+/MS spectra of the mixtures obtained by oxidation of **13** in the absence of Zn^{2+}: (a) LC/ESI+/MS elution profile of the mixture at 5 min reaction time after reduction with $NaBH_4$ (eluant I); (b) ESI+/MS spectrum of the species eluting at 12.0 min; (c) LC/ESI+/MS elution profile of the mixture at 2 h reaction time after reduction with $NaBH_4$ (eluant I); (d) ESI+/MS spectrum of the species eluting at 20.3 min. Elutographic peaks corresponding to identified compounds are marked with structural numbers.

From the experiments so far described, a number of conclusions can be drawn. First of all, it can be argued that Zn^{2+} affects in part the kinetic, chemical and spectrophotometric course of 5-*S*-cysteinyldopa oxidation favoring in particular retention of the carboxylic group in the early benzothiazine intermediates, but does not seem to modify to any appreciable extent the general features of the final pigment. This would be supported by the observation in Figure 22 indicating similar spectra for synthetic pheomelanins prepared in the presence and in the absence of Zn^{2+}.

Another central point emerging from the present results is that not all the "benzothiazine" units supposed to contribute to the pheomelanin chromophore exhibit absorption spectra entirely consistent with the observed features of the final pigments.[257] In particular, those structural components based on the 2*H*-1,4-benzothiazine ring system or the trichochrome skeleton would exhibit absorption maxima at relatively higher wavelengths than 305 nm, where the most characteristic feature of the pheomelanin chromophore occurs. Moreover, such 2*H*-1,4-benzothiazine units would be reducible by borohydride with a detectable ipsochromic shift, an effect that was not observed on pheomelanin pigments. On the other hand, the 3-oxo-3,4-dihydrobenzothiazine structure, which is found both in a monomer intermediate and as a structural moiety in the trichochrome skeleton, displays absorption and chemical properties that suggest a major presence in the pheomelanin backbone. Indeed, the significance of 3-oxo-3,4-dihydrobenzothiazine moieties as a final evolution product of 3-carboxy-2*H*-1,4-benzothiazine moieties, their characteristic absorption at 305 nm and their insensitivity to sodium borohydride treatment would concur to support this conclusion.

Interestingly, a careful scrutiny of the literature would indicate that in addition to the 3-oxo-3,4-dihydrobenzothiazine system, also benzothiazole units absorb at significantly lower wavelengths compared to 2*H*-1,4-benzothiazines and might likewise contribute to the chromophore of pheomelanins. In particular, benzothiazole **62** has a maximum at 303 nm. Moreover, benzothiazoles are not reducible with sodium borohydride, and their formation is another possible evolution pathway of 2*H*-1,4-benzothiazines via ring contraction. This latter step may occur at various stages of pheomelanin build up, either before or after the pigment backbone has been

assembled. In this connection, it may be worth noting that early tentative structural models of pheomelanins incorporated benzothiazole but not benzothiazine units.[258,259]

In Figure 25 the absorption spectrum of natural pheomelanin is shown together with those of putative structural units, to permit a better appreciation of the above reasonings. It is well apparent that besides the two main chromophores accounting for the absorption around 305 nm (traces B and C), non-reducible 2,2'-bi(3-carboxybenzothiazine) and trichochrome-like units may contribute to the long wavelength absorption.

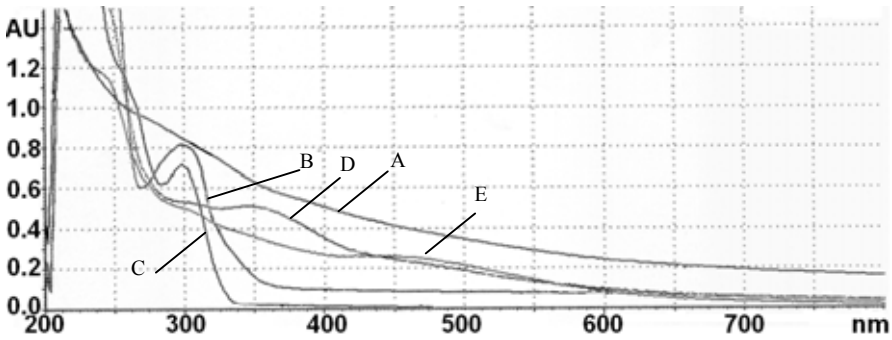

Figure 25. Absorption spectra at pH 7.4 of natural pheomelanin from human hair (trace A), 3-oxo-3,4-dihydrobenzothiazine **56** (B), benzothiazole **62** (C), dimers **57** (D) and trichochrome C **59** (E).

A scheme summarizing the origin of the main chromophoric units in pheomelanin is provided in Scheme 12.

Clearly, this is an oversimplification of the actual process of generation of the pheomelanin chromophore. The chromophoric changes accompanying oxidative conversion of 5-*S*-cysteinyldopa to pheomelanin have been interpreted for the first time in terms of structurally defined intermediates and pigment precursors, which have been analyzed for their absorption properties and reduction behavior.

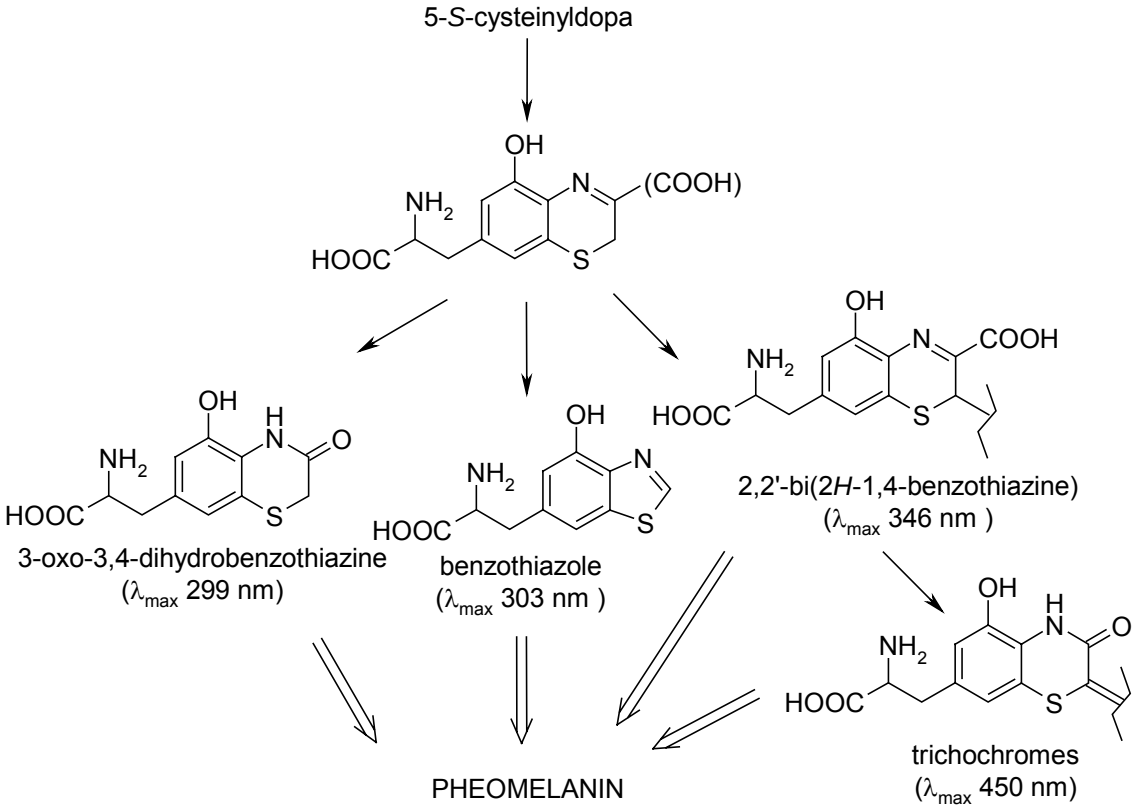

Scheme 12.

However, beyond a guess about the involvement of 3-oxo-3,4-dihydrobenzothiazine and benzothiazole units it is not possible to go. It is likely that the gradual broadening of the absorption spectrum of the first formed chromophores with consequent loss of the structural features in the final pigment is due to an oxidative breakdown of dimeric trichochrome-like oligomers, but the effect of superposition of the absorptions due to different species can not be rationalized nor excluded at the present level of analysis.

3.CONCLUSIONS

Overall, the research work has led to definition of the reaction pathways of a number of polyphenols mostly of dietary origin with peculiar attention to their transformations when acting as antioxidant or antinitrosating agents under conditions of physiological relevance. Moreover, straightforward synthetic methodologies for preparation of new compounds designed by combination of polyphenols and thiols of natural origin have been developed and their potential has been assessed by current assays.

Of particular interest are the results obtained in the investigation of the oxidation chemistry of hydroxytyrosol, the well known antioxidant from extra virgin olive oil, which had not been previously explored. The peculiar effect of hydrogen peroxide on the normal course of the reaction was highlighted supporting the proposed role of olive phenols as hydrogen peroxide scavengers. Moreover, the specific H_2O_2-dependent oxidative pathway of 4-alkylcatechols was defined revolving on the marked nucleophilic character of hydroxylated product initially generated by addition of hydrogen peroxide to the *ortho*-quinone of hydroxytyrosol.

The unusual reactions of phenolic stilbene antioxidants reveratrol and piceatannol occurring mostly in red wines and grapes toward acidic nitrite under conditions of relevance to gastric compartments was characterized highlighting the hitherto overlooked susceptibility of these compounds to oxidative cleavage under mild conditions, and the formation of the dimer restrytisol B under non-enzymatic conditions. Nitration of resveratrol is also of chemical interest as it may provide an entry to novel functionalized stilbene derivatives *via* proper manipulation of the products nitrated on the stilbene double bond or the phenolic ring ..

The relative RNS scavenging properties of a series of glutathionyl conjugates (**36**,

37, **38b** and **39**) of dietary catechols (**1**, **4b**, **11** and **12**) was assessed in two different assays based on nitrosation and nitration processes. When tested in the DAN nitrosation assay at mildly acidic pH, which is by far the most relevant for toxic nitrosamine formation in the stomach, the most efficient antinitrosating agent proved the GSH conjugate of piceatannol for which a novel and convenient synthetic procedure was also developed. The lack of any relationship between the antinitrosating properties and the antioxidant capacity of the catechols investigated is another interesting outcome of this study, as is the differential behavior of certain polyphenols and their *S*-glutathionyl conjugates in the nitrosation and nitration assays. This raises the caveat that evaluation of the RNS scavenging properties of polyphenols may be biased by the type of assay. When considered also in the light of previous studies on the scavenging properties of caffeic acid derivatives, green tea catechins and related flavonoids against nitrous acid-derived RNS,[147] this study contributes to identify some crucial structural factors that may guide in the quest for novel efficient antinitrosating agents for cancer chemoprevention. Potential applications of the compounds prepared encompasses different fields, especially cosmetic and pharmaceutical industries. Many ingredients used in formulations of cosmetic and personal care products contain nitrogen and thus there is an hazard related to formation of *N*-nitrosamines, such as *N*-nitrosodiethanolamine (NDEA) which may arise by nitrosation of DEA, a wetting agent presents in shampoos, lotions and creams. Use of antinitrosating agents in combination with drugs is highly recommended as is the case of aminophenazone or piperazine, which have been shown to undergo nitrosation under simulated gastric conditions.

An extension of this research work concerns the preparation of a lipophilic antioxidant derived from hydroxytyrosol and lipoic acid, 5-*S*-lipoylhydroxytyrosol.

This represents the first derivative of hydroxytyrosol with a higher radical scavenging activity than the parent compound prepared trough a suitable modification of the catecholic nucleus but without alteration of the alcoholic or phenolic functionality. Such a compound may potentially be exploited in preparation of multi-functional foods as a natural antioxidant in contrast with the widely used synthetic phenolic, antioxidants whose employment has been questioned by the carcinogenic effects demonstrated in living organisms.

Well framed in this general context is the comparative investigation of the reactions of menthofuran , an important naturally occurring furan derivative found in various mint oils, with nitric acid and nitrous acid. In the presence of sulfuric acid, nitric acid induced mainly a fragmentation reaction of menthofuran into two carbonyl compounds eventually trapped by the unreacted starting material as bis-furanyl adducts The isolation yields of these compounds one of which was the important fragrant terpenoid dehydromenthofurolactone (anhydro Woodward-Eastman lactone). were relatively high and hence of synthetic interest.. By contrast, exposure of menthofuran to nitrous acid led to a quite different pattern of products, including notably an unusual dimer (**43**), featuring an unprecedented 2*H*-indol-2-one-1-oxyl-2*H*-benzo[b]furan-2-one oxime structure with three different nitrogen functionalities. The structure of this compound was elucidated by an integrated spectral and theoretical approach that exemplified the power of ^{15}N NMR spectroscopy in combination with DFT methods for elucidation of complex nitrogen containing structures. Characterization of these and other minor reaction products contributes to draw the nitrosation chemistry of 2,3,4-trisubstituted furans which had so far remained virtually uncharted.

In the field of endogenous antioxidants, one of the main outcome of the research was the development of the first direct synthesis of the human melanogen 2-S-cysteinyldopa by a convenient three-step procedure with in overall 30% yield. This is by far the highest yield for this biologically and clinically relevant amino acid, that has so far been obtained only as a minor side product in the synthesis of 5-S-cysteinyldopa. Availability of this melanogen on gram scale is expected to open up the doorway to novel insights into pheomelanin pigments which derive biogenetically by oxidation of cysteinyldopas.

Finally, it was possible to provide evidence that the commonly held axiom that the pheomelanin chromophore is made up of "benzothiazine" units is ambiguous and must be revisited in the light of a detailed analysis of the chemical and spectrophotometric features of the main intermediates involved in the build up of the pheomelanin chromophore.

4. EXPERIMENTAL SECTION

4.1 General methods

UV spectra were performed with a Beckmann DU 640 spectrophotometer. IR spectra were recorded on a FT-IR instrument. LC/MS analysis were carried out on an instrument equipped with an ESI ion source; an octylsilane-coated column, 150 mm × 4.6 mm, 5 μm particle size (Zorbax, Eclipse XDB-C8) at 0.4 mL/min was used.

High resolution (HR) electrospray ionization in positive ion mode (ESI+)/MS spectra were obtained in methanol/2% formic acid 1:1 v/v. ^{1}H and ^{13}C NMR spectra were recorded in $CDCl_3$ with a Bruker WM 400 spectrometer at 400.1 and 100.6 MHz, respectively. The instrument was equipped with a 5 mm ^{1}H/broadband gradient probe with inverse geometry. ^{1}H, ^{1}H COSY, ^{1}H, ^{13}C heteronuclear multiple quantum coherence, ^{1}H, ^{13}C HSQC-DEPT, ^{1}H, ^{13}C heteronuclear multiple bond correlation, ^{1}H, ^{15}N HMBC and rotating frame nuclear Overhauser effect spectroscopy (ROESY) experiments were run using standard pulse programs from the Bruker library. Double-quantum filtered (DQF) COSY spectrum was recorded at 600 MHz. Chemical shifts are reported in δ values downfield from TMS (^{1}H and ^{13}C NMR) or relative to NH_3 (liquid, 298 K) at 0.0 ppm (^{15}N NMR).

Analytical and preparative TLC was carried out on silica gel plates (0.25 and 0.50 mm, respectively) from Merck. Column chromatography was performed using silica gel (0.063-0.200 mm). Analytical HPLC was carried out on an instrument equipped with an UV-vis detector. The chromatographic separation was achieved on an octadecylsilane coated column, 250 mm × 4.6 mm, 5 μm (Sphereclone, Phenomenex) using binary gradient or isocratic elution conditions. For preparative purposes, HPLC was carried out on an instrument equipped with an UV detector set at 280 nm and the

chromatographic separation was achieved on a preparative Econosil C18 column (250 mm × 22 mm, 10 μm).

Tyrosol (2-(4-hydroxyphenyl)ethanol) was from Fluka; Caffeic acid, chlorogenic acid, 4-methylcatechol, 2-iodobenzoic acid, oxone® ($2KHSO_5$-$KHSO_4$-K_2SO_4), $Na_2S_2O_4$, $Na_2S_2O_5$, $NaIO_4$, $K_3Fe(CN)_6$, $NaNO_2$, [^{15}N]$NaNO_2$ (99%), GSH, *N*-acetylglycine, *N*-acetyl-L-cysteine and $NaBH_4$ were from Aldrich Chemie; hydrogen peroxide (30% solution in water) was from Carlo Erba; horseradish peroxidase type II (HRP) (EC 1.11.1.7) and mushroom tyrosinase was from Sigma. 4-methyl-1,2-benzoquinone[10] was prepared as reported. Resveratrol, (*R*)-Menthofuran, 2,3-diaminonaphthalene (DAN), 2,2-diphenyl-1-picrylhydrazyl radical (DPPH), L-tyrosine, 3-nitrotyrosine, hydroxyacetone, *rac*-3-methylcyclohexanone and DDQ were used as obtained. Cyclooctadiene-1,5[(*R*,*R*)1,2-ethanediylbis(*o*-methoxyphenyl)phenylphosphine]rhodium tetrafluoroborate was obtained by Acros organics. Diazomethane was obtained from *N*-methyl-*N*-nitroso-*p*-toluenesulfonamide by treatment with KOH/ethanol.

Caution: diazomethane is explosive and must be collected in peroxide-free ether in a dry ice/acetone bath and kept at –20 °C. Note that diazomethane is also toxic and carcinogenic and should be handled an a fume hood.

5-*S*-cysteinyldopa was prepared from L-Dopa and L-cysteine. 7-(2-Amino-2-carboxyethyl)-5-hydroxy-3,4-dihydro-2*H*-1,4-benzothiazine (**61**) 7-(2-amino-2-carboxyethyl)-5-hydroxy-3,4-dihydro-2*H*-1,4-benzothiazine-3-one (**56**), 2,2'-bi[7-(2-amino-2-carboxyethyl)-3-carboxy-5-hydroxy-2*H*-1,4-benzothiazine] (**57**), trichochrome C (**59**), and 6-(2-amino-2-carboxyethyl)-4-hydroxybenzothiazole (**62**) were obtained as reported. Pheomelanin from red human hair was isolated as previously described.

4.2 Oxidative chemistry of hydroxytyrosol: hydrogen peroxide-dependent hydroxylation and hydroxyquinone/*o*-quinone coupling pathways.

Preparation of hydroxytyrosol (2-(3,4-dihydroxyphenyl)ethanol) (1)

The reaction was carried out as reported[170] with modification. In brief, a solution of tyrosol (200 mg, 1.4 mmol) in methanol (20 mL) was treated with IBX (600 mg, 2.1 mmol) under vigorous stirring at –25°C. Aliquots of the reaction mixture were periodically withdrawn and analyzed by HPLC with an UV detector set at 280 nm. The chromatographic separation was achieved using binary gradient elution conditions as follows: water/trifluoroacetic acid (97:3), solvent A; acetonitrile, solvent B; from 2 to 20% B, 0-40 min; from 20 to 55% B, 40-55 min; 55% B, 55-65 min; flow rate, 1 mL/min (eluant I). After 1 h the reaction mixture was reduced with a solution of $Na_2S_2O_4$ (300 mg) in water (10 mL) and then extracted with ethyl acetate (3 × 15 mL). The combined organic layers were dried over sodium sulphate and taken to dryness. The residue obtained (640 mg) was fractionated on a silica gel column (30 cm × 2 cm) using a gradient of $CHCl_3$-CH_3OH containing 0.5% acetic acid (from 98:2 to 90:10) as the eluant. Fractions eluted with $CHCl_3$/CH_3OH 90:10 were collected and taken to dryness to afford pure **1** (99 mg, 30% yield) as an oily solid.

Oxidation of 1 and 4-methylcatechol: general procedure

A solution of **1** (10 mg, 65 μmol) or of 4-methylcatechol (8 mg, 65 μmol) in 0.1 M phosphate buffer, pH 7.4 (65 mL) was treated with HRP (3 U/mL) and H_2O_2 (4 molar equivalents) under vigorous stirring. After 1 h the reaction mixture was reduced with $NaBH_4$ (20 mg), acidified to pH 3 with 3 M HCl and extracted with ethyl acetate (3 × 10 mL). The combined organic layers were dried over sodium sulphate and taken to dryness. The residue was treated with acetic anhydride (500 μL) and pyridine (25 μL)

at room temperature for 16 h. The mixture was taken to dryness and analyzed by TLC (eluant cyclohexane-ethyl acetate 1:1) and HPLC (gradient elution: water, solvent A; acetonitrile, solvent B; from 2 to 30% B, 0-15 min; from 30 to 60% B, 15-45 min; 60% B, 45-55 min; flow rate, 1 mL/min (eluant II). In the case of **1**, other experiments were performed (i) with H_2O_2 varying in the range of 2-10 molar equivalents; (ii) purging the solution with a stream of argon for at least 15 min prior to addition of the solution of the oxidant thoroughly purged with argon; (iii) with $K_3Fe(CN)_6$ (21 mg, 65 μmol) as the oxidant; after 20 min the reaction mixture was worked up and analysed as above. When required oxidation of **1** with $K_3Fe(CN)_6$ was carried out in the presence of H_2O_2 varying in the range of 1-3 molar equivalents.

Isolation of the tetraacetyl derivative of 2-(2,4,5-trihydroxyphenyl)ethanol (16) and of the heptaacetyl derivative of 2,3,3',4',6-pentahydroxy-5,6'-bis(2-hydroxyethyl)biphenyl (17)

For preparative purposes, the reaction of **1** with HRP/H_2O_2 was carried out as described above using 90 mg of the starting material. After work up of the reaction mixture, the residue (50 mg) was treated with acetic anhydride (1 mL) and pyridine (50 μL) at room temperature for 16 h and then purified by preparative TLC (eluant cyclohexane-ethyl acetate 1:1) to give the acetylated derivatives of **16** (R_f 0.47, 42 mg, 21% yield) and **17** (R_f 0.32, 4 mg, 2% yield).

Compound **16** *(tetraacetyl derivative)*.UV λ_{max} (CH_3OH): 267 nm; ESI+/MS: *m/z* 339 ($[M+H]^+$, 82), 361 ($[M+Na]^+$, 87), 377 ($[M+K]^+$, 36). ^1H and ^{13}C NMR data are reported in Table 1.

Compound **17** *(eptaacetyl derivative)*.UV λ_{max} (CH_3OH): 268, 311 nm; ESI +/MS: *m/z* 617 ($[M+H]^+$, 100), 639 ($[M+Na]^+$, 30), 655 ($[M+K]^+$, 21). ^1H and ^{13}C NMR data are reported in Table 1.

Isolation of the triacetyl derivative of 1,2,4-trihydroxy-5-methylbenzene (18) and of the pentaacetyl derivative of 2,3,3',4',6-pentahydroxy-5,6'-dimethylbiphenyl (19)

For preparative purposes, the reaction of 4-methylcatechol with HRP/H_2O_2 was carried out as described in the general procedure using 100 mg of the starting material. For isolation of **5** the reaction was carried out using 10 molar equivalents of H_2O_2. After work up of the reaction mixture, the residue was treated with acetic anhydride (1 mL) and pyridine (50 μL) at room temperature for 16 h and then purified by preparative TLC (eluant cyclohexane-ethyl acetate 6:4) to give the triacetyl derivative of **18** (R_f 0.61, 30 mg, 14% yield) and the pentaacetyl derivative of **19** (R_f 0.46, 20 mg, 21% yield).

Compound **18** *(triacetyl derivative)*. UV λ_{max} (CH_3OH): 268 nm; ^{1}H NMR δ(ppm): 2.15 (s, 3H), 2.25 (s, 3H), 2.26 (s, 3H), 2.29 (s, 3H), 6.95 (s, 1H), 7.04 (s, 1H); ^{13}C NMR δ(ppm): 15.9 (CH_3), 20.6 (2 × CH_3), 20.7 (CH_3), 117.2 (CH), 124.9 (CH), 128.7 (C), 139.4 (C), 140.0 (C), 146.4 (C), 168.0 (C), 168.2 (C), 168.6 (C); ESI+/MS: *m/z* 267 ($[M+H]^+$, 100), 289 ($[M+Na]^+$, 57), 305 ($[M+K]^+$, 4).

Compound **19** *(pentaacetyl derivative)*. UV λ_{max} (CH_3OH): 268 nm; ^{1}H NMR δ(ppm): 1.94 (s, 3H), 1.96 (s, 3H), 2.11 (s, 3H), 2.21 (s, 3H), 2.25 (s, 3H), 2.28 (s, 3H), 2.29 (s, 3H), 6.88 (s, 1H), 7.07 (s, 1H), 7.14 (s, 1H); ^{13}C NMR δ(ppm): 16.2 (CH_3), 19.1 (CH_3), 19.9 (2 × CH_3), 20.6 (3 × CH_3), 124.2 (2 × CH), 125.1 (CH), 128.4 (C), 129.5 (C), 129.8 (C), 136.4 (C), 139.3 (C), 139.7 (C), 140.3 (C), 141.7 (C), 144.8 (C), 168.2 (5 C); ESI+/MS: *m/z* 473 ($[M+H]^+$, 100), 505 ($[M+Na]^+$, 23).

Reaction of 4-methyl-1,2-benzoquinone with 2-hydroxy-5-methyl-1,4-benzoquinone

A solution of the triacetyl derivative of **18** (6 mg, 23 μmol) in acetone (100 μL) was added to 0.025 M sodium phosphate buffer (pH 12) (12 mL) that had been previously purged with a stream of argon for 15 min. After 2 min, the solution was acidified to pH 7 with $NaH_2PO_4 \times H_2O$ (29 mg) and treated with $NaIO_4$ (5 mg, 23 μmol) predissolved in H_2O (8 mL). After 30 s, a solution of 4-methyl-1,2-benzoquinone[10] (3 mg, 23 μmol) in acetone (145 μL) was added and after 3 min the mixture was worked up, acetylated and analysed as reported under the general procedure.

Computational methods

Quantum-mechanical computations were carried out with the Gaussian03 revision B.05 program[19] using the PBE0 density functional.[20] The 6-311+G(d,p) basis set was used for geometry optimisations. Frontier orbitals were calculated at the HF/6-31+G(d,p) level. The most recent version[21] of the Polarizable Continuum Model (PCM) was used to model the effects of the solvent medium.

4.3 Acid-Promoted Reaction of the Stilbene Resveratrol with Nitrite Ions.

Preparation of 3,5-dihydroxybenzaldoxime.

3,5-Dihydroxybenzaldoxime was prepared by a general procedure reported in literature.[44] Briefly, to 3,5-dihydroxybenzaldehyde (50 mg, 0.36 mmol) dissolved in water (4.2 mL) a solution of $NH_2OH \cdot HCl$ (14 mg, 0.20 mmol) and $CH_3COONa \times 3\ H_2O$ (27 mg, 0.20 mmol) in water (4.8 mL) was added, and the mixture was taken under stirring at 80 °C. After 2 h, the mixture was cooled and extracted with ethyl acetate (3 × 3 mL). The combined organic extracts were dried over Na_2SO_4 and evaporated to dryness. The residue was dissolved in ethyl acetate and fractionated by preparative TLC to give 3,5-dihydroxybenzaldoxime (R_f 0.43, 30 mg, 54% yield).

3,5-Dihydroxybenzaldoxime. ^{1}H NMR δ: 6.38 (1H, t, J= 2.0 Hz), 6.63 (2H, d, J= 2.0 Hz), 7.96 (1H, s); ESI+/MS: *m/z* 154 ($[M+H]^+$). 3,5-Dihydroxybenzaldoxime was reacted with $NaNO_2$ under the same conditions as for **4a** and the reaction mixture was periodically analyzed by HPLC (gradient elution: water, solvent A; acetonitrile, solvent B; from 2 to 30% B, 0-25 min; from 30 to 60% B, 25-70 min; 60% B, 70-75 min, eluant A).

Reaction of 4a with $NaNO_2$. General procedure.

To a solution of 4a (10 mg, 44 μmol) in methanol (0.5 mL), 0.1 M phosphate buffer (pH 3.0) (44 mL) was added followed by $NaNO_2$ (15 mg, 0.22 mmol), and the mixture was taken under vigorous stirring at room temperature. After 3 h, at complete consumption of the substrate (HPLC analysis with detection at 280, 320 nm, eluant A), the mixture was extracted with ethyl acetate (3 × 30 mL) and the combined organic layers were dried over Na_2SO_4 and taken to dryness. The residue was dissolved in methanol and analyzed by HPLC (eluant A), TLC and LC/MS. In other experiments, the reaction of 4a was run (i) as above with 1a at 3×10^{-6} or 25×10^{-6} M

concentration, with 0.2×10^{-3} M $NaNO_2$ added in eight portions at 15 min intervals, and at 37 °C; (ii) under an argon atmosphere; (iii) under an $^{18}O_2$ atmosphere. When required $Na^{15}NO_2$ was used in the reaction of 25×10^{-6} M 4a and the mixture was worked up as above and directly analyzed by NMR and LC/MS. For kinetic experiments 4a (2.5×10^{-5} M) was reacted with 1×10^{-3} M $NaNO_2$ added in one portion. In control experiments, the reaction was carried out under the conditions of the general procedure without added $NaNO_2$. Reaction of 4a (3.5×10^{-2} M) with $NaNO_2$ (0.35 M) was also run in acetonitrile containing 2.5% acetic acid; the reaction course was followed by HPLC (eluant A). Reaction of 3,4',5-trimethoxystilbene (2.5×10^{-4} M) with $NaNO_2$ (1×10^{-3} M) was carried out at pH 3.0 and the reaction course was followed by HPLC (gradient elution: water, solvent A; acetonitrile, solvent B; from 20 to 80% B, 0-45 min; 80% B, 45-55 min).

Reaction of 4a with CAN.

To a solution of **4a** (10 mg, 44 μmol) in methanol (0.5 mL), 0.1 M phosphate buffer (pH 3.0) (175 mL) was added followed by CAN (24 mg, 44 μmol), and the mixture was taken under vigorous stirring. After 1h, the mixture was extracted with ethyl acetate (3×50 mL) and the combined organic layers were dried over Na_2SO_4 and taken to dryness. The residue was analyzed by HPLC (eluant A).

Reaction of 4a with $K_3Fe(CN)_6$.

To a solution of **4a** (10 mg, 44 μmol) in methanol (0.5 mL) 0.1 M phosphate buffer (pH 7.0) (175 mL) was added followed by $K_3Fe(CN)_6$ (14 mg, 44 μmol) and the mixture was taken under stirring. After 1h, the mixture was acidified with HCl 0.5 M to pH 3 and extracted with ethyl acetate (3×50 mL), and the combined organic layers were dried over Na_2SO_4 and taken to dryness. The residue was analyzed by HPLC (eluant A).

Isolation of *rac*-(2*R*,3*R*)-3-(3,5-dihydroxyphenyl)-2-(4-hydroxyphenyl)-2,3-dihydrobenzofuran-5-carbaldehyde (20), (*E*)-3,4',5-trihydroxy-α-nitrostilbene (21a), (*E*)-3,4',5-trihydroxy-3'-nitrostilbene (22),[31] (*E*)-3,4',5-trihydroxy-2,3'-dinitrostilbene (23), 3,5-dihydroxybenzaldehyde, 3,5-dihydroxyphenylnitromethane, 4-hydroxybenzaldehyde and 4-hydroxy-3-nitrobenzaldehyde.

For preparative purposes, the reaction of **4a** with $NaNO_2$ was carried out as in the general procedure using 400 mg of starting material. After work up of the reaction mixture, the residue (380 mg) was fractionated by preparative TLC to give **21a** (R_f 0.36, 18 mg, 4% yield, > 95% purity), **20**[29] (R_f 0.40, 10 mg, 2% yield, > 90%purity), **22** (R_f 0.55, 5 mg, 1% yield, > 98% purity), 4-hydroxybenzaldehyde (R_f 0.69, 8 mg, 4% yield), **23** (R_f 0.77, 4 mg, 1% yield, > 90% purity), and 4-hydroxy-3-nitrobenzaldehyde (R_f 0.84, 4 mg, 1% yield). The fraction (5 mg) eluting at R_f 0.48 was found to consist of 3,5-dihydroxybenzaldehyde and 3,5-dihydroxyphenylnitromethane.

21a, **22**, 3,5-dihydroxybenzaldehyde, 4-hydroxybenzaldehyde or the R_f 0.48 band were exposed to $NaNO_2$ under the standard reaction conditions and the products formed were analyzed by HPLC (eluant A) and TLC.

21a. UV λ_{max} (CH_3OH): 276, 356 nm; (CH_3OH/0.1 M $NaHCO_3$, pH 8) 302, 451 nm. ^1H and ^{13}C NMR: see Table 2. HR ESI-/MS: found *m/z* 272.0563 ($[M-H]^-$), calcd for $C_{14}H_{10}NO_5$ *m/z* 272.0559.

22. UV λ_{max} (CH_3OH): 303, 323, 396 nm; (CH_3OH/0.1 M $NaHCO_3$, pH 8) 331, 464 nm. ^1H and ^{13}C NMR: see Table 2; ^1H NMR (CD_3OD) δ: 6.20 (1H, t, *J*= 2.0 Hz), 6.49 (2H, d, *J*= 2.0 Hz), 6.96 (1H, d, *J*= 16.4 Hz), 7.01 (1H, d, *J*= 16.4 Hz), 7.13 (1H, d, *J*=

8.8 Hz), 7.83 (1H, dd, *J*= 8.8, 2.0 Hz), 8.14 (d, 1H, *J*= 2.0 Hz). HR ESI-/MS: found *m/z* 272.0555 ([M-H]$^-$), calcd for $C_{14}H_{10}NO_5$ *m/z* 272.0559.

23. UV λ_{max} (CH_3OH): 300, 394 nm; (CH_3OH/0.1M $NaHCO_3$, pH 8) 317, 399 nm. ^1H and ^{13}C NMR: see Table 2; HR ESI+/MS: found *m/z* 319.0561 ([M+H]$^+$), calcd for $C_{14}H_{11}N_2O_7$ *m/z* 319.0566; found *m/z* 341.0380 ([M+Na]$^+$), calcd for $C_{14}H_{10}N_2O_7Na$ *m/z* 341.0386.

R_f 0.48 band: ^1H NMR resonances for 3,5-dihydroxyphenylnitromethane δ: 5.48 (2H, s), 6.42 (1H, t, *J*= 2.0 Hz), 6.50 (2H, d, *J*= 2.0 Hz); ^{13}C NMR resonances for 3,5-dihydroxyphenylnitromethane δ: 81.8 (CH_2), 103.9 (CH), 110.6 (2 × CH), 135.0 (C), 160.8 (2 × C); LC/ESI+/MS: t_R 13.9 min, *m/z* 192 ([M+Na]$^+$); HR ESI+MS: found 192.0279 ([M+Na]$^+$), calcd for $C_7H_7NO_4Na$ *m/z* 192.0273.

Isolation of *rac*-5-{(2*R*, 3*R*)-2-(4-hydroxyphenyl)-5-[(1*E*)-2-(3,5-dihydroxyphenyl)vinyl]-2,3-dihydrobenzofuran-3-yl}benzene-1,3-diol (24).

For preparative purposes the reaction of **4a** (2.5×10^{-5} M) with $NaNO_2$ (8 molar equivalents) was carried out using 50 mg of starting material. After work up of the reaction mixture, the residue (45 mg) was fractionated by preparative TLC to give **24**[17,18] (R_f 0.09, 2 mg, 4% yield, purity > 95%), **21a** (2 mg, 3% yield), **22** (3 mg, 5% yield) and 4-hydroxybenzaldehyde (1 mg, 4% yield). **24** was exposed to $NaNO_2$ under the standard reaction conditions and the products formed were analyzed by HPLC (eluant A) and TLC.

Isolation of *rac*-5,5'-[(2*R*,3*R*,4*R*,5*S*)-2,5-bis(4-hydroxyphenyl)-tetrahydrofuran-3,4-diyl]bisbenzene-1,3-diol (25).

The reaction of **4a** (2.5×10^{-5} M) with $NaNO_2$ (8 molar equivalents) was carried out using 50 mg of the starting material. After work up of the reaction mixture, the residue (45 mg) was fractionated on a Sephadex LH-20 column (50 cm × 2 cm) using

95% ethanol as the eluant. Fractions were collected based on HPLC analysis (eluant A) and further purified by preparative HPLC (water-acetonitrile 70:30 v/v) to give **25**[15] (t_R 24.2 min eluant A, 1 mg, 1% yield, > 95% purity).

Isolation of *trans*-ε–viniferin.

Wood from grapewine plants infected with fungi associated with esca (*Phaeoacremonium aleophilum*, *Phaeomoniella chlamydospora*, *Fomitiporia mediterranea*) was lyophilized and milled under nitrogen to obtain a fine powder. After treatment with petroleum ether 40-60 to remove lipids, the powder was extracted twice (3h and overnight) with methanol (1:15 w/v) in the dark with stirring . The extracts were filtered and taken to dryness. The residue was dissolved in methanol and purified by silica gel column chromatography using chloroform methanol 80:20 v/v as the eluant. The fraction containing *trans*–ε-viniferin (HPLC analysis: water- acetonitrile gradient from 80:20 to 33:67 in 90 min, t_R 56.9 min) was further fractionated by preparative TLC (chloroform methanol 80:20 v/v) to give the pure compound[33] (R_f 0.51).

4.4 Acid-Promoted Reaction of the Stilbene Piceatannol with Nitrite Ions.

Preparation of piceatannol (*trans*-3,3',4,5'-tetrahydroxystilbene, 4b).

A solution of resveratrol (150 mg, 0.66 mmol) in methanol (9 mL) was treated with *o*-iodoxybenzoic acid (IBX) (450 mg, 1.6 mmol) under vigorous stirring at –78 °C. Aliquots of the reaction mixture were periodically withdrawn and analyzed by HPLC with detection at 280 and 320 nm, using binary gradient elution conditions as follows: 3% trifluoroacetic acid, solvent A; acetonitrile, solvent B; from 2 to 20% B, 0-40 min; from 20 to 55% B, 40-55 min; 55% B, 55-65 min; flow rate, 1.0 mL/min. After 70 min the reaction mixture was reduced with a solution of $Na_2S_2O_4$ (300 mg) in water (26 mL), acidified to pH 3 with 3 M HCl and extracted with chloroform (3 × 10 mL) and then with ethyl acetate (3 × 10 mL). The combined ethyl acetate layers were dried over sodium sulfate and taken to dryness to give **4b** (93 mg, 58% yield, >98% purity).

2,3-Diaminonaphthalene (DAN) assay.

4b and caffeic acid were incubated separately at 0-1 mM concentration in 50 mM sodium acetate buffer (pH 4.0, 200 μL) in the presence of DAN (0.2 mM) and sodium nitrite (20 mM). After 30 min 50 mM sodium phosphate buffer (pH 7.4, 1.8 mL) was added to stop the reaction. Naphtho[2,3-*d*]triazole was quantified by measuring the fluorescence of each sample using an excitation wavelength of 375 nm and an emission wavelength of 450 nm.

Reaction of 4b with $NaNO_2$. Isolation of (*E*)-3,3',4,5'-tetrahydroxy-β-nitrostilbene (21b) and 3,4-dihydroxybenzaldehyde.

The reaction of **4b** (20 μM) with $NaNO_2$ (80 μM) was run in 0.1 M phosphate buffer (pH 3.0) at 37°C and analyzed by HPLC (gradient elution: 3% TFA, solvent A; acetonitrile, solvent B; from 2 to 30% B, 0-15 min; from 30 to 60% B, 15-45 min; 60% B, 45-55 min, eluant B). After 2h the reaction mixture was extracted with ethyl

acetate and the combined organic layers were dried over sodium sulfate and taken to dryness. For preparative purposes the reaction was carried out using 45 mg of the starting material. After work up of the reaction mixture, the residue (65 mg) was fractionated by preparative HPLC (3% TFA-acetonitrile 70:30 v/v) to give **21b**[27](t_R 18.0 min eluant B, 36 mg, 68% yield) and 3,4-dihydroxybenzaldehyde (t_R 11.0 min eluant B, 5 mg, 19% yield).

21b. UV λ_{max} (CH_3OH): 256, 277 and 373 nm; ^1H and ^{13}C NMR: see Table 3. ESI-/MS: *m/z* 288 ($[M-H]^-$), ESI+/MS: *m/z* 312 ($[M+Na]^+$).

4.5 Antinitrosating properties of catecholic compounds and of their *S*-glutathionyl conjugates.

Preparation of 2-*S*-glutathionylcaffeic acid (27) and of 2-*S*-glutathionylchlorogenic acid (28).

2-*S*-glutathionylcaffeic acid (**27**) and 2-*S*-glutathionylchlorogenic acid (**28**) were prepared by a general procedure reported in literature (*23*). Briefly, to a solution of **11** or **12** (100 mg) in methanol 0.1 M sodium phosphate buffer (pH 7.4) was added up to a 2 mM final concentration followed by GSH (8 mM) and tyrosinase (50 U/mL) in the case of **11** and by GSH (10 mM) and tyrosinase (100 U/mL) for **12**. The reaction mixture was taken under vigorous stirring at room temperature and periodically analyzed by HPLC with detection at 280 nm (0.5% acetic acid-methanol 75:25 v/v, flow rate 0.8 mL/min). After 1 h, the reaction mixture was acidified to pH 3 with 3 M HCl and then fractionated by preparative HPLC (0.5% acetic acid-methanol 80:20 v/v, flow rate 30 mL/min) to give **27** (*32*) (125 mg, 47% yield, > 98% purity) or **28** (*23*) (169 mg, 90% yield, > 98% purity).

Preparation of *trans*-2,5,6-tri-*S*-glutathionylpiceatannol (29a).

To a solution of **4b** (100 mg, 0.4 mmol) in methanol 400 mL of 0.1 M sodium phosphate buffer (pH 7.4) were added, followed by 4 molar equivalents of GSH (500 mg) and tyrosinase (50 U/mL), and the mixture was taken under vigorous stirring. Aliquots of the reaction mixture were periodically withdrawn and analyzed by HPLC (3% trifluoroacetic acid, solvent A; acetonitrile, solvent B; from 2 to 30% B, 0-15 min; from 30 to 60% B, 15-45 min; flow rate 1 mL/min, eluant A). After 2 h the reaction mixture was treated with $Na_2S_2O_5$, acidified to pH 3 with 3 M HCl, and washed with ethyl acetate.

The aqueous phase was fractionated by preparative HPLC (0.5% trifluoracetic acid-acetonitrile 90:10 v/v, flow rate 40 mL/min) to give **29a** (251 mg, 53% yield, > 98% purity).

29a. UV: λ_{max} (H_2O) 282, 304 nm; for ^1H and ^{13}C NMR spectra and positional assignment see Table 5. High resolution (HR) electrospray ionization in positive ion mode (ESI+)/MS: *m/z* 1160.2862, calcd for $C_{44}H_{58}N_9O_{22}S_3$ 1160.2858 ($[M+H]^+$).

Preparation of *trans*-5-*S*-glutathionylpiceatannol (29b).

A solution of resveratrol (100 mg, 0.4 mmol) in methanol (6 mL) was treated with IBX (300 mg, 1.0 mmol) under vigorous stirring at –78 °C. After 70 min a solution of GSH (540 mg, 1.8 mmol) in 0.1 M sodium phosphate buffer (pH 7.4) (6 mL) was added. Aliquots of the reaction mixture were periodically withdrawn and analyzed by HPLC (eluant A). After 50 min the reaction mixture was treated with $Na_2S_2O_5$ and acidified to pH 3 with 3 M HCl and washed with ethyl acetate. The water phase was fractionated by preparative HPLC (0.5% acetic acid-acetonitrile 82:18 v/v, flow rate 45 mL/min) to give 7b (130 mg, 43% yield, >98% purity).

29b. UV: λ_{max} (H_2O) 255, 311, 328 nm; for ^{1}H and ^{13}C NMR spectra and positional assignment see Table 5; HR ESI+/MS: *m/z* 550.1490, calcd for $C_{24}H_{28}N_3O_{10}S$ 550.1495 ($[M+H]^+$).

Preparation of *trans*-5-*S*-glutathionylhydroxytyrosol (30).

The reaction was run on 100 mg of tyrosol as described above for the preparation of **29b** but at -25 °C and with 1.5 molar equivalents of IBX. Aliquots of the reaction mixture were periodically withdrawn and analyzed by HPLC (0.2% trifluoroacetic acid, solvent A; acetonitrile, solvent B; from 0 to 5% B, 0-5 min; from 5 to 40% B, 5-40 min; from 40 to 70% B, 40-55 min; flow rate 0.7 mL/min). The reaction mixture was worked up as above and the water phase was fractionated by preparative HPLC (0.2% trifluoracetic acid-acetonitrile 85:15 v/v, flow rate 30 mL/min) to give **30** (*27*) (110 mg, 66% yield, > 98% purity).

Reaction of catechols with nitrite ions.

To a solution of the appropriate catechol (1.2×10^{-5} mol) in methanol 30 mL of 0.05 M sodium acetate buffer (pH 4.0) or 0.5 M HCl were added followed by $NaNO_2$ (1.2×10^{-5} mol) under stirring. Aliquots of the reaction mixture were periodically withdrawn and analyzed by HPLC (1% acetic acid-acetonitrile 85:15 v/v, flow rate 0.7 mL/min). When required the reaction was carried out under an argon atmosphere. In another experiments i) catechols were reacted all together with nitrite ions under the above conditions or ii) each catechol was reacted with nitrite ions at pH 4.0 in the presence of equimolar amounts of the corresponding glutathionyl conjugate.

2,3-Diaminonaphthalene (DAN) assay.

Catechols and their glutathionyl conjugates were incubated separately at 0-1 mM concentration in 50 mM sodium acetate buffer (pH 4.0, 200 μL) in the presence of DAN (0.2 mM) and sodium nitrite (20 mM). After 30 min 50 mM sodium phosphate

buffer (pH 7.4, 1.8 mL) was added to stop the reaction. Naphtho[2,3-*d*]triazole was quantified by measuring the fluorescence of each sample using an excitation wavelength of 375 nm and an emission wavelength of 450 nm.

Inhibition of tyrosine nitration.

Tested compounds were incubated separately at 25-150 μM concentration in 0.5 M HCl at 37 °C in the presence of tyrosine (400 μM) and nitrite (400 μM). After 4h 30 min the mixture was put on ice to stop the reaction and 3-nitrotyrosine formation was quantified by HPLC analysis (1% acetic acid/acetonitrile 85:15 v/v, flow rate 0.7 mL/min) at 275 nm (calibration ranges for 3-nitrotyrosine of 15-50 μM).

4.6 Antioxidant properties of a new derivative of hydroxytyrosol with α-lipoic acid.

Preparation of DHLA (6,8-dimercaptoottanoic acid).

To 500.0 mg of lipoic acid, previously dissolved in 10.0 mL of an aqueous solution of $NaHCO_3$ (0.25 M), were added 370.0 mg of $NaBH_4$ and the mixture was taken under stirring at –25 °C. After 2 h the reaction mixture was acidified until pH 1 with HCl 6 M and extracted with toluene (3x 5 mL). The residue was analysed by ^1H NMR to give DHLA in a pure form (352.0 mg, 70 % yield).

Preparation of *trans*-5-*S*-lipoylhydroxytyrosol (31).

The reaction was run on 100 mg of tyrosol as described above for the preparation of **30** but using dihydrolipoic acid as nucleophile (292.0 mM). After 15 min the reaction mixture was extracted with ethyl acetate (3×15 mL) and the combined organic layers were dried over sodium sulfate and taken to dryness. The residue (910 mg) was fractionated on a silica gel column (30 cm × 2 cm) using a gradient of $CHCl_3$-CH_3OH containing 0.5% acetic acid (from 98:2 to 90:10) as the eluant. Fractions eluted with $CHCl_3$/CH_3OH 93:7 were collected and taken to dryness to afford pure **31** (31.5 mg, 12 % yield) as an oily solid.

5-*S*-lipoylhydroxytyrosol (31)

ESI+/MS: *m/z* 361.1 ($[M+H]^+$), 383.1 ($[M+Na]^+$);

UV: λ_{max} (H_2O) 256, 291 nm;

^1H NMR (CD_3OD) δ (ppm): 1.54 (m, 7H), 1.84 (m, 1H), 2.26 (t, 2H), 2.65 (t, 2H), 2.91 (m, 2H), 3.07 (m, 1H), 3.67 (t, 2H), 6.62 (d, 1H, J=2.0 Hz), 6.71 (d, 1H, J= 2.0 Hz).

ABAP assay.

Linoleic acid (1.3 mM) was incubated in micelles of SDS (0.1 M) in phosphate buffer at pH 7.4 at 37°C. After 10', when the system was at a constant temperature, was added ABAP (0.5 mM) and after 32', when the rate of linoleic acid autoxidation was constant, was added the inhibitor (2μm). The reaction profile was followed spectrophotometrically until 74' reading the absorbance at 234 nm. The percent of inhibition for each compound was calculated as the ratio of the rates of formation of conjugates dienes in presence and in absence of the inhibitor. The inhibition values reported represent the media ± SD obtained by six separate experiments. For the elaboration of data was calculated the ratio:

$\Delta A_2 / \Delta A_1$

where $\Delta A_2 = \overline{A}_{74'} - \overline{A}_{42'}$; $\Delta A_1 = \overline{A}_{42'} - \overline{A}_{10'}$ with: $\overline{A} = A_{\text{solution}} - A_{\text{blank}}$.

Every measure was repeated twice and the media of the absorbance and ΔA, with the relative errors, were calculated for each spectrophotometric measure, for all the inhibition tests.

For errors about the media was used the following relation:

$$\delta x_i = [(1/N-1) \sum (x_i - \bar{x})^2]^{1/2}; \qquad \delta \bar{x} = \delta x / \sqrt{N}$$

For ΔA and $\Delta A_2 / \Delta A_1$ the errors were calculated applying the rules about the errors propagations.

For the percent of inhibition of the six tests made for each inhibitor was applicated the formula reported:

$$x_{\text{best}} = \sum_{i=1}^{N} w_i x_i / \sum_{i=1}^{N} w_i \quad ; \quad \delta x_{\text{best}} = (\sum_{i=1}^{N} w_i)^{1/2} \qquad \text{where } w_i = 1/\delta_i^2.$$

The assay was repeated on **1**, **31** and e α-tocopherol.

2, 2-Diphenyl-1-picrylhydrazyl radical (DPPH) assay (*33*).

To 3.0 mL of a freshly prepared 0.2 mM solution of DPPH in methanol compounds under exam (50 μM) were added separately. The reaction was monitored spectrophotometrically at 25 °C over 0-300 s, reading the changing of absorbance at 515 nm every 20 s. The reported values represent the media ± SD obtained by five separate experiments.

For the elaboration of data was calculated the ratio:

$\overline{A}_{4'20''}/\ \overline{A}_{0''}$

The errors were calculated applying the rules of the error of the media and the one about the errors propagations.

For kinetic parameters was selected a time of 20 s and to $\overline{A}_{20''}$ e $\overline{A}_{0''}$ were applicated the following relations:

$y = A + Bx$, where A = intercept e B = slope.

The intercept was calculated as*:*

$A = (\sum x_i^2)(\sum y_i) - (\sum x_i)(\sum x_i y_i) / \Delta;\quad \delta A^2 = \delta y^2 \sum x_i^2 / \Delta$

And the slope as:

$B = N(\sum x_i y_i) - (\sum x_i)(\sum y_i) / \Delta\ ;\ \delta B^2 = N\,\delta y^2 / \Delta$

where $\Delta = N(\sum x_i^2) - (\sum x_i)^2$

B was actual the kinetic constant *k*. So applying the relation:

$n = (\overline{A}_{20''}/\ \overline{A}_{0''})/\ \varepsilon\, C$

where ε= molar extinction coefficient of DPPH; C= inhibitor concentration

was possible to determine the stechiometric coefficient of the tested compound *n*. As a consequence was possibile to determine K_I with the relation:

$K_I = k \times n.$

The assay was repeated on **1**, **31**, DHLA and α-tocopherol.

4.7 Nitration *vs*. nitrosation chemistry of menthofuran: remarkable fragmentation and dimerization pathways and expeditious entry into dehydromenthofurolactone.

Reaction of 5 with HNO_3/cat. H_2SO_4. Isolation of 2,2-Bis[(*R*)-3,6-dimethyl-4,5,6,7-tetrahydrobenzofuran-2-yl]propan-1-ol (32), (6*R*, 6'*R*)-2,2'-[(*R*)-3-methylcyclohexane-1,1-diyl]bis-3,6-dimethyl-4,5,6,6-tetrahydrobenzofuran (33) and (*R*)-3,6-Dimethyl-2-nitro-4,5,6,7-tetrahydrobenzofuran (34).

To a cooled (5 °C) solution of **5** (485 mg, 3.22 mmol) in CH_2Cl_2 (2 mL), 40% HNO_3 ($\leq$0.1% nitrogen oxides content, 1 mL) and H_2SO_4 (2 drops) were added, resulting in the instantaneous development of a purple color. After 2 h, the reaction was quenched by the addition of sat. $NaHCO_3$ (15 mL) and extracted with petroleum ether. After washing with brine and evaporation, the crystalline residue was purified by gravity column chromatography on silica gel (petroleum ether-ethyl acetate 9:1 as the eluant) to afford crude **32** and **33** as brownish powders. Recrystallization from petroleum ether afforded as colorless material **32** (108 mg, 28% yield, >98% purity) and **33** (167 mg, 39% yield, >98% purity). In other experiments, the reaction of **5** was run as above but using 20% HNO_3. Purification of the reaction mixture by gravity column chromatography (petroleum ether-ethyl acetate 95:5 as the eluant) afforded **34** (100 mg, 18% yield, >95% purity) along with **32** (22 mg, 5% yield) and **33** (32 mg, 7% yield).

32. White powder (hexane), mp 98 °C (hexane); $[\alpha]^{D}_{25}$ +62 (*c* 0.90, $CHCl_3$); IR (KBr) (ν_{max}, cm^{-1}): 3400, 1770, 1714, 1681, 1650, 1574, 1455, 1378, 1291, 1223, 1032; ^1H NMR (400 MHz, $CDCl_3$) δ: 1.01 (6'-CH_3, d, *J*= 6.4 Hz), 1.37 (H-4b', m), 1.58 and 1.60 (3'-CH_3, s), 1.68 (H-3, s), 1.84 (H-4a', m), 1.91 (H-6', m), 2.17 (H-7b', m), 2.30 (H-5a,b', m), 2.65 (H-7a', dd, *J* = 15.9, 5.5 Hz), 3.94 (H-1, br s); ^{13}C NMR (100

MHz, $CDCl_3$) δ: 8.11 and 8.15 (2 × 3'-CH_3), 20.1 (CH_2, C-4'), 21.57 (CH_3, C-3), 21.60 (6'-CH_3), 29.8 (CH, C-6'), 31.4 (CH_2, C-5'), 31.4 (CH_2, C-7'), 44.3 (C, C-2), 69.2 (CH_2, C-1), 115.29 and 115.35 (C, 2 × C-3'), 118.7 (C, C-3a'), 147.6 (C, C-7a'), 148.8 (C, C-2'); HR ESI+/MS: *m/z* 379.2220 ($[M+Na]^+$), calcd for $C_{23}H_{32}NaO_3$ *m/z* 379.2249.

33.[9b] Colorless needles, mp 135 °C (lit. 130°C[9b]); IR (KBr) (ν_{max}, cm^{-1}): 1670, 1454, 1376, 1223, 1111, 868 (lit. 1640[9b]); ^1H NMR (400 MHz, $CDCl_3$) δ: 0.82 (d, J = 6.5 Hz, 3H), 0.95 (m, 1H), 1.05 and 1.08 (d, J = 6.5 Hz, 2 × 3H), 1.34 (s, 3H), 1.38-1.42 (m, 2H), 1.50-1.65 (m, 6H), 1.84 (s, 3H), 1.70-1.95 (m, 4H), 2.05-2.18 (m, 2H), 2.20-2.35 (m, 4H), 2.48 (m, 2H), 2.66 (m, 2H); ^{13}C NMR (100 MHz, $CDCl_3$) δ: 7.2 (CH_3), 9.1 (CH_3), 20.2 (CH_2), 20.3 (CH_2), 21.6 (CH_3), 21.8 (CH_3), 22.8 (CH), 23.1 (CH_2), 28.8 (CH_3), 29.8 (2 × CH), 31.5 (4 × CH_2), 34.3 (CH_2), 34.8 (CH_2), 43.0 (CH_2), 43.8 (C), 112.6 (C), 115.0 (C), 118.6 (C), 120.0 (C), 146.7 (C), 146.9 (C), 149.0 (C), 152.9 (C); HR ESI+/MS: *m/z* 417.2791 ($[M+Na]^+$), calcd for $C_{27}H_{38}NaO_2$ *m/z* 417.2770.

34. Foam, $[\alpha]_D^{25}$ +11 (*c* 0.90, MeOH); IR (KBr) (ν_{max}, cm^{-1}): 1616, 1551, 1484, 1374, 1293, 1233, 1118; ^1H NMR (400 MHz, $CDCl_3$) δ: 1.10 (6-CH_3, d, J = 6.4 Hz), 1.40 (H-4b, m), 1.84 (H-4a, m), 2.00 (H-6, m), 2.23 (H-7b, dd, J = 17.8, 9.8 Hz), 2.34 (3-CH_3, br s), 2.40 (H-5a,b, m), 2.75 (H-7a, dd, J = 17.8, 5.5 Hz); ^{13}C NMR (100 MHz, $CDCl_3$) δ: 10.5 (3-CH_3), 19.6 (CH_2, C-4), 21.2 (6-CH_3), 29.1 (CH, C-6), 30.3 and 31.2 (CH_2, C-5 and C-7), 122.5 (C, C-3a), 126.4 (C, C-3), 145.0 (C, C-2), 154.5 (C, C-7a, C); HR ESI+/MS: *m/z* 196.0985 ($[M+H]^+$), calcd for $C_{10}H_{14}NO_3$ *m/z* 196. 0974.

Preparation of bis-menthofuranylidene adducts 32 and 33.

To a solution of **5** in toluene (2.5 mL/mmol), the carbonyl compound, hydroxyacetone for **32** and *rac*-3-methylcyclohexanone for **33** (0.5 eq.), and one drop of conc. H_2SO_4 (or 10 mg/mmol acidic Dowex resin) were added. After stirring at rt

for 12-48 h, the reaction was worked up by washing with sat. $NaHCO_3$ (or filtration for Dowex removal), and the filtrate was concentrated. The adduct was purified by crystallization from hexane or, alternatively, by gravity column chromatography. The yields were 45% for **32** and 52% for **33**.

Oxidation of 5 with DDQ. **Isolation of (*R*)-3,6-Dimethyl-5,6-dihydrobenzofuran-2(4*H*)-one (Dehydromenthofurolactone, anhydro Woodward-Eastman lactone, 8).**

To a solution of **5** (200 mg, 1.33 mmol) in acetonitrile (6 mL), DDQ (605 mg, 2.66 mmol, 2 molar eqs) was added. After stirring at rt for 1 h, the reaction was worked up by filtration over Celite. The filtration cake was washed with acetonitrile, and the pooled filtrates were evaporated. The residue was purified by gravity column chromatography on silica gel (hexane-ethyl acetate 8:2 as the eluant) to afford **8** (97 mg, 44% yield) as a colorless oil.

8. Oil, IR (Liquid film) (ν_{max}, cm^{-1}): 1735, 1661, 1445, 1327, 1259, 1212, 1113; ^1H NMR (400 MHz, $CDCl_3$): δ 1.14 (d, J = 6.4 Hz, 3H), 1.48 (m, 1H), 1.87 (br s, 3H), 1.95 (m, 1H), 2.49 (m, 1H), 2.59 (m, 1H), 2.71 (dt, J = 16.5, 5.0 Hz, 1H), 5.60 (d, J = 4.1 Hz, 1H); ^{13}C NMR (100 MHz, $CDCl_3$): δ 8.4 (CH_3), 21.2 (CH_3), 21.9 (CH_2), 29.8 (CH), 31.0 (CH_2), 114.1 (CH), 119.8 (C), 148.2 (C), 149.2 (C), 171.6 (C); HR ESI+/MS: *m/z* 165.0908 ($[M+H]^+$), calcd for $C_{10}H_{13}O_2$ *m/z* 165.0916.

Reaction of 5 with nitrite.

To a solution of **5** (10 mg, 67 μmol) in dichloromethane (14 mL) 0.1 M phosphate buffer (pH 3.0) (56 mL) (1:4 v/v, with respect to the organic layer) was added, followed by sodium nitrite (14 mg, 203 μmol), and the biphasic system was taken under vigorous stirring at rt. After 2 h and 30 min, the organic layer was separated, the acqueous phase was washed with dichloromethane (3 × 15 mL), and the combined

organic layers were dried over sodium sulfate and taken to dryness. The residue was analyzed by TLC (eluant cyclohexane/ethyl acetate 1:1) and LC-MS (Binary gradient elution conditions were used as follows: 1% TFA, solvent A; acetonitrile, solvent B; from 30 to 60% B, 0-40 min; from 60 to 95% B, 40-45 min). When required $Na^{15}NO_2$ was used in the reaction of **5** with nitrite and the mixture was worked up and analyzed as above. In other experiments, the reaction of **5** was run as above but with purging of the biphasic system with argon for at least 30 min prior to the addition of sodium nitrite. In control experiments, the reaction was carried out under the conditions of the general procedure without added nitrite.

Isolation of 5,6,7,7a-tetrahydro-7a-hydroxy-3,6-dimethyl-4*H*-benzofuran-2-one (41), 1,4,5,6-tetrahydro-3,6-dimethyl-2H-indol-2-one (42), and (*Z*)-(6*R*, 7*R*, 7a*S*)-4,5,6,7-tetrahydro-7a-[(6*R*, 7a*S*)-4',5',6',7'-tetrahydro-7a'-hydroxy-3',6'-dimethyl-2*H*-indol-2-one-1-oxyl)]-3,6-dimethyl-7-nitro-2*H*-benzo[b]furan-2-one oxime (43).

For preparative purposes, the reaction of **5** with $NaNO_2$ or $Na^{15}NO_2$ was carried out as described in the general procedure using 1 g of the starting material. After work up of the reaction mixture, the residue (1 g) was fractionated by silica gel column chromatography (3 cm × 85 cm) using petroleum ether 40°-60°-ethyl acetate with 0.5% acetic acid as the eluant (8:2 to 4:6 gradient mixtures) to give nine fractions. Fractions V, VI and VII were purified on preparative TLC using chloroform/ethyl acetate 1:1 as eluant to give **41**[4a] (R_f 0.67, 12 mg, 1% yield, >95% purity), **42** (R_f 0.44, 11 mg, 1% yield, >95% purity) and **43** (R_f 0.55, 28 mg, 1% yield, >95% purity).

42. $[\alpha]^{D}_{25}$ +21.5° (*c* 0.79, $CHCl_3$); UV λ_{max} (CH_3OH): 277 nm; IR ($CHCl_3$) (ν_{max}, cm^{-1}): 2926, 2869, 1775, 1703, 1558, 1458, 1377, 1346, 1309, 1140; HR ESI+/MS: *m/z*

164.1066 ([M+H]$^+$), calcd for $C_{10}H_{14}NO$ *m/z* 164.1075; ^1H, ^{13}C NMR and ^{15}N data: see Table 7.

43. $[\alpha]^D_{25}$ -12.0° (*c* 0.59, $CHCl_3$); UV λ_{max} (CH_3OH): 249, 285, 364 nm; IR ($CHCl_3$) (ν_{max}, cm^{-1}): 2928, 2853, 1726, 1678, 1558, 1461, 1383, 1156; HR ESI+/MS: *m/z* 422.1921 ([M+H]$^+$), calcd for $C_{20}H_{28}N_3O_7$ *m/z* 422.1927; *m/z* 444.1736 ([M+Na]$^+$), calcd for $C_{20}H_{27}N_3O_7Na$ *m/z* 444.1747; ^1H, ^{13}C NMR and ^{15}N data: see Table 7.

Compound **43** was treated with diazomethane and analyzed by TLC and LC-MS. In other experiments **43** was treated with 2 M NaOH and the reaction mixture analyzed by LC-MS.

Computational details

All calculations were performed with the Gaussian 03 suite. The 6-31+G(d,p) basis set was adopted for geometry optimization, while NMR shielding tensors were computed within the Gauge-Including Atomic Orbitals (GIAO) ansatz at the PBE0/6-311+G(d,p) level. Computed isotropic shieldings were converted into chemical shifts using as reference the values obtained at the same level for cyclohexane (δ_C= 27.10, δ_H = 1.429, in $CDCl_3$).

Although large solvent effects on solute geometries and spectroscopic parameters are not expected in the relatively apolar $CDCl_3$ solutions, some test calculations were carried out using the polarizable continuum model (PCM) to simulate the influence of the solvent. In the PCM approach, the solvent is represented by an infinite dielectric medium characterized by the relative dielectric constant of the bulk, and a set of optimized radii (in the present instance, the UAHF radii are used to build an effective cavity occupied by the solute within the solvent. In particular, geometry optimization and computation of NMR parameters were repeated in the presence of the PCM for the three most stable conformers of **43**, and the resulting averaged chemical shifts

were compared with those obtained in vacuo. However, changes in computed carbon shifts are smaller than 1.4 ppm, and the correlation coefficient between experimental and computed carbon shifts is 0.99962 (versus 0.99965 in vacuo).

Model I

The four possible diastereoisomers of the model structure were generated and optimized at the PBE0/6-31+G(d,p) level; during this phase, both a chair and a twist-boat conformation (Figure S1) of the six-membered ring were explored.

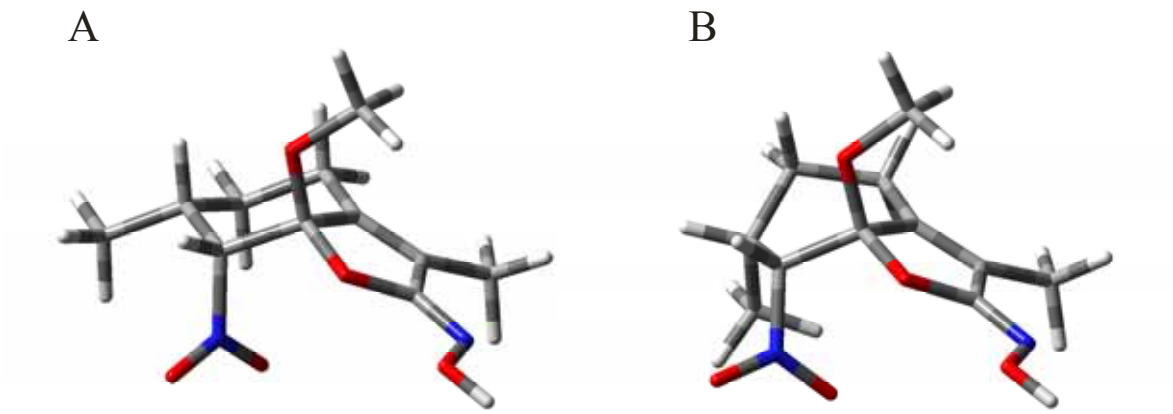

Figure S1. Optimized [PBE0/6-311+G(d,p)] structures of the chair conformer (panel A) and the twist-boat conformer (panel B) of the 7*R*,7a*S* diastereoisomer of model I.

Table S1 lists energies and atomic coordinates of the resulting optimized structures. GIAO NMR computations [PBE0/6-311+G(d,p)], followed by Boltzmann averaging, allowed to determine the correlation coefficients between experimental and computed carbon shifts, which are reported in Table S1 along with other indicators of the agreement with experimental data.

Table S1. Atomic coordinates (Å), energies, correlation coefficients between experimental and computed carbon shifts, largest absolute chemical shift deviation from the linear correlation, and H6-C6-C7-H7 dihedral values for the four diastereoisomers of model I (two conformers each).

	7R,7aR						***7S,7aR***					
ρ	0.9985						0.9989					
Δδ (ppm)	5.2						5.6					
	Chair			**Twist-boat**			**Chair**			**Twist-boat**		
ΔE (kcal mol^{-1})	0.0 [a]			1.7			0.0 [b]			1.0		
$\theta_{H6\text{-}C6\text{-}C7\text{-}H7}$ (degrees)	-52.0			42.4			75.5			153.2		
Atom	X	Y	Z	X	Y	Z	X	Y	Z	X	Y	Z
O	-1.034	0.996	0.052	-1.146	1.035	0.180	1.096	0.489	0.854	1.096	0.599	0.723
C	-2.140	0.272	0.258	-2.208	0.215	0.384	1.991	-0.032	-0.031	1.977	0.095	-0.185
C	-1.842	1.161	-0.258	-1.859	1.172	-0.072	1.346	-1.018	-0.899	1.405	-1.064	-0.868
C	0.383	2.442	0.120	0.357	2.268	0.709	-1.134	-1.767	-1.072	-0.918	-2.210	-0.677
C	1.535	2.180	-0.865	1.798	1.901	0.302	-2.188	-0.699	-1.416	-2.274	-1.630	-0.241
C	2.242	0.835	-0.636	1.796	1.014	-0.946	-2.539	-0.221	-0.235	-2.349	-0.126	-0.517
C	1.192	-0.295	-0.663	1.157	-0.358	-0.659	-1.289	-0.847	-0.430	-1.346	-0.633	-0.373
C	0.042	-0.092	0.327	-0.053	-0.249	0.314	-0.154	-0.169	-0.661	-0.081	-0.203	-0.698
C	-0.547	1.283	0.075	-0.580	1.166	0.338	0.064	-1.089	-0.510	0.183	-1.255	-0.347
N	-3.286	0.762	0.536	-3.354	0.585	0.809	3.222	0.298	-0.105	3.140	0.565	-0.414
O	-3.289	2.147	0.468	-3.408	1.952	1.032	3.562	1.255	0.837	3.425	1.663	0.382
C	-2.858	2.194	-0.595	-2.817	2.299	-0.225	2.063	-1.704	-2.006	2.117	-1.801	-1.945
C	3.134	0.841	0.606	3.155	0.920	-1.634	-3.417	-0.474	-0.808	-3.757	-0.433	-0.343
N	1.864	-1.649	-0.561	2.141	-1.371	-0.124	-0.806	1.993	-0.410	-0.950	1.916	-0.304
O	1.399	-2.490	0.176	3.009	-0.988	0.640	-0.975	-3.112	-0.040	-0.489	-1.838	-1.430
O	2.836	-1.803	-1.287	1.995	-2.519	-0.506	-0.318	1.739	-1.500	-1.130	-2.948	-0.316
O	0.529	-0.263	1.616	0.363	-0.723	1.550	-0.544	-0.815	1.838	-0.350	-0.705	1.974
C	-2.651			-2.565			0.344	-2.314		0.658	-2.529	

	0.441	0.241		0.628	0.767			1.816			1.537	
H	-	-	-	-	-	-	4.485	1.437	0.631	4.292	1.936	0.065
	4.194	2.369	0.709	4.308	2.079	1.351						
H	-	2.146	0.103	-	2.209	0.495	2.930	-	-	3.034	-	-
	3.700			3.637				2.252	1.623		2.259	1.560
H	-	2.016	-	-	2.285	-	2.443	-	-	2.418	-	-
	3.269		1.594	3.270		1.221		0.971	2.724		1.112	2.741
H	-	3.199	-	-	3.263	-	1.409	-	-	1.488	-	-
	2.432		0.561	2.326		0.069		2.405	2.530		2.586	2.372
H	-	3.375	-	0.039	3.191	0.211	-	-	-	-	-	-
	0.133		0.131				0.878	2.346	1.965	0.919	2.400	1.757
H	0.783	2.556	1.136	0.311	2.465	1.788	-	-	-	-	-	-
							1.544	2.473	0.336	0.752	3.181	0.192
H	1.132	2.208	-	2.368	2.814	0.103	-	-	-	-	-	-
			1.886				1.810	0.095	2.246	3.081	2.134	0.784
H	2.277	2.984	-	2.308	1.373	1.112	-	-	-	-	-	0.826
			0.795				3.108	1.186	1.760	2.443	1.818	
H	2.887	0.650	-	1.101	1.469	-	-	1.063	-	-	0.035	-
			1.502			1.668	3.122		0.632	2.023		1.553
H	3.907	1.608	0.489	3.446	1.906	-	-	-	0.334	-	-	-
						2.011	4.339	0.826		4.449	0.042	1.045
H	2.575	1.041	1.521	3.931	0.577	-	-	-	1.269	-	0.249	0.672
						0.946	2.914	1.327		4.128		
H	3.643	-	0.732	3.127	0.234	-	-	0.216	1.611	-	1.512	-
		0.119				2.488	3.694			3.789		0.522
H	0.739	-	-	0.793	-	-	-	1.303	1.388	-	0.941	1.321
		0.324	1.661		0.816	1.580	1.544			1.790		
H	-	0.700	2.657	-	0.231	2.779	0.437	-	1.602	0.802	-	1.936
	1.006			1.031				2.645			2.449	
H	0.119	-	3.583	-	-	3.451	-	-	3.245	0.305	-	3.526
		0.333		0.122	1.152		0.092	2.181			1.804	
H	-	-	2.556	-	-	2.288	1.334	-	2.518	1.608	-	2.612
	1.131	1.084		1.444	1.442			1.395			0.999	

	7*R*,7a*S*						**7*S*,7a*S***					
ρ	0.9991						0.9990					
Δδ (ppm)	5.2						4.4					
	Chair			**Twist-boat**			**Chair**			**Twist-boat**		
ΔE (kcal mol^{-1})	0.0 [c]			7.6			0.0 [d]			4.8		
$\theta_{H6\text{-}C6\text{-}C7\text{-}H7}$ (degrees)	54.0			-18.4			177.2			99.0		
Atom	X	Y	Z				X	Y	Z			
O	-	0.641	0.792	-	0.511	0.784	1.048	-	0.030	1.018	-	-
	1.128			1.145				0.991			1.058	0.146
C	-	0.240	-	-	0.105	-	2.128	-	-	2.097	-	-
	2.005		0.171	1.908		0.267		0.258	0.347		0.245	0.282
C	-	-	-	-	-	-	1.842	1.175	-	1.759	1.130	0.083
	1.460	0.886	0.929	1.234	0.957	1.015			0.251			
C	0.840	-	-	1.096	-	-	-	2.439	0.408	-	2.221	0.855
		2.086	0.780		2.069	0.707	0.329			0.465		
C	2.141	-	-	2.346	-	0.051	-	2.228	-	-	1.807	0.569
		1.286	0.965		1.593		1.585		0.452	1.918		
C	2.472	-	0.234	2.525	-	-	-	0.862	-	-	1.022	-
		0.390			0.068	0.005	2.253		0.240	2.046		0.742
C	1.313	0.549	0.627	1.321	0.637	0.706	-	-	-	-	-	-

							1.232	0.256	0.473	1.243	0.293	0.697
C	-0.004	-0.234	0.761	0.056	-0.250	0.782	0.009	-0.094	0.426	-0.082	-0.276	0.328
C	-0.260	-1.162	-0.396	-0.064	-1.179	-0.397	0.584	1.286	0.204	0.466	1.127	0.449
N	-3.141	-0.777	-0.393	-3.057	-0.574	-0.563	3.243	-0.738	-0.744	3.250	-0.613	-0.689
O	-3.399	-1.827	-0.475	-3.458	-1.563	-0.322	3.245	-2.123	-0.736	3.295	-1.969	-0.969
C	-2.168	-1.492	-2.088	-1.811	-1.579	-2.236	2.832	2.220	-0.626	2.736	2.250	0.019
C	3.775	0.378	0.028	2.793	0.399	-1.437	-3.461	0.714	-1.163	-1.637	1.853	-1.960
N	1.177	1.671	-0.358	1.045	1.951	0.041	-1.844	-1.619	-0.260	-2.120	-1.494	-0.406
O	0.802	1.400	-1.488	0.395	1.955	-0.988	-1.465	-2.505	-1.005	-1.688	-2.571	-0.772
O	1.492	2.782	0.029	1.551	2.933	0.559	-2.667	-1.746	-0.629	-3.178	-1.315	-0.169
O	0.151	-0.876	1.994	0.208	-0.891	2.017	-0.394	-0.357	-1.726	-0.579	-0.803	-1.513
C	-0.932	-1.700	2.399	-0.817	-1.812	2.359	0.621	-0.284	2.715	0.354	-0.930	2.576
H	-4.249	-2.155	-0.162	-4.297	-1.853	-0.052	4.122	-2.336	-1.072	-4.202	-2.095	-1.268
H	-2.329	-0.741	-2.868	-2.033	-0.813	-2.985	3.157	2.087	-1.662	3.214	2.286	-0.965
H	-3.157	-1.856	-1.790	-2.757	-2.079	-2.005	3.729	2.139	-0.003	3.536	2.106	0.752
H	-1.600	-2.324	-2.511	-1.126	-2.312	-2.669	2.416	3.223	-0.511	2.253	3.210	0.217
H	0.989	-2.830	0.018	0.875	-3.108	-0.429	-0.623	2.494	1.466	-0.350	2.447	1.924
H	0.594	-2.637	-1.692	1.276	-2.077	-1.789	0.159	3.385	0.156	-0.204	3.141	0.320
H	2.976	-1.981	-1.116	2.281	-1.912	-1.096	-2.320	3.012	-0.235	-2.293	1.182	1.385
H	2.063	-0.674	-1.870	3.238	-2.065	-0.374	-1.315	2.335	-1.512	-2.556	2.696	0.526
H	2.584	-1.033	-1.117	3.410	-0.186	-0.590	-2.584	0.781	-0.802	-3.098	0.742	-0.854
H	4.605	-0.320	-0.116	3.650	-0.155	-1.833	-4.171	1.529	-0.991	-2.213	2.784	-1.995
H	3.726	1.022	-0.857	1.939	0.233	-2.099	-3.159	0.753	-2.217	-0.574	2.117	-1.943
H	4.010	1.010	0.890	3.040	1.463	-1.480	-3.991	-0.226	-0.990	-1.827	1.307	-2.890
H	1.522	1.044	1.577	1.588	0.901	1.729	-0.885	0.276	1.509	0.801	0.524	1.668
H	-1.860	-1.122	2.469	-1.795	-1.321	2.378	1.418	-1.007	2.514	1.166	-1.611	2.303
H	-0.665	-2.074	3.388	-0.572	-2.170	3.360	0.133	-0.534	3.658	-0.208	-1.349	3.411
H	-1.076	-2.544	1.715	-0.845	-2.661	1.665	1.047	0.726	2.782	0.769	0.043	2.866

a) Energy = -913.307546 hartree
b) Energy = -913.311686 hartree
c) Energy = -913.315579 hartree
d) Energy = -913.313852 hartree

Based on correlation coefficients, the most promising candidate is the 7*R*,7a*S* diastereisomer. The second best candidate, namely the 7*S*,7a*S* structure, could be

ruled out based on the value of the H6-C6-C7-H7 dihedral (in the largely prevailing chair conformer), which is incompatible with the small vicinal scalar coupling observed. For the remaining diastereoisomers the agreement between computed and experimental carbon shifts is worse; however, the differences are not large, and therefore all three diastereoisomers (7*R*,7a*S*; 7*R*,7a*R*; 7*S*,7a*R*) were considered during a further exploration carried out at the level of the complete dimer (see below).

Model II

The two possible diastereoisomers of the model were generated and optimized as for model I. The resulting structural, energetic and spectroscopic parameters are reported in Table S2.

Table S2. Atomic coordinates (Å), energies, correlation coefficients between experimental and computed carbon shifts, largest absolute chemical shift deviation from the linear correlation, and H6a/H6b-C6-C7-H7 dihedral values for the two diastereoisomers of model II.

	7a*R*						**7a*S***					
ρ	0.9990						0.9992					
Δδ (ppm)	6.4						5.8					
	Chair			**Twist-boat**			**Chair**			**Twist-boat**		
ΔE (kcal mol^{-1})	0.0 [a]			3.0			0.0 [b]			5.9		
$\theta_{H6\text{-}C6\text{-}C7\text{-}H7}$ (degrees)	68.3, -49.6			144.7, 27.1			-179.8, 61.7			146.3, 28.4		
Atom	X	Y	Z	X	Y	Z	X	Y	Z	X	Y	Z
N	-1.243	0.568	0.160	-1.210	0.660	0.128	1.206	-0.651	0.125	1.255	-0.588	0.158
C	-1.905	0.654	0.004	-1.983	0.505	0.177	1.969	0.517	0.199	1.934	0.641	0.151
C	-0.836	1.687	0.027	-1.013	1.629	0.179	0.993	1.637	0.131	0.873	1.681	0.142
C	1.741	1.590	0.228	1.519	1.832	0.300	-1.523	1.781	0.465	-1.700	1.610	0.136
C	2.620	0.864	0.804	2.656	0.815	0.439	-2.629	1.019	0.281	-2.660	0.574	0.727
C	2.557	0.665	0.677	2.535	0.281	0.622	-2.607	0.484	0.014	-2.595	0.801	0.024
C	1.096	1.138	0.775	1.231	1.094	0.450	1.237	1.066	0.346	1.164	1.161	0.441

C	0.164	-0.433	0.214	0.140	-0.351	0.340	-0.118	-0.360	0.417	-0.105	-0.399	0.344
C	0.349	1.069	0.167	0.200	1.146	0.136	-0.199	1.140	0.239	-0.299	1.086	0.133
O	-1.857	-1.692	0.369	-1.774	-1.764	0.494	1.805	-1.771	0.428	1.914	-1.660	0.428
C	-2.506	-2.436	0.658	-2.269	-2.684	0.475	2.247	-2.657	0.596	2.468	-2.508	0.572
O	-3.109	0.802	0.047	-3.195	0.543	-0.242	3.174	0.565	-0.333	3.138	0.777	-0.201
C	-1.173	3.133	-0.062	-1.448	3.024	-0.454	1.418	3.034	-0.416	1.186	3.105	-0.435
C	3.290	-1.181	0.562	3.751	-1.200	0.640	-3.725	-1.212	-0.724	-3.563	-0.888	-1.154
O	0.368	-0.869	1.541	0.256	-0.599	1.728	-0.177	-0.651	1.797	-0.165	-0.700	1.724
H	-3.306	-1.841	1.107	-3.071	-2.224	1.058	1.408	-2.976	-1.225	1.687	-2.884	-1.242
H	-2.929	-3.308	0.156	-2.663	-3.523	0.102	2.670	-3.516	-0.070	2.925	-3.336	-0.025
H	-1.789	-2.751	1.424	-1.465	-3.025	1.136	3.018	-2.177	-1.205	3.232	-1.973	-1.142
H	-1.693	3.352	-1.001	-1.909	3.099	-1.445	2.216	3.334	0.271	2.060	3.424	0.140
H	-1.859	3.410	0.746	-2.211	3.334	0.268	1.830	3.115	-1.427	1.440	3.240	-1.493
H	-0.283	3.763	0.003	-0.612	3.725	-0.401	0.589	3.739	-0.316	0.344	3.759	-0.198
H	2.138	1.412	1.237	1.482	2.490	1.178	-1.506	2.836	0.171	-1.988	1.859	-0.896
H	1.763	2.671	0.062	1.702	2.484	-0.565	-1.737	1.749	1.543	-1.756	2.551	0.697
H	3.658	1.202	-0.702	2.631	0.364	1.438	-2.509	1.171	-1.364	-3.687	0.954	0.686
H	2.289	1.155	-1.810	3.620	1.327	0.338	-3.605	1.439	-0.010	-2.408	0.444	1.784
H	3.074	-1.080	-1.553	2.482	0.227	-1.597	2.753	-0.621	1.096	2.903	-1.546	0.767
H	2.836	-0.827	1.490	3.879	-1.691	0.332	-3.615	-1.103	-1.810	-3.343	-0.119	-1.906
H	4.340	-0.867	0.542	4.669	-0.643	-0.859	-4.708	-0.815	-0.447	-4.600	-0.750	-0.828
H	3.271	-2.276	0.593	3.646	-1.984	1.398	-3.721	-2.283	-0.494	-3.496	-1.862	-1.653
H	1.026	-2.223	-0.622	1.442	-2.028	0.085	-1.055	-0.943	-1.422	-1.034	-0.899	-1.499
H	0.719	-0.925	-1.783	0.834	-1.365	-1.433	-1.200	-2.141	-0.126	-0.990	-2.240	-0.357
H	-0.148	-1.681	1.647	-0.193	-1.442	1.893	0.290	-1.489	1.923	0.386	-1.486	1.855

a) Energy = -709.025187 hartree
b) Energy = -709.029363 hartree

The agreement between computed and experimental NMR shifts favors slightly the 7a*S* configuration. Support to this assignment is provided by an analysis of crosspeak fine structure in the DQF-COSY of **43**. In particular, the correlation between the H-7' proton at 2.38 ppm and the H-6' proton shows a small (ca. 4.5 Hz, vicinal *J*) active

coupling and a large (13.5 Hz, geminal *J*) passive coupling, whereas the crosspeak of the other H-7' proton (1.10 ppm) with H6' displays a shape characteristic of a large (vicinal) active coupling overlapped to a passive (geminal) coupling of comparable magnitude. Since twist-boat conformations can be disregarded on account of their high relative energies, the observed set of constants is only compatible with the H7a/H7b-C6-C7-H7 dihedrals of 7a*S* (in the chair conformation).

*Compound **43***

Structure **43** recombines the 7*R*,7a*S* diastereisomer of model I with model II in its 7a*S* configuration. Starting conformations of **43** were generated by systematic combination of the following dihedral values: C2-C7a-O-N1', -60, 60, and 180°; C7a-O-N1'-C2', -90 and 90°; N1'-C7a'-O-H, -60, 60, and 180°. Unrestrained optimizations resulted into 10 distinct minima, 3 of which lay within 3 kcal mol^{-1} from the absolute minimum and are expected to be significantly populated under the experimental conditions. Atomic coordinates, relative energies, and some relevant structural parameters for these conformations are reported in Table S3.

Table S3. Atomic coordinates (Å), relative energies (kcal mol^{-1}), correlation coefficients between experimental and computed carbon shifts, largest absolute chemical shift deviation from the linear correlation, and selected structural parameters of the three most stable conformers of **43.**

ρ	0.9996								
Δδ (ppm)	2.7								
	Conformer #1			**Conformer #2**			**Conformer #3**		
ΔE (kcal mol^{-1})	0.0 [a]			1.7			2.1		
$\theta_{H6\text{-}C6\text{-}C7\text{-}H7}$ (degrees)	54.2			54.8			52.8		
$d_{H7\text{-}H7'}$ (Å)	3.31, 3.96			3.32, 4.42			3.75, 4.29		
Atom	X	Y	Z	X	Y	Z	X	Y	Z
O	0.948	-1.146	0.729	-1.044	-0.238	1.342	0.844	1.235	0.420
C	1.184	-0.737	2.013	-1.212	-1.593	1.403	1.462	2.293	-0.185

C	1.805	0.584	2.024	-1.882	-2.081	0.200	2.415	1.823	-1.188
C	2.481	2.171	0.082	-2.583	-0.837	-1.973	3.115	-0.576	-1.891
C	3.463	1.706	-1.006	-3.492	0.402	-1.978	3.671	-1.548	-0.837
C	2.840	0.702	-1.982	-2.809	1.653	-1.412	2.580	-2.101	0.085
C	2.208	-0.517	-1.279	-2.216	1.433	-0.005	1.741	-1.006	0.775
C	1.284	-0.075	-0.133	-1.357	0.164	0.034	1.271	0.056	-0.229
C	1.875	0.987	0.745	-1.986	-1.028	-0.626	2.330	0.483	-1.206
N	0.868	-1.426	3.037	-0.777	-2.315	2.361	1.247	3.517	0.098
O	0.223	-2.603	2.662	-0.059	-1.541	3.275	0.281	3.663	1.084
C	2.250	1.251	3.275	-2.299	-3.496	0.023	3.302	2.743	-1.946
C	3.822	0.272	-3.068	-3.726	2.872	-1.448	3.138	-3.094	1.101
N	3.259	-1.460	-0.771	-3.300	1.360	1.030	2.513	-0.354	1.886
O	3.972	-1.085	0.146	-4.038	0.389	1.020	3.479	0.330	1.584
O	3.353	-2.532	-1.343	-3.393	2.307	1.792	2.147	-0.586	3.024
O	0.122	0.312	-0.859	-0.156	0.608	-0.632	0.210	-0.479	-1.022
N	-0.910	0.729	-0.031	0.895	-0.258	-0.409	-0.919	-0.844	-0.290
H	0.007	-3.008	3.509	0.198	-2.184	3.945	0.279	4.614	1.238
H	2.988	0.633	3.797	-3.002	-3.793	0.808	3.928	3.321	-1.259
H	1.405	1.387	3.958	-1.434	-4.163	0.097	2.710	3.464	-2.520
H	2.691	2.228	3.067	-2.771	-3.648	-0.950	3.948	2.195	-2.636
H	1.677	2.764	-0.375	-1.759	-0.706	-2.687	2.460	-1.128	-2.579
H	2.991	2.807	0.811	-3.141	-1.726	-2.281	3.924	-0.142	-2.486
H	3.800	2.575	-1.583	-3.800	0.620	-3.007	4.151	-2.393	-1.343
H	4.351	1.263	-0.540	-4.404	0.194	-1.407	4.442	-1.043	-0.245
H	1.980	1.190	-2.461	-1.925	1.864	-2.030	1.835	-2.625	-0.527
H	4.154	1.144	-3.639	-4.027	3.085	-2.478	3.617	-3.928	0.581
H	4.712	-0.202	-2.640	-4.638	2.704	-0.865	3.889	-2.632	1.752
H	3.367	-0.437	-3.767	-3.231	3.762	-1.048	2.344	-3.504	1.732
H	1.634	-1.114	-1.989	-1.609	2.287	0.299	0.877	-1.449	1.272
C	-1.353	2.036	-0.253	1.290	-1.104	-1.446	-1.239	-2.208	-0.321
O	-0.666	2.948	-0.673	0.599	-1.435	-2.391	-0.434	-3.116	-0.388
C	-2.047	-0.183	0.138	2.052	0.264	0.313	-2.123	-0.045	-0.593
C	-2.297	-1.095	-1.066	2.469	1.678	-0.096	-2.302	1.147	0.343
O	-1.983	-0.914	1.332	1.883	0.282	1.702	-2.147	0.335	-1.948
C	-3.199	0.790	0.271	3.135	-0.691	-0.157	-3.223	-1.063	-0.381
H	-1.254	-1.552	1.296	1.297	-0.432	1.995	-1.311	0.782	-2.136
C	-2.796	2.056	0.080	2.696	-1.476	-1.156	-2.712	-2.293	-0.204
C	-4.541	0.179	0.445	4.487	-0.456	0.412	-4.624	-0.564	-0.374
C	-3.561	3.332	0.086	3.398	-2.502	-1.973	-3.382	-3.599	0.036
H	-3.385	3.888	-0.840	3.313	-2.267	-3.038	-3.064	-4.028	0.992
H	-4.634	3.158	0.198	4.456	-2.571	-1.710	-4.469	-3.501	0.041
H	-3.229	3.976	0.908	2.943	-3.489	-1.831	-3.099	-4.318	-0.740
C	-4.788	-0.783	-0.734	4.898	0.993	0.083	-4.759	0.660	0.544
H	-4.558	-0.386	1.386	4.445	-0.580	1.502	-4.881	-0.265	-1.401
H	-5.324	0.942	0.498	5.219	-1.168	0.021	-5.322	-1.356	-0.084
H	-4.900	-0.193	-1.655	5.071	1.074	-1.000	-4.649	0.342	1.591
H	-5.735	-1.314	-0.581	5.851	1.223	0.574	-5.768	1.078	0.445
C	-3.655	-1.798	-0.927	3.841	2.025	0.497	-3.713	1.733	0.236
H	-2.275	-0.494	-1.984	2.509	1.732	-1.192	-2.115	0.810	1.371
H	-1.487	-1.832	-1.141	1.707	2.383	0.252	-1.545	1.907	0.127
C	-3.922	-2.700	-2.127	4.263	3.434	0.094	-3.868	2.940	1.156
H	-3.609	-2.423	-0.025	3.741	1.990	1.590	-3.862	2.065	-0.802
H	-4.873	-3.233	-2.018	5.226	3.702	0.542	-4.864	3.386	1.060
H	-3.971	-2.117	-3.055	4.366	3.518	-0.995	-3.728	2.652	2.205
H	-3.131	-3.449	-2.246	3.526	4.176	0.419	-3.127	3.711	0.923

a) Energy = -1467.496892 hartree

NMR computations followed by Boltzmann averaging resulted into a set of computed carbon shifts that displays a very good agreement with the experimental values (Figure S2).

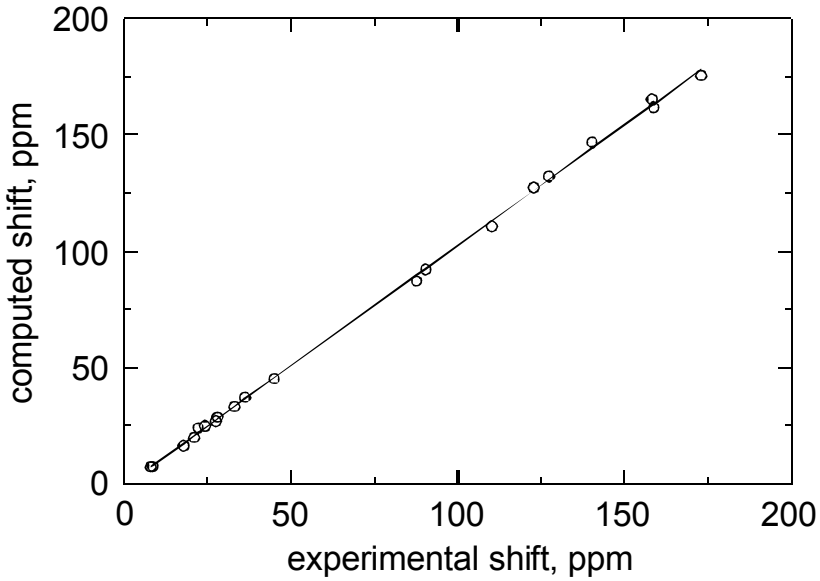

Figure S2. Linear correlation plot between computed [PBE0/6-311+G(d,p) // PBE0/6-31+G(d,p)] and experimental carbon chemical shifts for model **43**.

*Alternative diastereoisomers of **43***

A systematic conformational exploration of two alternative diastereoisomers of **43** was carried out along the same lines as for **43** itself.

In the case of the 7*R*,7a*R* diastereoisomer, starting structures with C2-C7a-O-N1'= 180° were evidently sterically crowded, and were not explored. Among the identified minima, a single conformer was significantly more stable than the others (by over 4 kcal mol^{-1}): the relevant structural parameters and NMR indicators are reported in Table S4.

Table S4. Atomic coordinates (Å), energy, correlation coefficient between experimental and computed carbon shifts, largest absolute chemical shift deviation

from the linear correlation, and selected structural parameters of most stable conformer of the 7*R*,7a*R* diastereoisomer of **43**.

ρ	0.9992		
Δδ (ppm)	4.7		
E (hartree)	-1467.491325		
$\theta_{H6\text{-}C6\text{-}C7\text{-}H7}$ (degrees)	-52.4		
$d_{H7\text{-}H7'}$ (Å)	4.77, 5.61		
Atom	X	Y	Z
O	0.800	1.563	0.094
C	0.758	1.936	1.405
C	1.493	0.983	2.234
C	2.869	-1.128	1.604
C	4.051	-0.995	0.629
C	3.620	-0.819	-0.837
C	2.679	0.400	-0.924
C	1.471	0.319	0.011
C	1.953	0.027	1.411
N	0.198	2.996	1.842
O	-0.396	3.730	0.824
C	1.656	1.152	3.702
C	3.058	-2.105	-1.444
N	2.333	0.706	-2.368
O	1.171	0.841	-2.705
O	3.291	0.830	-3.111
O	0.621	-0.677	-0.524
N	-0.572	-0.827	0.170
H	-0.750	4.493	1.293
H	0.682	1.110	4.202
H	2.087	2.131	3.933
H	2.295	0.372	4.123
H	3.231	-1.169	2.636
H	2.312	-2.053	1.415
H	4.667	-0.137	0.928
H	4.689	-1.883	0.699
H	4.507	-0.536	-1.414
H	3.848	-2.863	-1.459
H	2.211	-2.498	-0.879
H	2.732	-1.953	-2.478
H	3.239	1.290	-0.617
C	-0.761	-2.097	0.729
O	0.120	-2.814	1.164
C	-1.765	-0.453	-0.624

With respect to **43**, the agreement between computed and experimental carbon shifts is definitely worse; moreover, the relative stereochemistry at the C-7 and C-7a centers implies that the H-7 proton points away from the other ring, so that the H-7-H-7' distances are necessarily large, and cannot account for the observed ROE contacts.

For the 7*S*,7a*R* diastereoisomer, four conformers were found at relatively low energies: the relevant structural parameters and averaged NMR indicators are reported in Table S5.

Table S5. Atomic coordinates (Å), relative energies (kcal mol^{-1}), correlation coefficients between experimental and computed carbon shifts, largest absolute chemical shift deviation from the linear correlation, and selected structural parameters of the four most stable conformers of the 7*S*,7a*R* diastereoisomer of **43**.

ρ	0.9996											
Δδ (ppm)	3.1											
	Conformer #1			**Conformer #2**			**Conformer #3**			**Conformer #4**		
ΔE (kcal mol^{-1})	0.0 [a]			0.4			0.8			1.1		
$\theta_{H6\text{-}C6\text{-}C7\text{-}H7}$ (degrees)	74.8			79.3			74.7			73.7		
$d_{H7\text{-}H7'}$ (Å)	4.50, 5.46			4.64, 5.00			5.13, 5.21			4.18, 5.21		
Atom	X	Y	Z	X	Y	Z	X	Y	Z	X	Y	Z
O	0.943	1.370	-0.355	-0.910	1.088	0.586	1.077	0.677	-1.059	0.862	1.354	-0.153
C	0.890	1.888	0.907	-1.420	2.196	-0.027	1.399	1.996	-0.898	0.832	1.704	1.166
C	1.350	0.904	1.882	-2.320	1.808	-1.109	2.085	2.199	0.374	1.403	0.642	1.990
C	2.355	-1.464	1.584	-3.101	-0.523	1.932	2.764	0.528	2.237	2.570	-1.581	1.345
C	3.634	-1.594	0.738	-3.845	-1.389	0.902	3.673	-0.658	1.871	3.786	-1.531	0.405
C	3.367	-1.526	-0.774	-2.905	-2.093	0.089	2.927	-1.784	1.140	3.402	-1.316	-1.066
C	2.563	-0.268	-1.183	-1.900	-1.131	0.775	2.160	-1.290	-0.115	2.513	-0.064	-1.267
C	1.364	0.020	-0.256	-1.316	-0.055	-0.161	1.378	0.010	0.139	1.367	0.039	-0.242
C	1.657	-0.210	1.197	-2.288	-0.467	1.181	2.100	1.010	0.998	1.763	-0.346	1.154
N	0.518	3.076	1.184	-1.135	3.388	0.326	1.125	2.897	-1.756	0.401	2.820	1.609
O	0.152	3.784	0.047	-0.226	3.391	1.378	0.427	2.366	-2.835	-0.053	3.646	0.590
C	1.482	1.212	3.330	-3.109	2.798	-1.889	2.648	3.513	0.782	1.578	0.774	3.460
C	2.692	-2.795	1.301	-2.178	-3.279	0.546	2.005	-2.566	2.081	2.742	-2.555	1.678
N	3.478	0.922	-1.219	-2.591	-0.457	1.929	3.141	-1.084	-1.234	3.375	1.164	-1.203
O	3.761	1.358	-2.321	-2.207	-0.743	3.048	3.111	-1.889	-2.147	3.624	1.708	-2.264
O	3.909	1.347	-0.160	-3.513	-0.301	1.672	3.927	-0.153	-1.145	3.807	1.508	-0.116
O	0.364	-0.819	-0.832	-0.200	-0.544	0.885	0.152	-0.334	-0.827	0.384	-0.804	-0.850
N	-0.806	-0.902	-0.088	-0.835	-0.996	-0.064	-0.862	-0.689	-0.038	-0.794	-0.888	-0.133
H	-0.038	4.661	0.397	-0.136	4.327	1.585	0.274	3.137	-3.392	-0.274	4.458	1.059
H	0.516	1.507	3.752	-2.445	3.516	-2.380	1.864	4.276	0.802	0.612	0.928	3.951
H	2.165	2.054	3.481	-3.765	3.371	-1.226	3.401	3.847	0.061	2.197	1.647	3.694
H	1.856	0.350	3.886	-3.718	2.308	-2.651	3.108	3.458	1.771	2.046	-0.116	3.885
H	2.608	-2.648		-3.347	-1.328	-2.703	2.902	-2.385				

		1.452		3.811	0.023	2.597					1.666	
H	1.693	-	1.408	-	-	-	2.008	0.212	2.968	1.948	-	1.127
		2.321		2.449	1.148	2.556					2.457	
H	4.332	-	1.023	-	-	-	4.493	-	1.246	4.457	-	0.730
		0.801		4.546	0.752	0.354		0.290			0.729	
H	4.121	-	0.957	-	-	-	4.119	-	2.782	4.345	-	0.480
		2.551		4.433	2.155	1.421		1.074			2.471	
H	4.336	-	-	-	-	0.900	3.676	-	0.765	4.321	-	-
		1.436	1.284	3.526	2.494			2.494			1.122	1.635
H	3.342	-	-	-	-	-	2.605	-	2.887	3.440	-	-
		3.654	1.107	2.914	3.966	0.976		3.002			3.397	1.628
H	1.727	-	-	-	-	-	1.236	-	2.530	1.826	-	-
		2.981	0.825	1.474	2.983	1.327		1.933			2.836	1.153
H	2.531	-	-	-	-	0.200	1.486	-	1.553	2.492	-	-
		2.736	2.383	1.599	3.831			3.368			2.389	2.731
H	2.204	-	-	-	-	1.236	1.480	-	-	2.090	-	-
		0.360	2.209	1.079	1.682			2.066	0.471		0.045	2.272
C	-	-	0.369	1.430	-	-	-	-	-	-	-	0.429
	1.120	2.186			2.187	0.503	1.221	2.020	0.199	1.081	2.131	
O	-	-	0.649	0.889	-	-	-	-	0.044	-	-	0.752
	0.315	3.055			3.039	1.180	0.517	2.985		0.266	2.975	
C	-	-	-	1.878	-	0.347	-	0.199	-	-	-	-
	1.998	0.296	0.720		0.036		2.012		0.137	2.001	0.325	0.775
C	-	1.154	-	2.175	1.053	-	-	0.745	1.199	-	1.150	-
	2.229		0.298			0.690	2.516			2.227		0.478
O	-	-	-	1.643	0.502	1.616	-	1.307	-	-	-	-
	1.961	0.440	2.117				1.771		0.962	1.962	0.465	2.174
C	-	-	-	3.090	-	0.450	-	-	-	-	-	-
	3.103	1.187	0.192		0.935		3.062	0.746	0.691	3.088	1.181	0.149
H	-	0.046	-	0.887	1.106	1.560	-	1.057	-	-	-	-
	1.190		2.440				1.178		1.685	1.897	1.402	2.395
C	-	-	0.455	2.828	-	-	-	-	-	-	-	0.547
	2.596	2.249			2.166	0.017	2.608	2.010	0.729	2.559	2.202	
C	-	-	-	4.347	-	0.876	-	-	-	-	-	-
	4.506	0.751	0.425		0.270		4.403	0.153	0.926	4.500	0.765	0.368
C	-	-	1.133	3.704	-	-	-	-	-	-	-	1.318
	3.271	3.388			3.359	0.167	3.271	3.275	1.145	3.207	3.297	
H	-	-	2.185	3.677	-	-	-	-	-	-	-	2.376
	2.972	3.446			3.725	1.198	3.237	4.011	0.335	2.928	3.243	
H	-	-	1.081	4.739	-	0.104	-	-	-	-	-	1.242
	4.358	3.304			3.135		4.313	3.108	1.428	4.296	3.256	
H	-	-	0.670	3.352	-	0.468	-	-	-	-	-	0.955
	2.971	4.335			4.179		2.748	3.724	1.997	2.865	4.272	
C	-	0.718	-	4.637	0.874	-	-	0.473	0.394	-	0.734	-
	4.689		0.018			0.115	4.897			4.672		0.079
H	-	-	-	4.208	0.145	1.882	-	0.634	-	-	-	-
	4.718	0.850	1.500				4.320		1.687	4.758	0.948	1.422
H	-	-	0.105	5.182	-	0.913	-	-	-	-	-	0.239
	5.210	1.399			0.976		5.113	0.900	1.294	5.183	1.367	
H	-	0.804	1.076	4.904	0.441	-	-	-	1.109	-	0.911	1.000
	4.617					1.089	5.113	0.333		4.560		
H	-	1.050	-	5.510	1.444	0.228	-	1.001	0.217	-	1.039	-
	5.696		0.296				5.841			5.691		0.346
C	-	1.628	-	3.445	1.822	-	-	1.432	1.017	-	1.587	-
	3.640		0.660			0.299	3.876			3.651		0.834
H	-	1.225	0.788	2.303	0.584	-	-	-	1.908	-	1.313	0.592
	2.083					1.675	2.608	0.088		2.048		
H	-	1.798	-	1.324	1.739	-	-	1.446	1.595	-	1.738	-
	1.474		0.762			0.765	1.773			1.483		1.022
C	-	3.084	-	3.758	2.905	-	-	1.988	2.344	-	3.072	-
	3.841		0.251			1.326	4.383			3.846		0.544
H	-	1.555	-	3.248	2.305	0.667	-	2.270	0.323	-	1.422	-
	3.750		1.751				3.727			3.795		1.911
H	-	3.442	-	4.640	3.485	-	-	2.511	2.215	-	3.402	-
	4.835		0.539			1.034	5.337			4.851		0.829
H	-	3.203	0.835	3.959	2.468	-	-	1.184	3.074	-	3.282	0.524
	3.743					2.312	4.540			3.713		

H	-3.097	3.733	-0.725	2.920	3.602	-1.435	-3.669	2.697	2.776	-3.120	3.679	-1.094

a) Energy = -1467.490125 hartree

In this case, the agreement of computed versus experimental NMR parameters is comparable to **43**; however, the predicted H-7-H-7' distances are always long, at variance with the experimental observation of ROE contacts.

4.8 New synthetic approach to the endogenous antioxidant 2-*S*-cysteinyldopa. Synthesis of 2-acetylamino-3-(3,4-dihydroxyphenyl)propenoic acid (52).

The reported procedure[16] was followed with slight modifications. 3,4-Dihydroxybenzaldehyde (1.0 g, 7.3 mmol), *N*-acetylglycine (1 g, 8.5 mmol), and sodium acetate (2.3 g, 28 mmol) were heated at 120 °C in acetic anhydride (7.8 mL) under stirring. After 5 h the reaction mixture was diluted with 0.1 M phosphate buffer (pH 7.4) and extracted with ethyl acetate. The residue obtained from the organic layers was taken up in 0.2 M HCl (74 mL) and refluxed for 1 h. After ethyl ether washing the mixture was taken to dryness to afford **52**[16] (1.0 g, 60% yield) as yellowish powder (>95% pure by HPLC and ^{1}H NMR analysis). ESI+/MS: *m/z* 238 $[M+H]^+$, 260 $[M+Na]^+$.

(*Z*)-2-acetylamino-3-[2-(2-acetylamino-2-carboxyethylthio)-3,4-dihydroxyphenyl]propenoic acid (53)

A solution of **52** (500 mg, 2.1 mmol) in 0.01 M phosphate buffer (pH 7.4) (1.15 L) was sequentially treated with *N*-acetyl-L-cysteine (688 mg, 4.2 mmol) and mushroom tyrosinase (50 U/mL) and the mixture is taken under vigorous stirring at rt. After 2 h a complete consumption of the starting product is obtained (HPLC evidence, 0.1 M formic acid/methanol 88:12) and the mixture is acidified to pH 3 and fractionated by preparative HPLC (10 μm particle size 250 × 22 mm Econosil C18, eluant as above, 30 mL/min) to afford **53** (460 mg, 55% yield). Purity > 95 % as determined by ^{1}H NMR analysis.

(*Z*)-2-acetylamino-3-[2-(2-acetylamino-2-carboxyethylthio)-3,4 dihydroxyphenyl]propenoic acid (**53**). HR ESI+/MS: found *m/z* 399.1049 ($[M+H]^+$), calcd for $C_{16}H_{19}N_2O_{10}$ *m/z* 399.1040; UV λ_{max} (CH_3OH) 257, 314; $[\alpha]_D$ +44 (c=0.25, CH_3OH) ^{1}H NMR (DMSO-d_6) δ (ppm) 1.82 (3H,s, $COC\underline{H_3}$ cys), 1.87 (3H, s, $COC\underline{H_3}$), 2.85 (1H, dd, J=13.2, 10.0 Hz, $-SC\underline{H_2}$), 3.32 (1H, dd, J= 13.2, 4.4 Hz, $-SC\underline{H_2}$), 3.98 (1H, m, $-CH_2C\underline{H}$), 6.80 (1H, d, J=8.4 Hz, H-6'), 6.96 (1H, d, J=8.4 Hz, H-5'), 7.63 (1H,s, H-3) 8.16 (1H, d,

J=8.0 Hz, NHCOCH$_3$ cys), 9.11 (1H, s, NHCOCH$_3$); ^{13}C NMR (DMSO-d$_6$) δ (ppm) 22.5 (COCH$_3$ cys), 22.6 (COCH$_3$), 35.2 (-SCH$_2$), 52.2 (CHCH$_2$), 115.6 (C-5'), 120.0 (C-2'), 120.4 (C-6') , 126.0 (C-2), 128.7 (C-1'), 131.5 (C-3), 146.3 (C-4'), 147.2 (C-3'), 166.8 (C-1), 169.5 (-NHCO), 169.9 (-NHCO cys), 172.6 (COOHcys).

Synthesis of 14.

To a 100 mL hydrogenation bomb were added a solution of **53** (800 mg) in methanol (30 mL) and cyclooctadiene-1,5[(*R*,*R*)1,2-ethanediylbis(*o*-methoxyphenyl)phenylphosphine]rhodium tetrafluoroborate (44 mg). The solution was purged by filling and evacuating with N_2 and finally with H_2, and then allowed to stand under stirring at 50 atm for 72 h. After removal of the solvent the residue was taken up in 3 M HCl (50 mL) and taken under reflux for 5 h under an argon atmosphere. Removal of the catalyst by filtration and evaporation of the acid gave a pale yellow oil which was dissolved in ethanol and added to ethyl acetate to afford **14** as a colorless powder.[6,8] Diastereoisomeric excess was determined by HPLC analysis using a Synergi Hydro-RP 80A column (250 × 4.6 mm, 4μm) using 0.1% trifluoroacetic acid/methanol 99:1 (0.7 mL/min) as the eluant, detection wavelength 280 nm. Retention times of **14** and its diastereoisomer under these conditions were 9.9 min and 10.8 min, respectively.

^{1}H NMR (D$_2$O): δ (ppm) 3.18 (1H, dd, *J*= 14.4, 9.2 Hz, -CHCH$_2$), 3.31 (1H, dd, *J*= 14.8, 4.4 Hz, CH$_{2cys}$), 3.45 (1H, dd, *J*= 14.8, 7.2 Hz, CH$_{2cys}$), 3.66 (1H, dd, *J*= 14.4, 6.0 Hz, -CHCH$_2$), 4.12 (1H, dd, *J*= 7.2, 4.4 Hz, CH$_{cys}$), 4.23 (1H, dd, *J*= 9.2, 6.0 Hz, CH), 6.84 (1H, d, *J*=8.0 Hz, H-6), 6.96 (1H, d, *J*=8.0 Hz, H-5); ^{13}C NMR (D$_2$O): δ= 36.1 (-CHCH$_2$), 36.4 (CH$_{2cys}$), 54.1 (CH$_{cys}$), 55.9 (-CHCH$_2$), 118.8 (C-5), 119.7 (C-2), 124.3 (C-6), 132.0 (C-1), 145.6 (C-4), 148.6 (C-3), 172.0 (COOH$_{cys}$), 173.3 (COOH).

4.9 The "Benzothiazine" Chromophore of Pheomelanins: a Reassessment.

Preparation of synthetic pheomelanin.

To a solution of 5-*S*-cysteinyldopa (100 mg) in 0.1 M phosphate buffer (pH 6.8) (25 mL) horseradish peroxidase (16.7 units/mL final concentration) and hydrogen peroxide (38 μL) were added. The mixture was allowed to stand at room temperature under vigorous stirring for 2 h and then acidified to pH 3. The melanin precipitate was collected by centrifugation and washed three times with 1% acetic acid, once with water and then lyophilized. In other experiments the reaction was run in the presence of $ZnSO_4 \times 7H_2O$ (111 mg, 1.2 molar equivalents), with 100 units/mL of peroxidase and 228 μL of hydrogen peroxide, added in two portions at 5 h interval. The mixture was taken under stirring for 24 h and then acidified to pH 3, and the melanin precipitate was collected as above.

In both cases, aliquots of the reaction mixtures were periodically withdrawn, reduced with $NaBH_4$ when required, and analyzed by HPLC, LC/MS or UV-visible spectroscopy. High performance liquid chromatography (HPLC) analyses were performed on an Agilent 1100 series instrument equipped with an UV detector set at 280, 340 or 460 nm. An octadecylsilane-coated column, 150 mm × 4.6 mm, 5 μ particle size (Zorbax, Eclipse XDB-C18) at 0.4 mL/min was used. The following eluant systems were used: 0.1% TFA, solvent A; methanol, solvent B: from 10 to 15% B, 0-15 min; from 15 to 60% B, 15-55 min; from 60 to 80% B, 55-65 min (eluant I); 0.5% TFA, solvent A; methanol, solvent B: from 35 to 45% B, 0-25 min; from 45 to 80%B, 25-45 min (eluant II).

5. REFERENCES

1. Bravo, L. *Nutr Re*v. **1998**, *56*, 317–333.

2. Yang, C. S. *Nutrition* **1999**, *15*, 946–949.

3. Sun, A. Y.; Simonyi, A.; Sun, G. Y. *Free Radic.l Biol. Med.* **2002**, *32*, 314–318.

4. Arts, I. C.; Hollman, P. C. *Am. J. Clin. Nutr.* **2005**, *81*, 317S–325S.

5. Scalbert, A.; Manach, C.; Morand, C.; Remesy, C.; Jimenez, L. *Crit. Rev. Food Sci. Nutr.* **2005**, *45*, 287–306.

6. Stavric, B. *Clin. Biochem.* **1994**, *27*, 319–332.

7. Mukhtar, H.; Ahmad, N. *Am. J. Clin. Nutr.* **2000**, *71*, 1698S–1702S.

8. Galati, G.; Teng, S.; Moridani, M. Y.; Chan, T. S.; O'Brien, P. J. *Drug Metabol. Drug Interact.* **2000**, *17*, 311–314.

9. Yang, C. S.; Landau, J. M.; Huang, M. T.; Newmark, H. L. *Annu. ReV. Nutr.* **2001**, *21*, 381–406.

10. Barnes, S., Lamartiniere, C. A. In Cancer Chemoprevention Volume 1: Promising Cancer Chemopreventive Agents, Kelloff, G. J.Hawk, E. T., Sigman, C. C., Eds.; Humana Press: Totowa, NJ, 2004; pp 359–369.

11. Whitsett, T. G., Jr.; Lamartiniere, C. A. *Expert Rev. Anticancer Ther.* **2006**, *6*, 1699–1706.

12. Patel, D.; Shukla, S.; Gupta, S. *Int. J. Oncol.* **2007**, *30*, 233–245.

13. Balunas, M. J.; Kinghorn, A. D. *Life Sci.* **2005**, *78*, 431–441.

14. Zhao, J.; Wang, J.; Chen, Y.; Agarwal, R. *Carcinogenesis* **1999**, *20*, 1737–1745.

15. Ebeler, S. E.; Brenneman, C. A.; Kim, G. S.; Jewell, W. T.; Webb, M. R.; Chacon- Rodriguez, L.; MacDonald, E. A.; Cramer, A. C.; Levi, A.; Ebeler, J. D.; Islas-Trejo, A.; Kraus, A.; Hinrichs, S. H.; Clifford, A. J. *Am. J. Clin. Nutr.* **2002**, *76*, 865–872.

16. Lambert, J. D.; Yang, C. S. *Mutat. Res.* **2003**, *523–524*, 201–208.

17. Soleas, G. J.; Grass, L.; Josephy, P. D.; Goldberg, D. M.; Diamandis, E. P. *Clin. Biochem.* **2006**, *39*, 492–497.

18. Wagner, K. H.; Elmadfa, I. *Ann. Nutr. Metab.* **2003**, *47*, 95–106.

19. Lee, K. W.; Lee, H. J.; Surh, Y. J.; Lee, C. Y. *Am. J. Clin. Nutr.* **2003**, *78*, 1074–1078.

20. Butterfield, D.A.; Castegna, A.; Pocernich, C. B.; Drake, J.; Scapagninib, G.; Calabresec, V. *J. Nutr. Biochem.* **2002**, *13*, 444-461.

21. Xie, D. Y.; Sharma, S. B.; Paiva, N. L.; Ferreira, D.; Dixon, R. A. *Science* **2003**, *299*, 396–399.

22. Schroder, J.; Schroder, G. *Z. Naturforsch. C*, **1990**, *45*, 1–8.

23. Rupprich, N.; Kindl, H. Hoppe. *Seylers Z. Physiol. Chem.* **1978**, *359*, 165–172.

24. Gutteridge, J.M. *Free Radic. Res. Commun*. **1993**, *19,* 141-158.

25. Kehrer, J.P. *Crit. Rev. Toxicol.* **1993**, *23*, 21- 48.

26. Becker, L.B. *Cardiovasc. Res.* **2004**, *61*, 461-470.

27. M. Valko; M. Izakovic; M. Mazur; C.J. Rhodes; J. Telser, *Mol. Cell. Biochem.* **2004**, *266*, 37–56.

28. Kovacic, P.: Jacintho, J. D. *Curr. Med. Chem.*, **2001**, *8*, 773–796.

29. Ridnour, L. A., Isenberg, J. S., Espey, M. G., Thomas, D. D., Roberts, D. D.; Wink, D. A. *Proc. Natl. Acad. Sci. U.S.A.*, **2005**, *102*, 13147–13152.

30. Valko, M.; Morris, H.; Cronin, M. T. D. *Curr. Med. Chem.*, **2005**.*12*, 1161–1208.

31. Droge, W. *Physiol. Rev.*, **2002**, *82*, 47–95.

32. Halliwell, B.; Gutteridge, J. M. C. (1999). *Free radical Biology and medicine* (3rd ed.). Oxford University Press.

33. Miller, D. M.; Buettner, G. R.; Aust, S. D. *Free Radic. Biol. Med.*, **1990**, *8*, 95–108.

34. Pastor, N.; Weinstein, H.; Jamison, E.; Brenowitz, M. *J. Mol. Biol.*, **2000**, *304*, 55–68.

35. Pinchuk I.; Schnitzer, E.; Lichtenberg, D.; *Biochim. Biophys. Acta- Lipids Lipid Metab.*, **1998**, *1389*, 155–172.

36. Nyska, A.; Kohen, R., *Toxicol. Pathol.* **2002**, *30*, 620–650.

37. Marnett, L.J. *Mut. Res.-Fund. Mol. Mech. Mutagen.,* **1999**, *424*, 83–95.

38. Golding, B.T.; Patel, N.; Watson , W.P. *J. Chem. Soc. Perkin*, **1989**, *1,* 668–69.

39.Riggins, J.N.; Marnett, L.J. *Mutat. Res.*, **2001**, *497*, 153–57.

40. Ji, C. ; Rouzer, C.A.; Marnett, L.J. ; Pietenpol, J.A. *Carcinogenesis,***1998**, *19*, 1275–83.

41. Stadtman, E. R. *Curr. Med. Chem.*, **2004**, *11*, 1105–1112.

42. Dalle-Donne, I.; Giustarini, D.; Colombo, R.; Rossi, R.; Milzani, A. *Trends Mol. Med.*, **2003**, *9*, 169–176.

43. Dalle-Donne, I.; Scaloni, A.; Giustarini, D.; Cavarra, E.; Tell, G.; Lungarella, G. *Mass Spectrom. Rev.*, **2005**, *24*, 55–99.

44. Han, X.; Shen, T.; Lou, H. *Int. J. Mol. Sci,* **2007**, *8*, 950-988.

45. Motohashi, H.; Yamamoto, M. *Trends Mol. Med.* **2004***, 10,* 549-557.

46. Fki, I.; Sahnoun, Z.; Sayadi, S. *J. Agric. Food Chem.* **2007**, *55,* 624-631.

47. Hartman, R.E.; Shah, A.; Fagan, A.M.; Schwetye, K.E.; Parsadanian, M.; Schulman, R. N.; Beth Finn, M.; Holtzman, D.M. *Neurobiol. Dis.* **2006**, *24,* 506-515.

48. Butterfield, D.A.; Castegna, A.; Pocernich, C. B.; Drake, J.; Scapagninib, G.; Calabresec, V. *J. Nutr. Biochem.* **2002**, *13*, 444-461.

49. Shakibaei, M.; John, T.; Seifarth, C.; Mobasheri, A. *Ann. N. Y. Acad. Sci.* **2007***, 1095,* 554-563.

50. Tsai, S.H.; Lin-Shiau, S.Y.; Lin, J.K. *Br. J. Pharmacol.* **1999***, 126,* 673-680.

51 Nonn, L.; Duong, D.; Peehl, D.M. *Carcinogenesis* **2007**, *28, 1188*-1196.

52. Kunnumakkara, A.B.; Guha, S.; Krishnan, S.; Diagaradjane, P.; Gelovani, J.; Aggarwal, B.B. *Cancer Res.* **2007**, *67,* 3853-3861.

53. Collett, G.P.; Campbell, F.C. *Carcinogenesis* **2004***, 25,* 2183-2189.

54. Kundu, J.K.; Chun, K.S.; Kim, S.O.; Surh, Y.J. *Biofactors* **2004**, *21,* 33-39.

55. Schwarz, D. and Roots, I. *Biochem. Biophys. Res. Commun.* **2003**, *303,* 902-907.

56. Lee, L.T.; Huang, Y.T.; Hwang, J.J.; Lee, P.P.; Ke, F.C.; Nair, M.P.; Kanadaswam, C.; Lee, M.T. *Anticancer Res.* **2002***, 22*, 1615-1627.

57. Yoon, S.H.; Kim, Y.S.; Ghim, S.Y.; Song, B.H.; Bae, Y.S. *Life Sci.* **2002***, 71,* 2145-2152.

58. Martin, S.; Andriambeloson, E.; Takeda, K.; Andriantsitohaina, R. *Br. J. Pharmacol.* **2002**, *135,* 1579-1587.

59. Oak, M.H.; Chataigneau, M.; Keravis, T.; Chataigneau, T.; Beretz, A.; Andriantsitohaina, R.; Stoclet, J.C.; Chang, S.J.; Schini-Kerth, V.B. *Arterioscler. Thromb. Vasc. Biol.* **2003**, *23,* 1001-1007.

60. Oak, M.H.; El Bedoui, J.; Anglard, P.; Schini-Kerth, V.B. *Circulation* **2004***, 110,* 1861-1867.

61. Bryan, N. S.; Rassaf, T.; Maloney, R. E.; Rodriguez, C. M.; Saijo, F.; Rodriguez, J. R.; Feelish, M. *Proc. Natl. Acad. Sci. U. S. A.*, **2004,** *101*, 4308.

62. Coss, A.; Cantor, K. P.; Reif, J. S.; Lynch, C. F.; Ward, M. H. *Am. J. Epidemiol.*, **2004**, *159*, 693.

63. Duncan, C.; Dougall, H.; Johnston, P.; Green, S.; Brogan, R.; Leifert, C.; Smith, L.; Golden, M.; Benjamin, N. *Nat. Med.*, **1995**, *1*, 546.

64. Ferguson, D. B. In *Human Saliva. Clinical Chemistry and Microbiology*; Tenovuo, J., Ed.; CRC Press: Boca Raton, FL, 1989; Vol. *I*, pp. 75-79.

65. McKnight G. M.; Smith, L. M.; Drummond, R. S.; Duncan, C. W.; Golden, M.; Benjamin, N. *Gut*, **1997**, *40*, 211.

66. Van Maanen, J. M. S.; Pachen, D. M. F. A.; Dallinga, J. W.; Kleinjans, J. C. S. *Cancer Detect. Prev.*, **1998**, *22*, 204.

67. *CRC Handbook of Chemistry and Physics*; Lide, D. R., Ed.; CRC Press: Boca Raton, FL, 1995, 75th ed.

68. Gold, D. R. *Clin. Chest. Med.*, **1992**, *13*, 215.

69. Nathan, C.; Xie, Q. W. *Cell*, **1994**, *78*, 915.

70. Moncada, S.; Palmer, R. M.; Higgs, E. A. *Pharmacol. Rev.*, **1991**, *43*, 109.

71. Tamir, S.; Tannenbaum, S. R. *Biochim. Biophys. Acta*, **1996**, *1288*, F31.

72. Ramachandran, A.; Levonen, A. L.; Brookes, P. S.; Ceaser, E.; Shiva, S.; Barone, M. C.; Darley-Usmar, V. *Free Radical Biol. Med.*, **2002**, *33*, 1465.

73. Pryor, W.; Squadrito, G. *Am. J. Physiol.*, **1996**, *268*, L699.

74. Beckman, J. S.; Koppenol, W. H. *Am. J. Physiol.*, **1996**, *271*, C1424.

75. Herold, S.; Rehmann, F. J. *Free Radical Biol. Med.*, **2003**, *34*, 531.

76. Beckman, J.S. *FASEB J.*, **2002**, *16*, 1144.

77. Lancaster, J. R., Jr.; Langreher, J. M.; Bergonia, H. A.; Murase, N., Simmons, R. L.; Hoffmann, R. A. *J. Biol. Chem.*, **1992**, *267*, 10994.

78. Prutz, W. A.; Monig, H.; Butler, J.; Land, E. J. *Arch. Biochem. Biophys.*, **1985**, *243*, 125.

79. Stamler, J. S. *Cell*, **1994**, *78*, 931.

80. Goldstein, S.; Czapski, G. *J. Am. Chem. Soc.*, **1996**, *118*, 3419.

81. van der Vliet, A.; Smith, D.; O'Neill, C. A.; Kaur, H.; Darley-Usmar, V.; Cross, C. E.; Halliwell, B. *Biochem. J.*, **1994**, *303*, 295.

82. Zhang, Y.; Hogg, N. *Free Radical Biol. Med.*, **2005**, *38,* 831.

83. Moore, K. P.; Mani, A. R. *Methods Enzymol.*, **2002**, *359,* 256.

84. Pryor, W. A.; Lightsey, J. W. *Science,* **1981**, *214*, 435

85. Baker, P. R. S.; Lin, J.; Schopfer, F. D.; Woodcock, S. R.; Groeger, A. L.; Batthyany, C.; Sweeney,S.; Long,M.H.; Iles,K.E.; Baker, L.M.S.; Branchaud, B.P.; Chen,Y.E.; Freeman, B.A. *J. Biol. Chem* **2005**, 280, 42464.

86. Balazy, M.; Poff, C. D. *Curr. Vasc. Pharmacol.* **2004**, *2*, 81.

87. O'Donnell, V. B.; Eiserich, J. P.; Chumley, P. H.; Kirk, M. ; Barnes, S.; Darley-Usmar, V. M.; Freeman, B. A. *Chem. Res. Toxicol.*, **1999**, *12*, 83.

88. Napolitano, A.; Camera, E.; Picardo, M.; d'Ischia, M. *J. Org. Chem.*, **2002**, *67*, 1125.

89. Yu, H.; Venkatarangan, L.; Wishnok, J. S.; Tannenbaum, S. R. *Chem. Res. Toxicol.*, **2005**, *18*, 1849.

90. Caulfield, J. L.; Wishnok, J. S.; Tannenbaum, S. R. *J. Biol. Chem.*, **1998**, *273*, 12689

91. Bartsch, H.; Oshima, H.; Pignatelli, B.; Calmels, S. *Pharmacogenetics*, **1992**, *2*, 272.

92. Halliwell, B.; Zhao, K.; Whiteman, M. *Free Radical Res.*, **1999**, *31*, 651.

93. Masuda, M.; Mower, H. F.; Pignatelli, B., Celan, I.; Friesen, M. D.; Nishino, H.; Ohshima, H. *Chem. Res. Toxicol.*, **2000**, *13*, 301.

94. Mirvish, S. S. *Cancer Lett.*, **1995**, *93*, 17.

95. Jourd'heuil, D.; Kang, D.; Grisham, M. B. *Front. Biosci.*, **1997**, *2*, d189.

96. , G. D.; Morse, M. A.; Kelloff, G. J. *Environ Health Perspect.*, **1997**, *S4*, 945.

97. Lin, H.; Hollenberg, P. F. *Chem. Res. Toxicol.*, **2001**, *14*, 562.

98. Hecht, S. S. *Mutat. Res.*, **1999**, *424*, 127.

99. Shu, L.; Hollenberg, P. F. *Carcinogenesis*, **1997**, *18*, 801.

100. Vissers, M. N.; Zock, P. L.; Katan, M. B. *Eur. J. Clin. Nutr.*, **2004**, *58*, 955.

101. Hecht, S. S. *Proc. Soc. Exp. Biol. Med.*, **1997**, *216*, 181.

102. Owen, R. W.; Mier, W.; Giacosa, A.; Hull, W. E.; Spiegelhalder, B.; Bartsch, H. *Food Chem. Toxicol.* **2000**, *38*, 647.

103. Oldreive, C.; Zhao, K.; Paganga, G.; Halliwell, B.; Rice-Evans, C. *Chem. Res. Toxicol.* **1998**, *11*, 1574.

104. Zhao, K.; Whiteman, M.; Spencer, J. P.; Halliwell, B. *Methods Enzymol.*, **2001**, *335*, 296.

105. Rundlöf, T.; Olsson, E.; Wiernik, A.; Back, S.; Aune, M.; Johansson, L.; Wahlberg, I. *J. Agric. Food Chem.,* **2000**, *48*, 4381.

106. Rice-Evans, C. *Curr. Med. Chem.*, **2001**, *8*, 797.

107. Kono, Y.; Shibata, H.; Kodama, Y.; Sawa, Y. *Biochem. J.*, **1995**, *312*, 947.

108. Keys, A. *Am. J. Clin. Nutr.* **1995**, *61*, 1321S-1323S.

109. Owen, R. W.; Haubner, R.; Wurtele, G.; Hull, E.; Spiegelhalder, B.; Bartsch, H. *Eur. J. Cancer Prev.* **2004**, *13*, 319-326.

110. Tuck, K. L.; Hayball, P. J. *J. Nutr. Biochem*. **2002**, *13,* 636-644.

111. Visioli, F.; Bellomo, G.; Galli, C. *Biochem. Biophys. Res. Commun.* **1998**, *247*, 60-64.

112. Owen, R. W.; Mier, W.; Giacosa, A.; Hull, W. E.; Spiegelhalder, B.; Bartsch, H. *Food Chem. Toxicol.* **2000**, *38*, 647-659.

113. Monti, S. M.; Ritieni, A.; Sacchi, R.; Skog, K.; Borgen, E.; Fogliano, V. *J. Agric. Food Chem.*, **2001**, *49*, 3969.

114. Rietjens, S. J.; Bast, A.; Haenen, G. R. M. M. *J. Agric. Food Chem.* **2007**, *55*, 7609-7614.

115. Visioli, F.; Bellomo, G.; Montedoro, G. F.; Galli, C. *Atherosclerosis* **1995**, *117*, 25-32.

116. Medina, I.; Tombo, I.; Satuè-Gracia, M. T.; German, J.B.; Frankel, E. N. *J. Agric. Food Chem.* **2002**, *50*, 2392-2399.

117. Pazos, M.; Lois, S.; Torres, J. L.; Medina, I. *J. Agric. Food Chem.* **2006**, *54*, 4417-4423.

118. Hashimoto, T.; Ibi, M.; Matsuno, K.; Nakashima, S.; Tanigawa, T.;Yoshikawa, T.; Yabe-Nishimura, C. *Free Radic. Biol. Med.* **2004**, *36*, 555-564.

119. Corona, G.; Tzounis, X.; Dessi, A.; Deiana, M.; Debnam, E. S.; Visioli, F.; Spencer, J. P. E. *Free Radic. Res.* **2006**, *40*, 647-658.

120. Johnson, B. M.; van Breemen, R. B. *Chem. Res.Toxicol.* **2003**, *16*, 838-846.

121. Jeandet, P; Bessis, R.; Sbaghi, M.; Meunier, P. ; Trollat, P. *J. Phytopathol.* 1995, *143*, 135-9.

122. Cantos, E.; Espin, J.C.; Fernandez, M.J.; Oliva, J.; Tomas-Barberan, F.A. *J. Agric. Food Chem.* **2003**, *51*, 1208-14.

122. Bavaresco, L.; Fregoni, C.; Cantu, E.; Trevisan, M. *Drugs. Exp. Clin. Res.* **1999**, *25*, 57-63.

123. Roberti, M.; Pizzirani, D.; Simoni, D.; *J. Med. Chem.* **2003**, *46*, 3546-54.

124. Brito, P.; Almeida, L. M.; Dinis, T. C. P. *Free Radical Res.* **2002**, *36*, 621-631.

125. Lorentz, P.; Roychowdhury, S.; Engelmann, M.; Wolf, G.; Horn, T. F. W. *Nitric Oxide* **2003**, *9*, 64-76.

126. Burkitt, M. J.; Duncan, J. *Arch. Biochem. Biophys.* **2000**, *381*, 253-263.

127. Olas, B.; Nowak, P.; Kolodziejczyk, J.; Ponczek, M.; Wachowicz, B. *J. Nutr. Biochem.* **2006**, *17*, 96-102.

128. Amorati, R.; Ferroni, F.; Pedulli, G. F.; Valgimigli, L. *J. Org. Chem.* **2003**, *68*, 9654-9658.

129. Caruso, F.; Tanski, J.; Villegas-Estrada, A.; Rossi, M. *J. Agric. Food Chem.* **2004**, *52*, 7279-7285.

130. Stivala, L. A.; Savio, M.; Carafoli, F.; Perucca, P.; Bianchi, L.; Maga, G.; Forti, L.; Pagnoni, U. M.; Albini, A.; Prosperi, E.; Vannini, V. *J. Biol. Chem.* **2001**, *276*, 22586-22594.

131. Leopoldini, M.; Marino, T.; Russo, N.; Toscano, M. *J. Phys. Chem. A* **2004**, *108*, 4916-4922.

132. Cao, H.; Pan, X.; Li, C.; Zhou, C.; Deng, F.; Li, T. *Bioorg. Med. Chem. Lett.* **2003**, *13*, 1869-1871.

133. Amorati, R.; Lucarini, M.; Mugnaini, V.; Pedulli, G. F.; Roberti, M.; Pizzirani, D. *J. Org. Chem.* **2004**, *69*, 7101-7107.

134. Inamori, Y.; Kato, Y.; Kubo, M.; Yasuda, M.; Baba, K.; Kozawa, M. *Chem. Pharm. Bull.* **1984**, *32*, 213-8.

135. Brinker, A.M.; Seigler, D.S. *Phytochemisty* **1991**, *30*, 3229-32.

136. Murais. M.; Handler, N.; Erker, T. *Bioorg. Med. Chem.* **2004**, *12*, 5571-8.

137. Roupe, K.A.; Fukuda, C.; Halls, S.; Teng, X.W.; Davies, N.M. *J. Pharm. Pharm. Sci.* **2004**, *7*, 92-185.

138. Renaud, S.; Gueguen, R.; Schenker, J.; d'Houtaud, A. *Epidemiology* **1998**, *9*, 184-8.

139. Constant, J. *Coron. Artery Dis.* **1997**, *8*, 645-9.

72) 140. Khojasteh-Bakht, S. C.; Koenigs, L. L.; Peter, R. M.; Trager, W. F.; Nelson, S. D. *Drug. Metab. Dispos*. **1998**, *26*, 701-704.

73) 141. Riddle, J. M. *Contraception and Abortion from the Ancient World to the Renaissance*. Harvard University Press, Cambridge, 1992, pp. 46-47.

74) 142. Thomassen, D.; Knebel, N.; Slattery, J. T.; McClanahan, R. H.; Nelson, S. D. *Chem. Res. Toxicol.* **1992**, *5*, 123-130.

75) 143. (a) Frérot, E.; Bagnoud, A.; Vuilleumier, C. *Flavour Frag. J*. **2002**, *17*, 218-226.

76) (b) Naf, F.; Velluz, A. *Flavour Fragr. J*. **1998**, *13*, 203-208.

77) 144. Mahmoud, S. S.; Croteau, R. B. *Proc. Natl. Acad. Sci. USA* **2003**, *100*, 14481-14486.

78) 145. Oishi, S.; Nelson, S. D. *J.Org. Chem.* **1992**, *57*, 2744-2747.

79) 146. *Herbal Medicine. Expanded Commission E Monographs*, American Botanical Council, 2000.

80) 147. d'Ischia, M.; Panzella, L.; Manini, P.; Napolitano, A. *Curr. Med. Chem.* **2006**, *13*, 3133-3144.

148. Scalbert, A.; Williamson, G. *J. Nutr.*, **2000**, *130*, 2073S.

81) 149. Clifford, M. N. *J. Sci. Food Agric.*, **1999**, *79*, 362.

150. Prota, G. *Fortschr. Chem. Org. Naturst.* **1995**, *64*, 94-148.

151. Kongshoj, B.; Thorleifsson, A.; Wulf, H. C. *Photodermatol. Photoimmunol. Photomed.* **2006**, *22*, 141-147.

152. Wenczl, E.; Van der Schans, G. P.; Roza, L.; Kolb, R. M.; Timmerman, A. J.; Smit, N. P.; Pavel, S.; Schothorst, A.A. *J. Invest. Dermat.* **1998,** *11*, 678-672.

153. Vincensi, M. R., d'Ischia, M.; Napolitano, A.; Procaccini, E.; Riccio, G.; Monfrecola, G.; Santoianni, P.; Prota, G. *Melanoma Res.* **1998**, *8*, 53-58.

154. Chedekel, M. R.; Smith, S. K.; Post, P. W.; Pokora, A.; Vessell, D. L. *Proc. Natl. Acad. Sci. USA* **1978**, *75*, 5395-5399.

155. Rees, J. L. *Annu. Rev. Genet.* **2003**, *37*, 67-90.

156. Wakamatsu, K.; Kageshita, T.; Furue, M.; Hatta, N.; Kiyohara, Y.; Nakayama, J.; Ono, T.; Saida, T.; Takata, M.; Tsuchida, T.; Uhara, H.; Yamamoto, A.; Yamazaki, N.; Naito, A.; Ito, S. **2002**, *12,* 245-253.

157. Napolitano, A.; Memoli, S.; Nappi, A. J.; d'Ischia, M.; Prota, G. *Biochim. Biophys. Acta* **1996**, *1291*, 75-82.

158. Memoli, S.; Napolitano, A.; d'Ischia, M.; Misuraca, G.; Palumbo, A.; Prota, G. *Biochim. Biophys. Acta* **1997**, *1346*, 61-68.

159. Chioccara, F.; Novellino, E. *Synth. Commun.* **1986**, *16*, 967-971.

160. Ito, S.; Inoue, S.; Yamamoto, Y.; Fujita, K. *J. Med. Chem.* **1981**, *24*, 673-677.

161. Ito, S. *Bull. Chem. Soc. Jpn.* **1983**, *56*, 365-366.

162. Ito, S.; Prota, G. *Experientia* **1977**, *33*, 1118-1119.

163. The common system for catecholamine nomenclature was adopted which assigns number 3 and 4 to the OH bearing carbons of the aromatic ring.

164. Zhang, F.; Dryhurst, G. *Bioorg. Chem.* **1995**, *23*, 193-216.

165. Ito, S.; Palumbo, A.; Prota, G. *Experientia* **1985**, *41*, 960-961.

166. Ito, S.; Wakamatsu, K. In *The Pigmentary System. Physiology and Pathophysiology*; Nordlund, J., J., Boissy, R. E., Hearing, V. J., King, R. A., Oetting, W. S., Ortonne, J. P., Eds; Blackwell Publishing: New York, 2006; pp 282-310.

167. Vogna, D.; Pezzella, A.; Panzella, L.; Napolitano, A.; d'Ischia, M. *Tetrahedron Lett.* **2003**, *44*, 8289-8292.

168. O'Dowd, Y.; Driss, F.; My-Chan Dang, P.; Elbim, C.; Gougerout-Pocidalo, M.; Pasquier, C.; El-Benna, J. *Biochem. Pharmacol.* **2004**, *68*, 2003-2008.

169. Roche, M.; Dufour, C.; Mora, N.; Dangles, O. *Org. Biomol. Chem*. **2005**, *3*, 423-430.

170. Pezzella, A.; Lista, L.; Napolitano, A.; d'Ischia, M. *Tetrahedron Lett.* **2005**, *46*, 3541-3544.

171. Adler, E.; Magnusson, R. *Acta Chem. Scand.* **1959**, *13*, 505-519.

172. Plesnicar, B. In *The Chemistry of Peroxides*; Patai, S. Ed.; John Wiley and Sons, Inc.: New York, 1983; pp 573-578.

173. Napolitano, A.; Crescenzi, O.; Pezzella, A.; Prota, G. *J. Med. Chem.* **1995**, *38*, 917-922.

174. Teichner, H.; Weil, H. *Chem. Ber.* **1905**, *38*, 3376-3377.

175. Weitz, E.; Schobbert, H.; Seibert, H. *Chem. Ber.* **1935**, *68*, 1163-1168.

176. Wehrli, P. A.; Pigott, F.; Fischer, U.; Kaiser, A. *Helv. Chim. Acta* **1972**, *55*, 3057-3061.

177. Bailey, S. I.; Ritchie, I. M. *Electrochim. Acta* **1985**, *30*, 3-12.

178. Critchlow, A.; Haslam, E.; Haworth, R. D.; Tinker, P. B.; Waldron, N. M. *Tetrahedron* **1967**, *23,* 2829-2847.

179. Palumbo, A.; d'Ischia, M.; Misuraca, G.; Prota, G. *Pigment Cell. Res.* **1992**, *Suppl. 2*, 299-303.

180. Murias, M.; Handler, N.; Erker, T.; Pleban, K.; Ecker, G.; Saiko, P.; Szekeres, T.; Jäger, W. *Bioorg. Med. Chem.* **2004**, *12*, 5571-5578.

181. Szewczuk, L. M.; Fori, L.; Stivala, L. A.; Penning, T. M. *J. Biol. Chem.* **2004**, *279*, 22727-22737.

182. Gehm, B. D.; Mc Andrews, J. M.; Chien, P. Y.; Jameson, J. L. *Proc. Natl. Acad. U.S.A.* **1997**, *94*, 14138-14143.

183. Li, S. Y.; Fuchino, H.; Kawahara, N.; Sekita, S.; Satake, M. *J. Nat. Prod.* **2002**, *65*, 262-266.

184. Klebanoff, S. J. *Free Radical Biol. Med.* **1993**, *14*, 351-360.

185. For the sake of simplicity, throughout this paper, the same numbering system as for **4a** was adopted for **22**, which assigns numbers 1-6 to the resorcin moiety and numbers 1'-6' to the phenol moiety.

186. Breuil, A.-C.; Adrian, M.; Pirio, N.; Meunier, P.; Bessis, R.; Jeandet, P. *Tetrahedron Lett.* **1998**, *39*, 537-540.

187. Nicotra, S.; Cramarossa, M. R.; Mucci, A.; Pagnoni, U. M.; Riva, S.; Forti, L. *Tetrahedron* **2004**, *60*, 595-600.

188. Cichewicz, R. H.; Kouzi, S. A.; Hamann, M. T. *J. Nat. Prod.* **2000**, *63*, 29-33.

189. Amalfitano, C.; Evidente, A.; Surico, G.; Tegli, S.; Bertelli, E.; Mugnai, L. *Phytopathol. Mediterr.* **2000**, *39*, 178-183.

190. Li, W-W; Ding, L-S.; Li, B-G.; Chen, Y-Z. *Phytochemistry* **1996**, *42*, 1163-1165.

191. Stivala, L. A.; Savio, M.; Carafoli, F.; Perucca, P.; Bianchi, L.; Maga, G.; Forti, L.; Pagnoni, U. M.; Albini, A.; Prosperi, E.; Vannini, V. *J. Biol. Chem.* **2001**, *276*, 22586-22594.

192. Caruso, F.; Tanski, J.; Villegas-Estrada, A.; Rossi, M. *J. Agric. Food Chem.* **2004**, *52*, 7279-7285.

193. Wright, J. S.; Johnson, E. R.; DiLabio, G. A. *J. Am. Chem. Soc.* **2001**, *123*, 1173-1183.

194. Leopoldini, M.; Marino, T.; Russo, N.; Toscano, M. *J. Phys. Chem. A* **2004**, *108*, 4916-4922.

195. Sako, M; Hosokawa, H.; Ito, T.; Iinuma, M. *J. Org. Chem.* **2004**, *69*, 2598-2600.

196. Takahama, U.; Oniki, T.; Hirota, S. *J. Agric. Food Chem.* **2002**, *50*, 4317-4322.

197. Al-Obaidi, U.; Moodie, R. B. *J. Chem. Soc., Perkin Trans. 2: Phys. Org. Chem. (1972-1999)*, **1985**, *3*, 467-472.

198. Oldreive, C.; Zhao, K.; Paganga, G.; Halliwell, B.; Rice-Evans, C. *Chem. Res. Toxicol.* **1998**, *11*, 1574-1579.

199. Fronza, G.; Fuganti, C.; Serra, S.; Cisero, M.; Koziet, J. *J. Agric. Food Chem.* **2002**, *50*, 2748-2754.

200. Napolitano, A.; Panzella, L.; Savarese, M.; Sacchi, R.; Giudicianni, I.; Paolillo, L.; d'Ischia, M. *Chem. Res. Toxicol.* **2004**, *17*, 1329-1337.

201. Napolitano, A.; Crescenzi, O.; Camera, E.; Giudicianni, I.; Picardo, M.; d'Ischia, M. *Tetrahedron* **2002**, *58*, 5061-5067.

202. Lee, J.G.; Kwak, K.H.; Hwang, J.P. *Tetrahedron Lett.* **1990**, *31*, 6677-6680.

203. Ley, J. P.; Bertram, H. –J. *Bioorg. Med. Chem.* **2001**, *9*, 1879-1885.

204. Lins, A. P.; Felicio, J. D.; Braggio, M. M.; Roque, L. C. *Phytochemistry* **1991**, *30*, 3144-3146.

205. Fulcrand, H.; Cheminat, A.; Brouillard, R.; Cheynier, V. *Phytochemistry* **1994**, *35*, 499-505.

206. Denmark, S.; Marcin, L. R. *J. Org. Chem*. **1993**, *58*, 3850.

207. All quantum-mechanical calculations were carried out with the Gaussian03 package [Gaussian 03, Revision C.02, Frisch, M. J. *et al*. Gaussian, Inc., Wallingford CT, 2004].

208. Adamo, C.; Barone, V. *J. Chem. Phys.* **1999**, *110*, 6158.

209. Francl, M. M.; Petro, W. J.; Hehre, W. J. S.; Binkley, J.; Gordon, M. S.; DeFrees, D. J.; Pople, J. A. *J. Chem. Phys.* **1982**, *77*, 3654. For a general introduction

to basis sets see: Foresman, J. B.; Frisch, A. *Exploring Chemistry with Electronic Structure Methods*; Gaussian Inc.: Pittsburg, PA, 1996, 2nd edition.

210. Cheeseman, J. R.; Trucks, G. W.; Keith, T. A.; Frisch, J. M. *J. Chem. Phys.* **1996**, *104*, 5497.

211. Benzi, C.; Crescenzi, O.; Pavone, M.; Barone, V. *Magn. Reson. Chem.* **2004**, *42*, S57.

212. a) Miertus, S.; Scrocco, E.; Tomasi, J. *Chem. Phys.* **1981**, *55*, 117; b) Cossi, M.; Scalmani, G.; Rega, N.; Barone, V. *J. Chem. Phys.* **2002**, *117*, 43; c) Scalmani, G.; Barone, V.; Kudin, K. N.; Pomelli, C. S.; Scuseria, G. E.; Frisch, M. J. *Theor. Chem. Acc.* **2004**, *111*, 90.

213. Barone, V.; Cossi, M.; Tomasi, J. *J. Chem. Phys.* **1997**, *107*, 3210.

214. Cotelle, P.; Vezin, H. *Tetrahedron Lett.* **2001**, *42*, 3303.

215. Napolitano, A.; d'Ischia, M. *J. Org. Chem.* **2002**, *67*, 803.

216. Geometry optimizations and frontier orbital computations were carried out at the PBE0/6-31+G(d,p)/PCM level on two conformers of the quinone, the most stable of which is shown.

217. Cao, H.; Pan, X.; Li, C.; Zhou, C.; Deng, F.; Li, T. *Bioorg. Med. Chem. Lett.* **2003**, *13*, 1869.

218. Kalyanaraman, B.; Sealy, R. C.; Liehr, J.G. *J. Biol. Chem.* **1989**, *264*, 11014.

219. Two conformers of the 4-phenoxyl radical of **1**, differing by a 180° rotation of the phenoxyl ring, were geometry optimized at the unrestricted PBE0/6-31+G(d,p) level, either in vacuo or using the PCM model.

220. De Lucia, M.; Panzella, L.; Crescenzi, O.; Napolitano, A.; Barone, V.; d'Ischia, M. *Bioorg. Med. Chem. Lett.* **2006**, *16*, 2238-2242.

221. Panzella, L.; Manini, P.; Napolitano, A.; d'Ischia, M. *Chem. Res. Toxicol.* **2005**, *18*, 722-729.

222. Pollard, S. E., Kuhnle, G. G. C., Vauzour, D., Vafeiadou, K., Tzounis, X., Whiteman, M., Rice-Evans, C., and Spencer, J. P. E. *Biochem. Biophys. Res. Commun.* **2006**, *350*, 960-968.

223. Panzella, L., Napolitano, A., and d'Ischia, M. *Bioorg. Med. Chem. Lett.* **2003**, *11*, 4797-4805.

224. Moridani, M. Y., Scobie, H., Jamshidzadeh, A., Salesi P., and O'Brien, P. J. *Drug. Metab. Dispos*. **2001**, *29*, 1432-1439.

225. Amorati, R., Fumo, M. G., Menichetti, S., Mugnaini, V., and Pedulli, G. F. *J. Org. Chem*. **2006**, *71*, 6325-6332.

226. Lozano C., Torres J. L., Julià L., Jimenez, A., Centelles, J. J., and Cascante M. *FEBS Letters* **2005**, *579*, 4219-4225.

227. Kerry, N., and Rice-Evans, C. *FEBS Lett.* **1998**, *437*, 167-171.

228. Braida, W., and Ong, S. K. *Water Air Soil Pollut.* **2000**, *118*, 13–26.

229. ago, B., Lundberg, G. O., Barbosa, R. M., and Laranjinha J. () *Free Radic. Biol. Med.* **2007**, *43*, 1233-1242.

230. Ley, J.P.; Bertram, H.J. *J. Agric. Food Chem.,* **2003**, *51*, 4596-4602.

231. Jin, G.; Yoshioka, H. *Biosci. Biotechnol. Biochem.,* **2005**, *69*, 440-447.

232. Gordon, M.H.; Paiva-Martins, F.; Almeida, M. *J. Agric. Food Chem.,* **2001**, *49,* 2480-2485.

233. Reed, L.J.; DeBusk, B.G.; Gunsalus, I.C.; Hornber Jr., C.S., *Science,* **1951,** *114,* 93-94.

234. Packer, L.; Witt, E.H. & Tritschler, H. *Free Radic. Biol. Med.,* **1995**, *19*, 227-250.

235. Ono, K.; Hirohata, M.; Yamada, M., *Biochem. Biophys. Res. Commun.,* **2006**, *341*, 1046-1052.

236. Tsuji-Naito, K.; Hatani, T.; Okada, T.; Tehara, T. *Bioorg. Med. Chem.,* **2007**, *15,* 1967-1975.

237. Gunsalus, I.; Barton, L.S.; Gruber, W. *J. Am. Chem. Soc.,* **1956**, *78*, 1763-1766.

238. Pryor, W. A.; Cornicelli, J. A.; Devall, L. J.; Tait, B.; Trivedi, B. K.; Witiak, D. T.; Wu, M. *J. Org. Chem.,* **1993,** *58,* 3521-3532.

239. (a) Ackman, R. G.; Brown, W. H.; Wright, G. F. *J. Org. Chem*. **1955**, *20*, 1147-1158. (b) Boyle, P. H.; Cocker, W.; McMurry, T. B. H.; Pratt, A. C. *J. Chem. Soc. C* **1967**, 1993-1998.

240. Compound **33** obtained from *rac*-3-methylcyclohexanone is actually a mixture of diastereomers,[239b] due to the chirality of the two menthofuranyl moieties, but the NMR spectra of the compounds obtained from *R*-menthofuran and *rac*-3-methylcyclohexanone showed only minor differences in the splitting pattern of the ^{1}H NMR resonances, while their IR spectra were completely superimposable.

241. The trapping reaction between **5** and carbonyl compounds is of general applicability and may lead to a variety of bis-furanyl adducts. For example, bis-furanyl adducts were easily obtained when **5** was treated with vanillin (54% yield), anisaldehyde (43%) and furfural (39%) in the presence of catalytic amounts of various acidic catalysts (H_2SO_4, *p*-toluensulfonic acid, acidic Dowex resin). The reaction gives better yields with electron rich carbonyl compounds, whereas no product was formed with benzaldehyde and aromatic aldehydes bearing electron-withdrawing groups (*o*- and *p*-nitrobenzaldehyde, *p*- chlorobenzaldehyde), suggesting that protonation of the aldehyde carbonyl group is the critical step. A more detailed

account of this reaction is out of the scope of this paper and will be reported elsewhere.

242. Shirota, F. N.; DeMaster, E. G.; Lee, M. J. C; Nagasawa, H. T. *Nitric Oxide* **1999**, *3*, 445-453.

243. Wong, H. N. C.; Xu, Z. L.; Chang, H. M. *Synthesis* **1992**, *8*, 793-797.

244. Vineyard, B. D.; Knowles, W. S., Sabacky, M. J., Bachman, G. L.; Weinkauff, D. J. *J. Am. Chem. Soc*. **1977**, *99*, 5946-5952.

245. Ye, T.; Simon, J. D. *Photochem. Photobiol.* **2003**, *77*, 41-45.

246. Di Donato, P.; Napolitano, A. *Pigment Cell. Res.* **2003**, *16*, 532-539.

247. Thomson, R. H. *Angew. Chem. Int. Ed.* **1974**, *13*, 305-312.

248. Simon, J. D.; Goldsmith, M. R.; Hong, L; Kempf , V. R.; McGuckin, L. E.; Ye, T.; Zuber, G. *Photochem Photobiol* 200682, 318-323.

249. Napolitano, A.; Di Donato, P.; Prota, G. *J. Org. Chem.* **2001**, *66*, 6958-6966.

250. Panzella, L., P. Manini, G. Monfrecola, M. d'Ischia and A. Napolitano *Pigment Cell Res.* **2007**, *20*, 128-133.

251. Napolitano, A., C. Costantini, O. Crescenzi and G. Prota *Tetrahedron Lett*. **1994**, 35, 6365-6368.

252. Napolitano, A., S. Memoli, O. Crescenzi and G. Prota *Org. Chem.* **1996**, ***61***, 598-604.

253. Bertazzo, A., C. Costa, M. Biasiolo, G. Allegri, G. Cirrincione, and G. Presti *Biol. Trace Elem. Res.* **1996**, ***52***, 37-53.

254. Nicolaus, R. A., G. Prota, C. Santacroce, G. Scherillo, and D. Sica () *Gazz. Chim. Ital.* **1969**, *99*, 323-350.

255. Napolitano, A., P. Di Donato and G. Prota *Biochim. Biophys. Acta* **2000**, *1475*, 47-54.

256. Di Donato, P., A. Napolitano and G. Prota *Biochim. Biophys. Acta* **2002**, ***1571***, 157-166.

257. Brown, C. and R. M. Davidson *Adv. Heterocycl. Chem.* **1985**, *38*, 135-176.

258. Fattorusso, E., L. Minale, S. De Stefano, G. Cimino and R. A. Nicolaus () *Gazz. Chim. Ital.* **1968**, *98*, 1443-1463.

259. Patil, D. G. and M. R. Chedekel *J. Org. Chem.* **1984**, ***49***, 997-1000.

LIST OF PUBBLICATIONS

1) De Lucia, M.; Panzella, L.; Pezzella, A.; Napolitano, A.; d'Ischia, M. "**Oxidative chemistry of the natural antioxidant hydroxytyrosol: hydrogen peroxide-dependent hydroxylation and hydroxyquinone/*o*-quinone coupling pathways**." *Tetrahedron*, **62**, 1273-8 (2006).

2) De Lucia, M.; Panzella, L.; Crescenzi, O.; Napolitano, A.; Barone, V.; d'Ischia, M. "**The catecholic antioxidant piceatannol is an effective nitrosation inhibitor via an unusual double bond nitration**." *Bioorg. Med. Chem. Lett.*, **16**, 2238-42 (2006).

3) Panzella, L.; De Lucia, M.; Amalfitano, C.; Pezzella, A.; Evidente, A.; Napolitano, A.; d'Ischia, M. **"Acid-promoted reaction of the stilbene antioxidant resveratrol with nitrite ions: mild phenolic oxidation at the 4'-hydroxystiryl sector triggering nitration, dimerization, and aldehyde-forming routes**." *J. Org. Chem.*, **71**, 4246-54 (2006).

4) De Lucia, M.; Mainieri, F.; Verotta, L.; Maffei, M.; Panzella, L.; Crescenzi, O.; Napolitano, A.; Barone, V.; Appendino, G.; d'Ischia, M. **"Nitration *vs*. nitrosation chemistry of menthofuran: remarkable fragmentation and dimerization pathways and expeditious entry into dehydromenthofurolactone.**" *J. Org. Chem.*, **72**, 10123-9 (2007).

5) Panzella, L.; De Lucia, M.; Napolitano, A.; d'Ischia, M. "**The first expedient entry to the human melanogen 2-*S*-cysteinyldopa exploiting the anomalous regioselectivity of 3,4-dihydroxycinnamic acid-thiol conjugation.**" *Tetrahedron Lett.*, **48**, 7650-52 (2007).

6) Napolitano, A.; De Lucia, M.; Panzella, L.; d'Ischia, M. **"The "benzothiazine" chromophore of pheomelanins: a reassessment."** *Photochem. Photobiol.* **84**, 593-9 (2008).

7) De Lucia, M.; Panzella, L.; Pezzella, A.; Napolitano, A.; d'Ischia, M. "**Plant catechols and their S-glutathionyl conugates as antinitrosating agents: expedient synthesis and remarkable potency of 5-S-glutathionylpiceatannol.**" *Chem. Res. Toxicol.* In press.

8) Napolitano, A.; De Lucia, M.; Panzella, L.; d'Ischia, M.

"***The chemistry of tyrosol and hydroxytyrosol: implications for oxidative stress***" In: "Olives and Olive Oil In Health and Disease Prevention" (Ed. C. Borger) Elsevier: San Diego, CA, 2008.